FAA-72-25

Report No. FAA-RD-72-141

VORTEX SENSING TESTS AT LOGAN AND KENNEDY AIRPORTS

T. Sullivan
D. Burnham
R. Kodis
Transportation Systems Center
55 Broadway
Cambridge, Ma. 02142

DECEMBER 1972
FINAL REPORT

Prepared for:

DEPARTMENT OF TRANSPORTATION
FEDERAL AVIATION ADMINISTRATION
Systems Research and Development Service
Washington, D.C. 20591

1. Report No. FAA-RD-72-141	2. Government Accession No.	3. Recipient's Catalog No.
4. Title and Subtitle VORTEX SENSING TESTS AT LOGAN AND KENNEDY AIRPORTS		5. Report Date December 1972
		6. Performing Organization Code DOT-TSC-FAA-72-25
7. Author(s) T.Sullivan, D.Burnham, R.Kodis		8. Performing Organization Report No.
9. Performing Organization Name and Address Department of Transportation Transportation Systems Center 55 Broadway, Cambridge, MA 02142		10. Work Unit No. R-3116
		11. Contract or Grant No. FA 305
12. Sponsoring Agency Name and Address Department of Transportation Federal Aviation Administration Systems Research & Development Service Washington, D.C. 20591		13. Type of Report and Period Covered Final Report
		14. Sponsoring Agency Code
15. Supplementary Notes		

16. Abstract

This report describes a series of tests of wake vortex sensing systems at Logan and Kennedy Airports. Two systems, a pulsed acoustic radar (acdar) and an array of ground level pressure sensors, were tested. Site restrictions limited the Logan work to preliminary evaluation. The tests at Kennedy Airport established the general operating characteristics of both tracking systems. It was found that the acoustic sensor can detect and track the vortices of all commonly used commercial aircraft, though with varying degrees of sensitivity. The pressure sensors generally behaved best during conditions of low to moderate winds when the vortices could often be tracked laterally up to several hundred feet from the aircraft flight path.

17. Key Words	18. Distribution Statement
Vortex Sensing Tests, Acoustic Sensors, Wind Pressure Sensors, Aircraft Wake Vortices	DOCUMENT IS AVAILABLE TO THE PUBLIC THROUGH THE NATIONAL TECHNICAL INFORMATION SERVICE, SPRINGFIELD, VIRGINIA 22151.

19. Security Classif. (of this report)	20. Security Classif. (of this page)	21. No. of Pages	22. Price
Unclassified	Unclassified	136	

PREFACE

The tests described in this report were carried out by the Communications Branch of the Transportation Systems Center for the Federal Aviation Administration. The ultimate objective of this work is to develop operational sensors as components of a wake vortex avoidance system for terminal areas. These particular tests were designed to establish the basic operating characteristics of a pulsed acoustic sensor and an array of wind pressure sensors.

The experimental work described in this and earlier reports has depended heavily upon the technical support of Mr. Myles P. Byrne. Much of the data analysis was carried out by Mr. John Winkler.

The enthusiastic cooperation of the Massachusetts Port Authority, The Port of New York Authority, and the FAA personnel at Logan and Kennedy International Airports is very much appreciated and has been essential to the success of the sensor tests.

We wish to thank W. P. Maiersperger for suggesting the use of Ball Engineering pressure sensors.

TABLE OF CONTENTS

LIST OF ILLUSTRATIONS

LIST OF ILLUSTRATIONS (CONT.)

LIST OF ILLUSTRATIONS (CONT.)

LIST OF ILLUSTRATIONS (CONT.)

LIST OF ILLUSTRATIONS (CONT.)

LIST OF ILLUSTRATIONS (CONT.)

LIST OF TABLES

1.0 INTRODUCTION

This report describes the further development and testing of TSC wake vortex sensing systems during the period from September 1971 to March 1972. Two systems, a pulsed acoustic radar (acdar) and an array of ground level pressure sensors, have been studied. An earlier report[1], described the status of these systems as of August 1971. At that time the acoustic sensor suffered from a number of difficulties:

1. The transducers were too sensitive to aircraft noise.
2. Measurements of the reference time delay were impossible under some conditions.
3. The amount of equipment needed to track both vortices was excessive.
4. The data analysis was extremely tedious.

This report describes substantial progress in overcoming the first three difficulties. The fourth awaits the delivery of a real time data processing system, which is scheduled for August 1972.

In August 1971, the ground-based pressure sensor was established as a promising component of a vortex tracking system, but only a single sensor had been used in tests prior to those discussed in this report. The original pressure sensor provided no means for identifying which vortex was located over the sensor. This report describes an improved pressure sensor which does provide vortex identification.

The sensor development described in this report was carried out at available test sites at Logan and Kennedy International Airports (Figures 1 and 2). The Logan site is located 2100 ft from the threshold of runway 22L, in a small grassy field which contains the 4R localizer. The available transverse distance is 550 ft between boundary fences which are asymmetrically located with respect to the runway centerline. Because this distance is

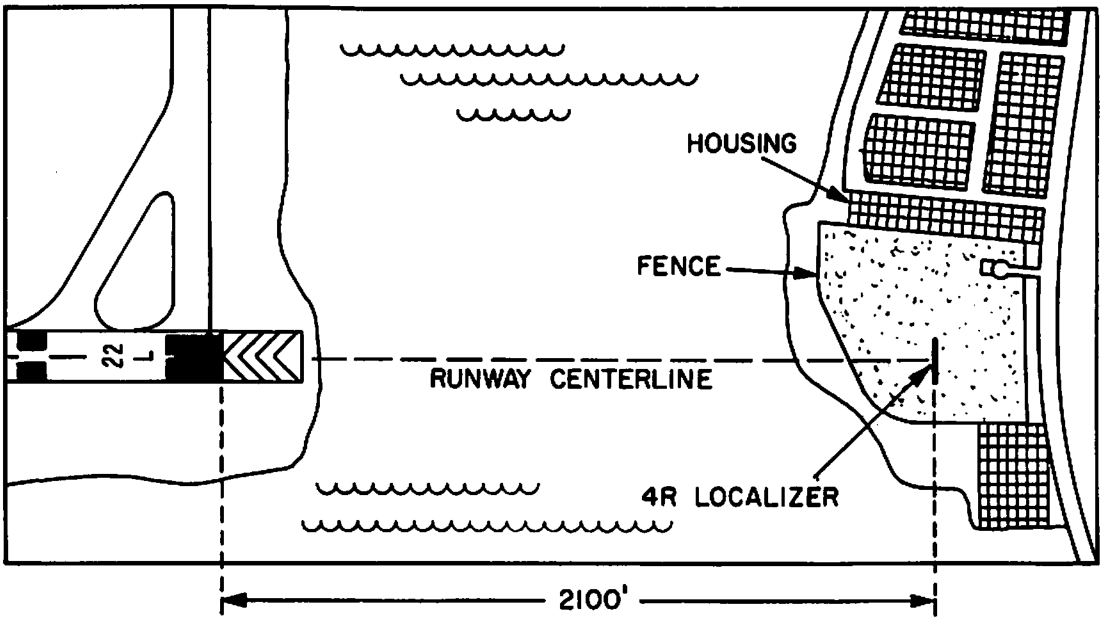

Figure 1. Test Site, Runway 22L, Logan Airport

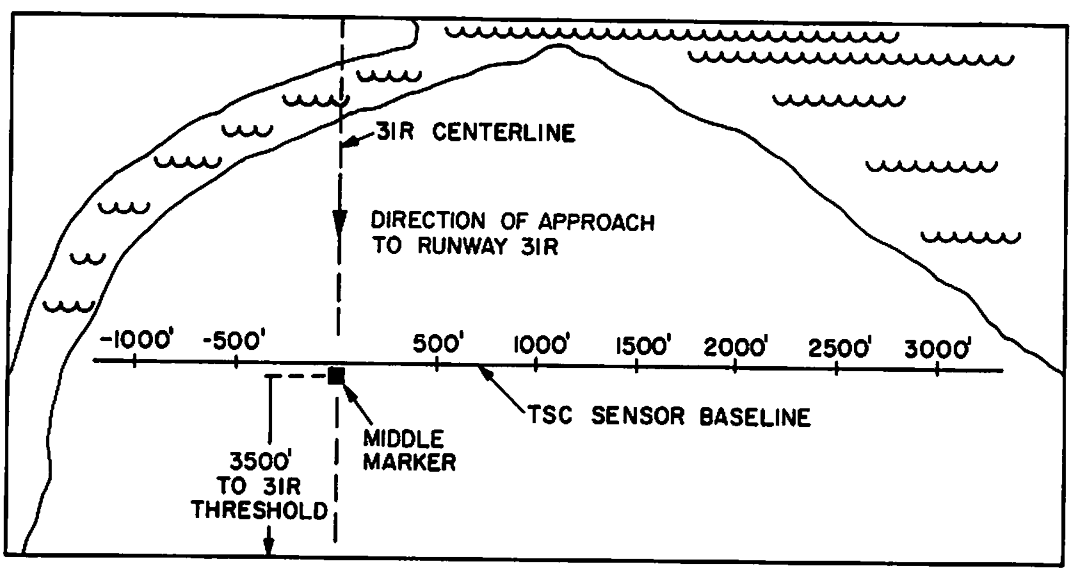

Figure 2. Test Site, Runway 31R, Kennedy Airport

inadequate for testing the tracking capabilities of the sensors, arrangements were made to operate the equipment in the vicinity of the middle marker of runway 31R at Kennedy Airport, where the available transverse distances are 1000 ft to the northeast and 3000 ft to the southwest. The land is sandy (unsuitable for vehicle travel) and fairly level ($\pm$7 ft). The mobile laboratory van was parked on the paved pad at the middle marker (Figure 3). For most data runs, photographs of the type shown in Figure 3 were taken automatically to establish the altitude and lateral position of the aircraft as it passed over the sensor baseline.

The sensor tests at Kennedy Airport established the general operating characteristics of both vortex tracking systems. However, since there was no independent means of monitoring the vortex locations, the absolute accuracy of the tracks obtained can not be determined. A comparison of the tracks obtained with each system for the same vortex shows only moderately good agreement. In addition, the interpretation of the vortex signal, and in particular, its disappearance, is not possible in the absense of some other means of determining the nature and time of the vortex dissipation. These questions will be studied in future tests at NAFEC (National Aviation Facilities Experimental Center) where the vortices are made visible by smoke and can be tracked photographically.

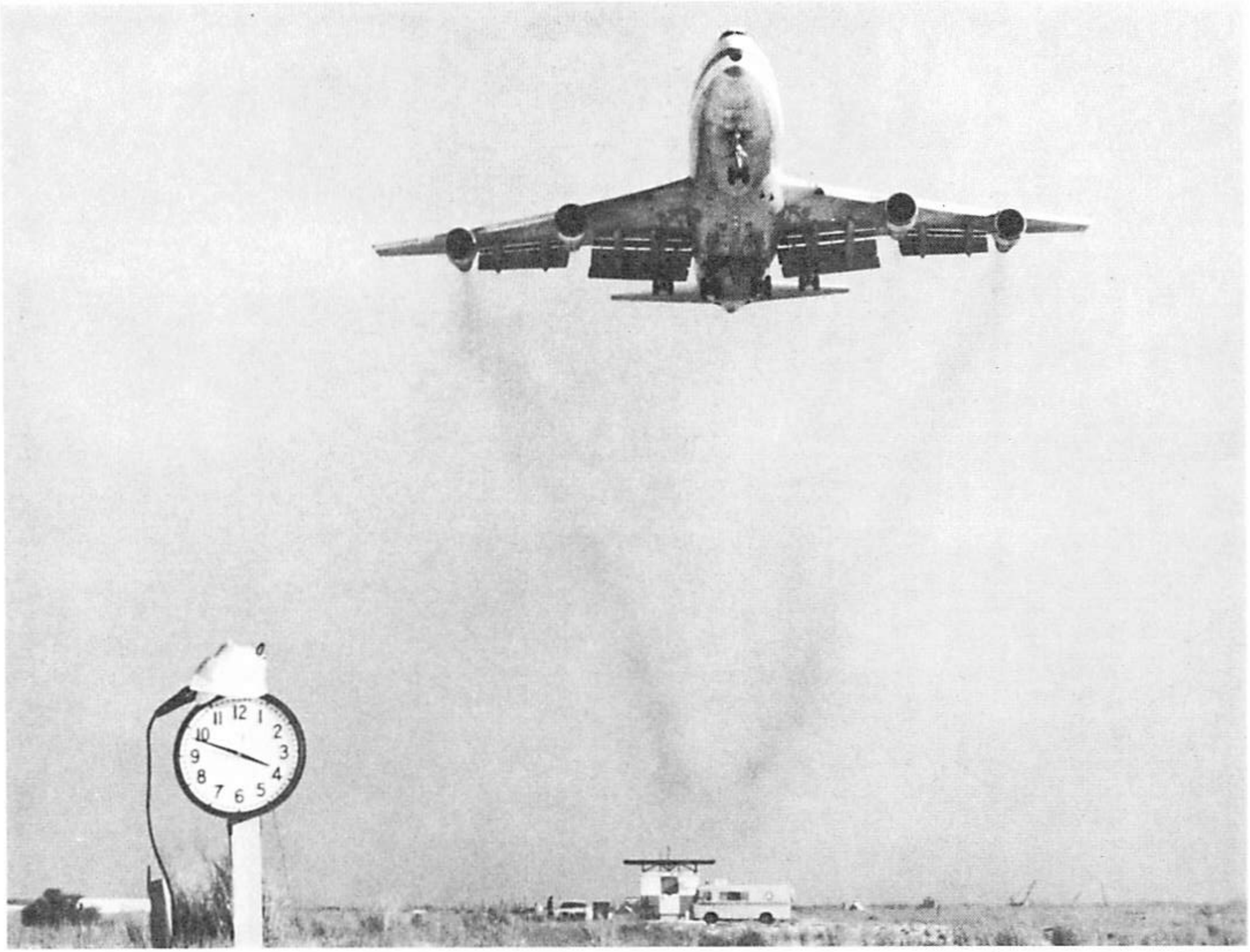

Figure 3. Photograph of Aircraft over Sensor Baseline at Kennedy Runway 31R, middle marker

2.0 ACOUSTIC SENSING SYSTEM

2.1 SUMMARY OF DEVELOPMENTS IN THE PULSED ACOUSTIC SENSING TECHNIQUE

The most significant improvements since the last report (#DOT-TSC-FAA-72-2) are the following:

1. The development of a transmit-receive (T-R) mode of operation in which one speaker acts as both transmitter and receiver (Section 2.1.1).
2. An increase in system sensitivity, achieved by reducing the sidelobes of the transceiver response (Section 2.1.2).
3. The design and development of a high powered pulse amplifier which can drive each speaker at its rated power of 60 watts (Section 2.1.3).
4. The development of a scheme for choosing speaker position and pulse timing so that adequate spatial coverage can be achieved (Section 2.1.4).
5. The use of more sophisticated data analysis (Section 2.1.5).
6. An increase in the size of the signal propagating along the ground, achieved by elevating the transceivers eight to ten ft (Section 2.1.6).

These points will be discussed in greater detail in the following sections.

2.1.1 Transceiver Mode of Operation

In all previous tests loudspeakers were used as transmitters, and microphones as receivers. Since the speakers are true transducers (i.e. can also act as receivers), it was decided to use them as transceivers, eliminating the need for separate microphones. Each speaker alternately transmits and receives. Switching is accomplished by a six-channel diode circuit similar to that used by the National Oceanic and Atmospheric Administration.[2] The switching circuit acts as an electronic gate with the parameters shown in Figure 4a. During the transmitting interval, ϕ, the speaker is connected to the output of the power amplifier and acts as a transmitter. The power pulse delivered to the speaker has the waveshape shown in Figure 4b, where the pulse length, θ, is much shorter than the pulse period, T:

$$\theta \approx 2\text{-}3 \text{ ms.} \ll T \approx 100\text{-}500 \text{ ms.}$$

During the remainder of the period the transducer is electronically switched to the input terminals of a low-level preamplifier and becomes a receiver. (See the block diagram of Fig. 4c.).

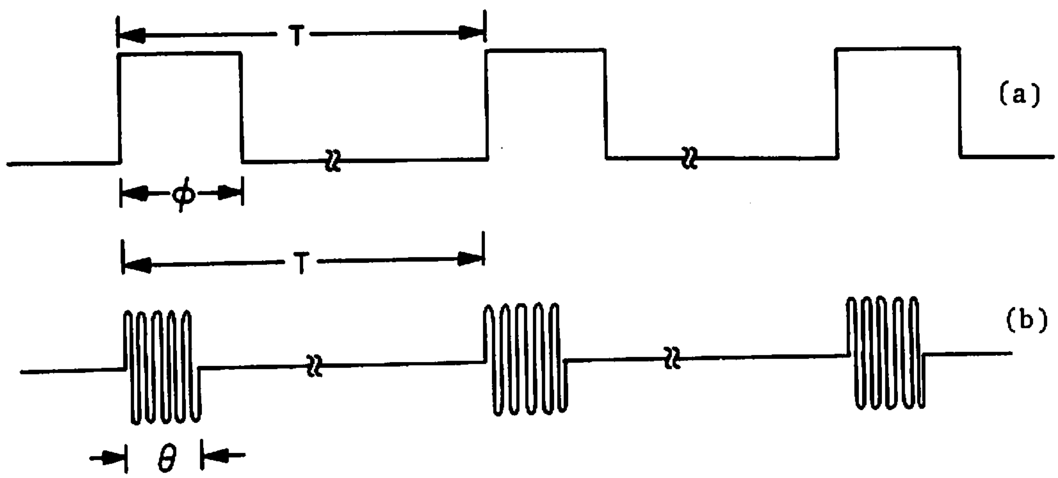

Figure 4. Transceiver Timing

A significant problem arises from the difference in signal level between these two modes of operation. Whereas the received signals are typically less than a millivolt, the transmitted signals are on the order of 100 volts. The speaker response to this high-powered pulse contains a decaying transient, as shown in Figure 5. In order that this transient may fall to a low level before the transducer is switched to the receiver preamplifier, the

2.0 ACOUSTIC SENSING SYSTEM

2.1 SUMMARY OF DEVELOPMENTS IN THE PULSED ACOUSTIC SENSING TECHNIQUE

The most significant improvements since the last report (#DOT-TSC-FAA-72-2) are the following:

1. The development of a transmit-receive (T-R) mode of operation in which one speaker acts as both transmitter and receiver (Section 2.1.1).
2. An increase in system sensitivity, achieved by reducing the sidelobes of the transceiver response (Section 2.1.2).
3. The design and development of a high powered pulse amplifier which can drive each speaker at its rated power of 60 watts (Section 2.1.3).
4. The development of a scheme for choosing speaker position and pulse timing so that adequate spatial coverage can be achieved (Section 2.1.4).
5. The use of more sophisticated data analysis (Section 2.1.5).
6. An increase in the size of the signal propagating along the ground, achieved by elevating the transceivers eight to ten ft (Section 2.1.6).

These points will be discussed in greater detail in the following sections.

2.1.1 Transceiver Mode of Operation

In all previous tests loudspeakers were used as transmitters, and microphones as receivers. Since the speakers are true transducers (i.e. can also act as receivers), it was decided to use them as transceivers, eliminating the need for separate microphones. Each speaker alternately transmits and receives. Switching is accomplished by a six-channel diode circuit similar to that used by the National Oceanic and Atmospheric Administration.[2] The switching circuit acts as an electronic gate with the parameters

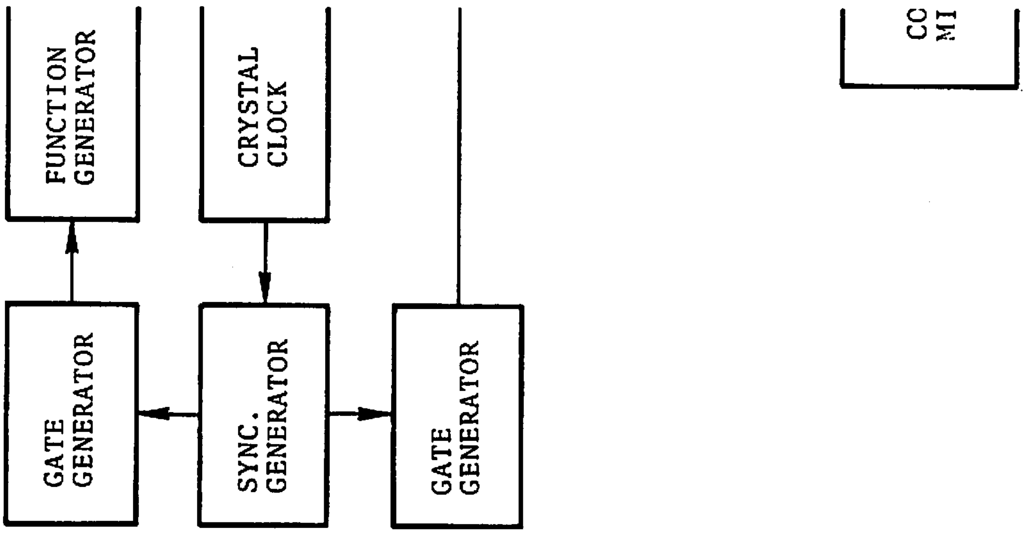

Figure 4c. Bl

shown in Figure 4a. During the transmitting interval, ϕ, the speaker is connected to the output of the power amplifier and acts as a transmitter. The power pulse delivered to the speaker has the waveshape shown in Figure 4b, where the pulse length, θ, is much shorter than the pulse period, T:

$$\theta \approx 2\text{-}3 \text{ ms.} << T \approx 100\text{-}500 \text{ ms.}$$

During the remainder of the period the transducer is electronically switched to the input terminals of a low-level preamplifier and becomes a receiver. (See the block diagram of Fig. 4c.).

gate time ϕ, of the switching circuit must be much greater than the pulse duration, θ. In these experiments ϕ was set at 20-30 msec.*

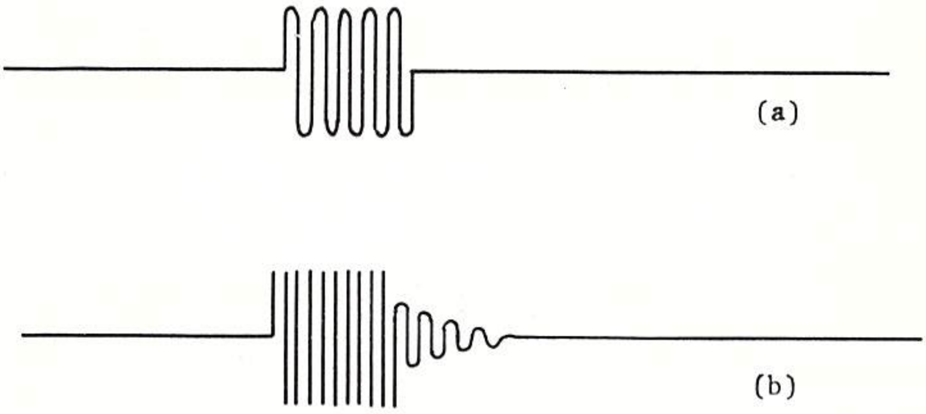

Figure 5. Signal Voltage Across Speaker
a) Normal size
b) Greatly magnified

Another type of interference is due to nearby reflections from the ground. This problem can be controlled by adjusting the antenna beam shape (e.g., tilting the acoustic dishes up). Both problems are greatly alleviated by transmitting different frequencies in the two directions of propagation. Thus, the speaker which is transmitting at frequency f_1 receives a signal at frequency f_2. Electronic filtering** then eliminates a great deal of the ringing at frequency f_1. The frequencies chosen were 3KHz and 2KHz as shown in Figure 6.

*This ringing problem was particularly bothersome in one of the speakers, in which the amplitude of the transient increased gradually with time. Eventually, this speaker was taken out of service.

**The electronic filters used to obtain the acoustograms in this report have the following characteristics:

Recording:	2KHz, 3 pole, high pass.
Playback:	2 or 3KHz, 4 pole, high pass; 2 or 3KHz, 2 pole, Q = 5-8, bandpass.

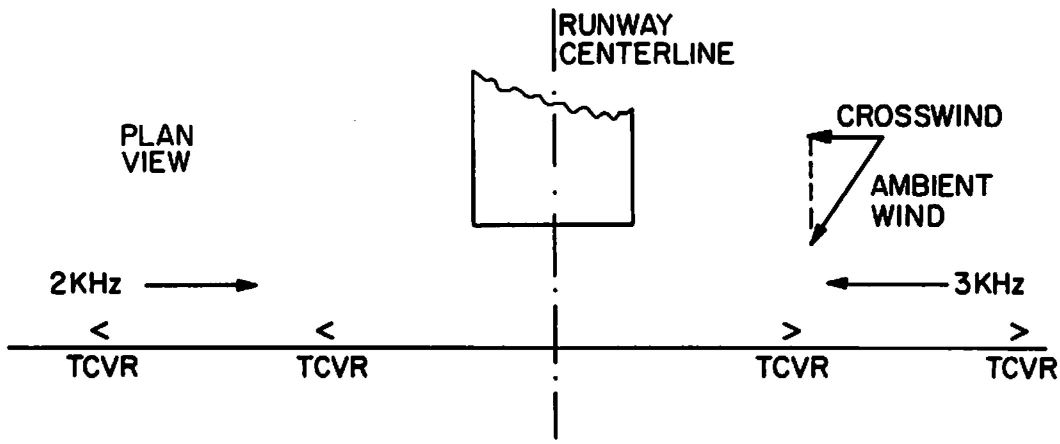

Figure 6. Frequency Choice as a Function of Wind

The lower frequency was chosen for propagation against the crosswind component of the ambient wind since lower atmospheric attenuation at 2KHz compensates for the added losses due to upwind propagation. This procedure increases significantly the amplitude of the received signal for this direction of propagation.

2.1.2 Modification of the Antenna Pattern

The sidelobes of the receiving antenna were greatly reduced by using horn-type speakers instead of microphones in the parabolic reflectors. A more complete discussion of the relative merits of several different speaker horns is given in Appendix A. The combination chosen consists of a University SH horn with an ID-60T driver mounted in a parabolic reflector (Figure 7). When an aircraft passes through the sensitive volume of the radar, it creates enough noise in the receivers to mask any useful information. This noise may be observed at the beginning of each acoustogram. In earlier tests, using microphones as receivers, this noise persisted for 10-15 seconds after the passage of the aircraft due to the omnidirectionality of the microphone response. The lower sidelobe response of the new system reduces this waiting time to two or three seconds, as may be seen in most of the acoustograms in this report.

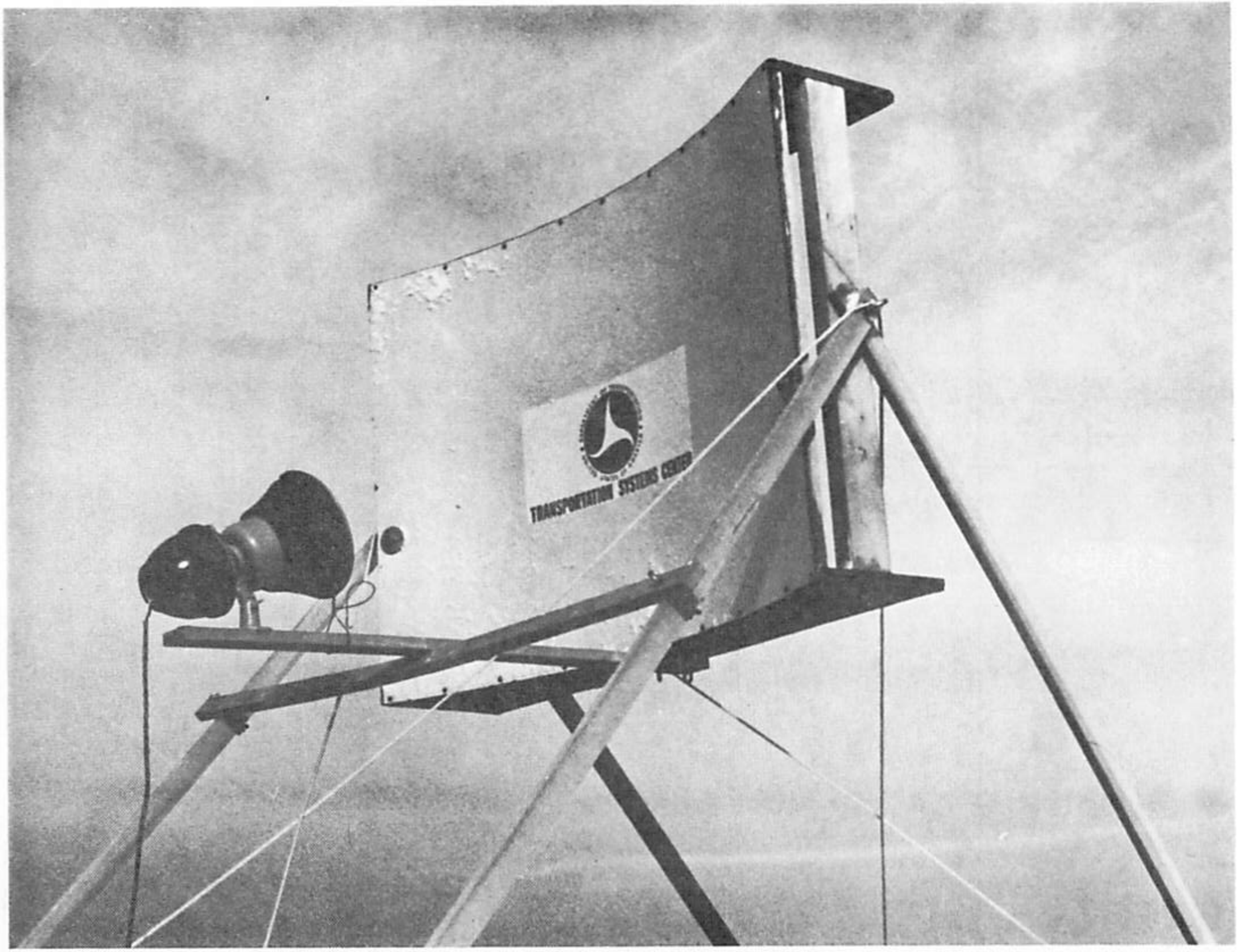

Figure 7. Antenna System used in Kennedy Tests

2.1.3 Development of High Power Pulse Amplifier

The original acoustic system used two commercial public-address amplifiers to drive the loudspeakers. These amplifiers proved to be inadequate for two reasons:

1. Their power rating was insufficient to operate the speakers at full power (60 W per speaker).
2. They generated considerable noise after the transmitted pulse was turned off, especially when operated near maximum power (35 W and 75 W respectively for the two amplifiers).

These difficulties led to the design of a new pulse amplifier which has performed satisfactorily. The amplifier operates in a switching mode rather than as a linear amplifier, in order to eliminate output noise during the time the speaker is acting as a receiver. Because the duty cycle is low (about 1%) and the pulse length is short (2-3 msec), very high peak power (500 W per channel) can be supplied by capacitor discharge from a compact unit with low average power requirements.

2.1.4 Choice of Speaker Position and Pulse Timing

When a speaker is used as both transmitter and receiver, it is important to choose its location carefully. If the available land permits, it is desirable to deploy the transducers symmetrically about the runway centerline in order to track the vortices equally well in both directions. It is also advantageous to space the sensors evenly so that each received signal can be unambiguously defined on the output display. Satisfying this requirement also depends on the available land. Since all the pulses are transmitted at the same time and each received signal has its own non-interfering time slot, this procedure can be considered a form of time multi-plexing. Figure 8 shows a representative acoustogram containing only signals transmitted directly along the ground, and the corresponding positions of the sensors. The signals received from speakers 5 and 6 are at a very low level for two reasons:

1. They are received through the back lobe of the antenna and therefore have very low gain,
2. They are transmitted at 2KHz and are therefore attenuated by the filtering (tuned to 3KHz).

For a symmetrical, evenly spaced system, such as that shown in Figure 8, the following relations hold:

$$T_2 = \left(p + \frac{q}{n}\right) T, \qquad (1a)$$

$$T_1 = \frac{m}{n} T + B, \qquad (1b)$$

$$\tau_m = \frac{T}{n} - B, \qquad (1c)$$

where T is the period of the pulse signal, m, p, and q are integers ($0 < q < n$; $0 \leq p$), and

n = number of sensors on one side of the runway, i.e. total number/2,

τ_m = the maximum time delay expected from the vortex delayed pulse,

B = the time when the first ground pulse appears on the acoustogram,

T_1 = the spacing between the first receivers encountered by pulses propagating in either direction (may be negative).

T_2 = the spacing between adjacent speakers transmitting in the same direction ($T_2 > 0$).

B must be larger than ϕ (Figure 4) since the speaker is not in the receiver mode during this part of the period.

The position of the first ground pulse depends on the direction and magnitude of the ambient crosswind. The shift in position from the zero wind condition is equal to Lw_c/c^2, where w_c is the magnitude of the crosswind, L is the baseline length, c the velocity of sound,

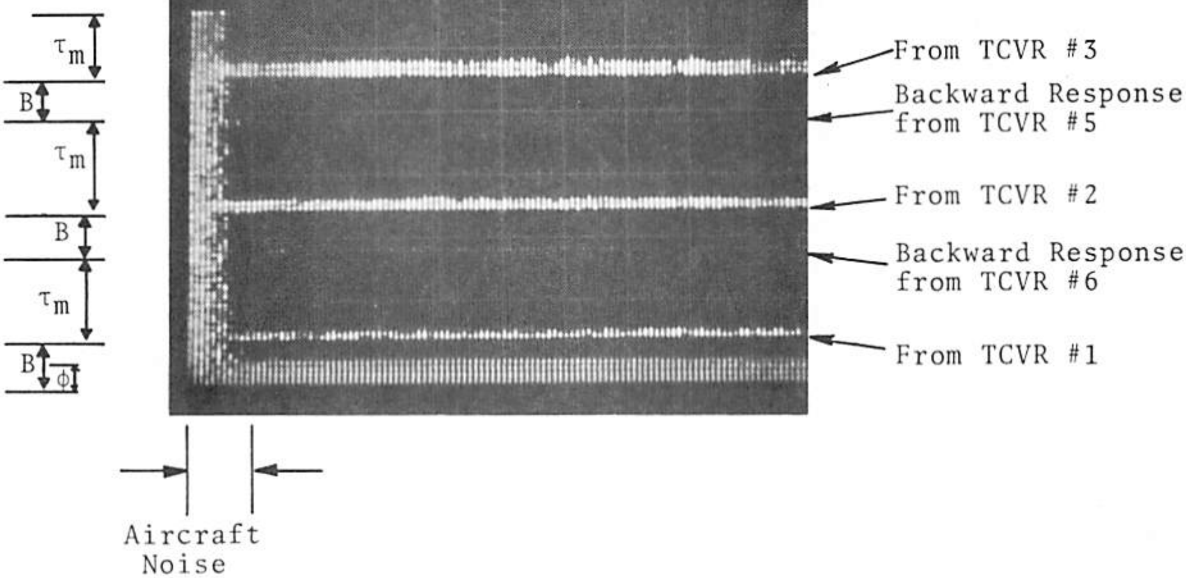

(a)

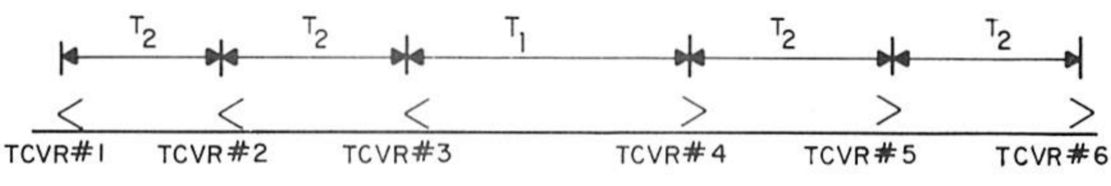

(b)

Figure 8. Sample Acoustogram
a) Signals received in transceiver #4
b) Sensor position for sample acoustograms

and $w_c \ll c$. If the crosswind is toward the receiver, then this shift is toward the dead time ϕ. Thus B must be large enough to keep the position of the ground pulse from moving into the dead time. In our experiments, B was chosen to be 50 milliseconds, which allows for crosswinds of approximately 12 knots over a 1000 foot baseline with ϕ = 30 msec.

If B - ϕ is not adequate to insure unobscured ground pulses, the period T may be decreased slightly in order to delay the arrival time of all the ground pulses. This procedure keeps the initial ground pulse out of the dead time at the expense of shortening the maximum time available for observing signals. The alternative of relocating all the speakers is operationally impractical.

If a vortex is roughly halfway between the transmitter and receiver and fairly close to the ground (i.e. $h < L/4$), then from Figure 9 the following small angle approximations hold:

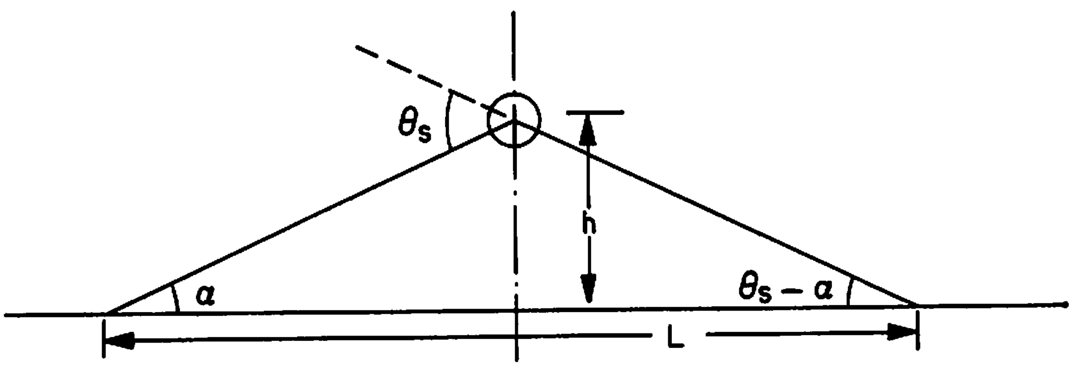

Figure 9. Small Angle Approximation Geometry

$$\tau = \frac{\theta_s h}{2} \tag{2a}$$

$$\tau = \frac{2h^2}{L} \tag{2b}$$

$$h = \left(\frac{L\tau}{2}\right)^{1/2} \tag{2c}$$

$$\tau = \frac{\theta_s^2 L}{8} \tag{2d}$$

where θ_s is the scattering angle in radians and τ is the time delay of the signal received from the vortex pulse. All distances are normalized to c, the speed of sound, and are expressed in units of time. These equations are not all independent but each finds a useful application.

The operational characteristics of the acoustic sensing system may be determined from Equations (2a) - (2d). The maximum scattering angles θ_m (landing configuration) are observed from the vortices generated by B-727's and are in the range of 1.2 - 1.4 radians. A sensing system generally would be required to track vortices from a maximum height h_m, (probably equal to the aircraft height) down to the minimum height reached in ground effect (theoretically $\pi b/8$, where b is the wing span). These limits h_m, h_ℓ and θ_m determine the baseline separations of the system. Once h_m and θ_m are chosen, τ_m may be calculated from (2a): $\tau_m = \theta_m h_m/2$. The sensor separation, L_m, required to observe signals from vortices at this maximum height and scattering angle may be calculated from (2b) and generally results in a relatively long baseline. As the vortex descends, the time delays observed with a long baseline can become very small, and the calculation of the position is then not very accurate (Appendix B). In fact, the minimum height h_ℓ determines the maximum baseline L_ℓ which will allow the delayed pulse to be distinguished from the direct pulse. The minimum usable delay, τ_ℓ, is about five msec, which according to Equation (2b) leads to a value of L_ℓ = 1000 msec (1100') for h_ℓ = 50 msec.

In a typical application (see the Kennedy set-ups in Section 2.3) L_ℓ and L_m are approximately the same. In this case several other sensors with shorter baselines and, hence, larger time delays are used to monitor the vortex in the region close to the ground.

2.1.5 Data Analysis

Two time delays with either a common receiver or transmitter are required to locate the position of a vortex. The multiple speaker system allows for the possibility of observing several time delays and making a redundant calculation of the vortex position. These calculations do not all yield the same results because of errors in data reduction and other systematic errors (Appendix B). The best location is calculated using a least squares iterative technique which minimizes the discrepancy between measured and calculated time delays. An outline of this procedure is as follows:

1. An initial position (x_o, h_o) is calculated using the two largest time delays (with the requirement of a common transmitter or receiver).
2. Using this position the expected time delay, α_{nm}, is calculated for all other combinations of speakers.
3. The sum of the squares of the time delay errors is given by:

$$\sum_{nm} \left(\tau_{nm} - \alpha_{nm}\right)^2 = \varepsilon$$

   where τ_{nm} is the observed time delay using transmitter n and receiver m.

4. The x_o position is indexed by an amount Δx and ε is calculated again. This procedure is continued until the value of x yielding minimum ε is found.
5. The same procedure is then followed for h_o, indexing by Δh.
6. Steps 4 and 5 are alternated, and Δx and Δh are decreased until the location yielding the minimum value of ε is found to the desired accuracy. This result is the best estimate of the vortex location.

A sample computer printout is shown in Figure 10, where T(n,m) is the time delay τ_{nm}. The values of $E = \tau_{nm} - \alpha_{nm}$ give an indication of the accuracy of the time delay measurement. The time delays, which would be observed if the vortex were actually at the final calculated position, may be found by adding the corresponding values of E to T(n,m).

2.1.6 Speaker Elevation

In our early work it was often difficult to observe the ground pulse on some of the receivers. This difficulty was due to several factors, viz. slopes in the land, ground-level wind-shear effects, and relatively low transmitted power. Support stands were designed and constructed to raise the transceiver 8-10 ft above the ground to help reduce this problem. A photograph of one of these stands with the transceiver mounted on it is shown in Figure 11. Appendix C contains a more detailed discussion of the direct signals observed in the experiments.

2.2 TESTS AT LOGAN AIRPORT, APPROACH END OF RUNWAY 22L

The controlling factor in deciding the speaker position and timing for the location at Logan is the available land (Figure 1). Two transceivers were placed on either side of the runway center-line, and with the help of Equations (2a)-(2d), the configuration shown in Figure 12 was chosen (for aircraft altitudes of 100-150 feet). Altec Lansing horns with University and Altec Lansing driver units were used as transceivers (Figure 13). All speakers were placed on the ground but one, which was elevated to a height of about 10 ft by means of the support structure shown in Figure 14. It was impossible to detect direct pulses when this speaker was at ground level because of the sharp downward slope of the land.

```
TIME =  3        3 5-- 3 6     X0= 20.264798  H0= 115.28036
X= 86.264798     H= 146.66786  AV E^2= 2.4292972
T( 1, 4)= 47     E=-.75355467
T( 1, 5)= 26     E= 2.5533916
T( 1, 6)= 23     E=-3.9036706E-02
T( 2, 4)= 55     E= .20423256
T( 2, 5)= 39     E=-1.5088211
T( 2, 6)= 32     E=-.10124947
T( 3, 4)= 0      E= 99.361846
T( 3, 5)= 80     E= 1.3487925
T( 3, 6)= 77     E=-1.2436358

TIME =  5        3 4-- 3 5     X0= 87.275517  H0= 133.45133
X= 104.11927     H= 138.74508  AV E^2= 2.5202156
T( 1, 4)= 45     E=-1.7576081
T( 1, 5)= 25     E= .76243234
T( 1, 6)= 20     E= .4950575
T( 2, 4)= 51     E=-.18198046
T( 2, 5)= 34     E=-.66193999
T( 2, 6)= 28     E= 7.0685163E-02
T( 3, 4)= 84     E= 2.4758509
T( 3, 5)= 69     E=-4.1086562E-03
T( 3, 6)= 66     E=-2.2714835

TIME =  10       3 4-- 3 5     X0= 179.47255  H0= 122.90888
X= 173.6288      H= 123.94013  AV E^2= 1.2946815
T( 1, 4)= 43.5   E=-1.0046676
T( 1, 5)= 22     E=-.53752927
T( 1, 6)= 17     E=-.70316435
T( 2, 4)= 47     E= .4005162
T( 2, 5)= 26     E= .36765453
T( 2, 6)= 21.5   E=-.29798055
T( 3, 4)= 65.5   E= .85668105
T( 3, 5)= 44     E= 1.3238194
T( 3, 6)= 42     E=-1.8418157

TIME =  15       3 4-- 3 5     X0= 257.928    H0= 114.96358
X= 246.58425     H= 115.78858  AV E^2= 1.0958724
T( 1, 4)= 51     E= .4314833
T( 1, 5)= 20     E= 9.0280883E-02
T( 1, 6)= 14     E= .36017381
T( 2, 4)= 54     E= .92937194
T( 2, 5)= 23     E= .58816952
T( 2, 6)= 17     E= .85806245
T( 3, 4)= 68     E=-1.7457124
T( 3, 5)= 34     E= .9130852
T( 3, 6)= 30     E=-.81702188

TIME =  20       3 5-- 3 6     X0= 299.67     H0= 97.713324
X= 331.295       H= 97.919574  AV E^2= 1.4657889
T( 1, 4)= 0      E= 72.595694
T( 1, 5)= 16.5   E=-.21940541
T( 1, 6)= 9.5    E= 1.0873458
T( 2, 4)= 0      E= 74.623405
T( 2, 5)= 19     E=-.69169469
T( 2, 6)= 11     E= 1.6150565
T( 3, 4)= 0      E= 80.256534
T( 3, 5)= 24     E=-5.8565173E-02
T( 3, 6)= 19     E=-.75181398
```

Figure 10. Sample Computer Printout for the Calculation of the Position of one Vortex.
Note: T=0 implies no scattered signal was observed for this transceiver combination.

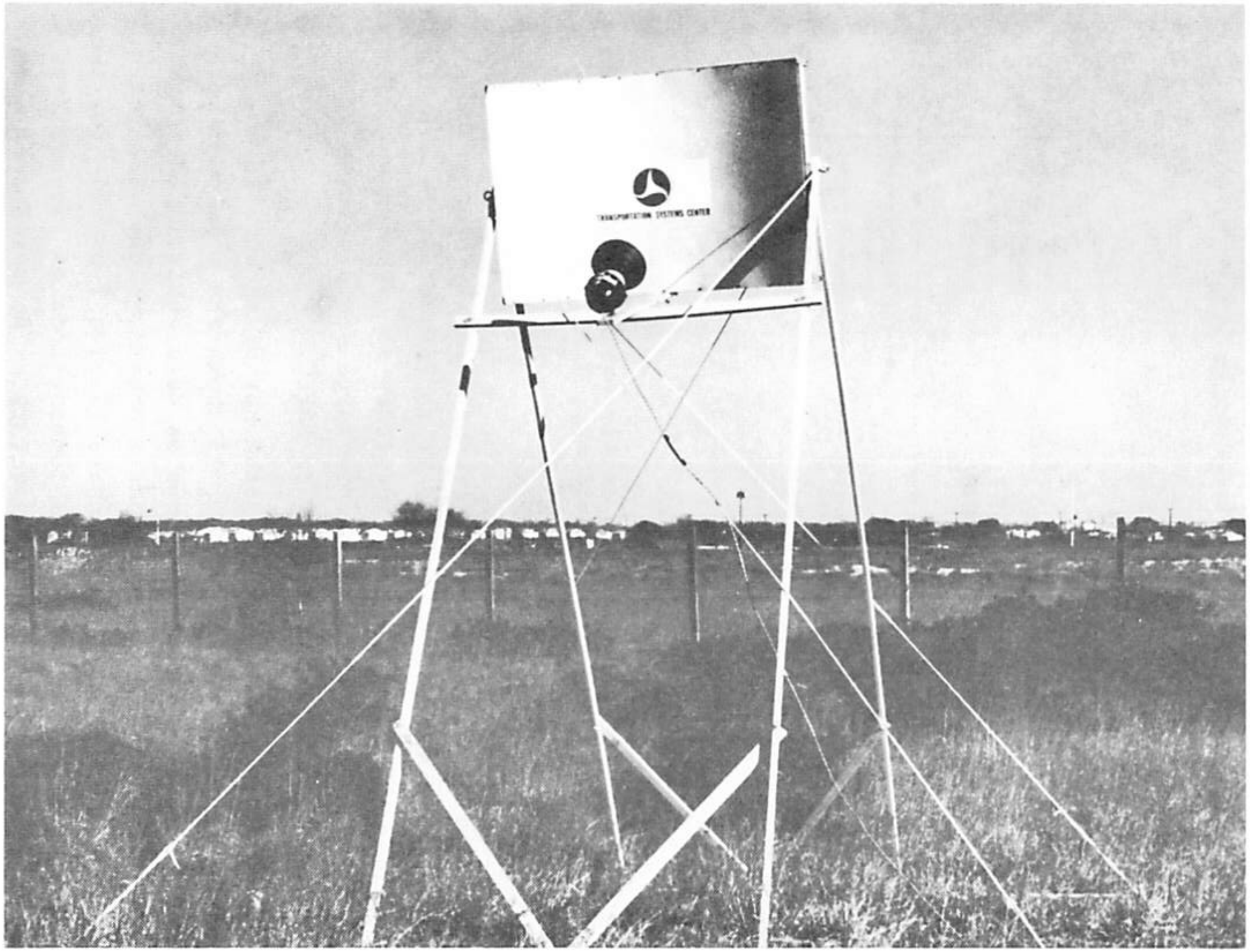

Figure 11. Acoustic Sensor with its Support Stand. Speaker is about Eight Feet above the Ground.

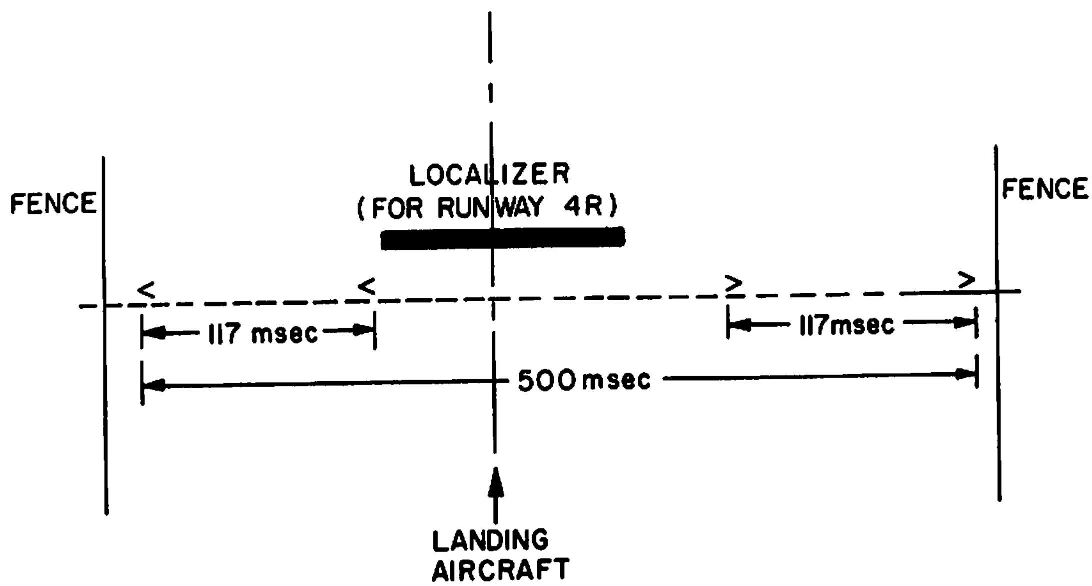

Figure 12. Speaker Locations at Logan Airport, Runway 22L. τ_m=87.5ms.; B=30ms.; T_1=265ms.; T_2=117.5ms.; n=2; q=1; p=0; m=2.

Because the baselines at Logan are necessarily short, the vortices usually drift out of the sensitive volume fairly quickly (20-40 seconds). For this reason, the tests at Logan Runway 22L were designed to check out the system before large scale testing at either Kennedy International Airport or NAFEC.

The advantage of a redundant system may be shown with an example from the Logan tests. Figure 15 shows the tracks of both vortices obtained using the least squares data analysis (described in Section 2.1.5). For most of the data points, a time delayed signal was observed in all four channels (Tables 1 and 2) For these data points there are four different combinations of transceivers which can be used to compute a vortex track. The results of each combination for the right vortex are shown in Figure 16. It can be seen that the averaging done by the redundancy in the least squares program produces a more realistic track.

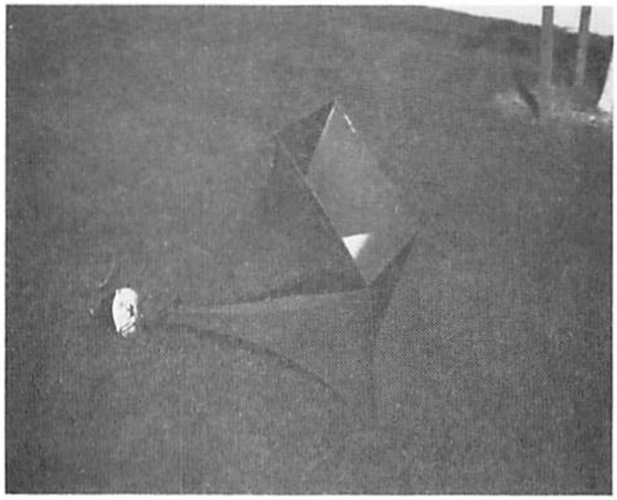

(a)

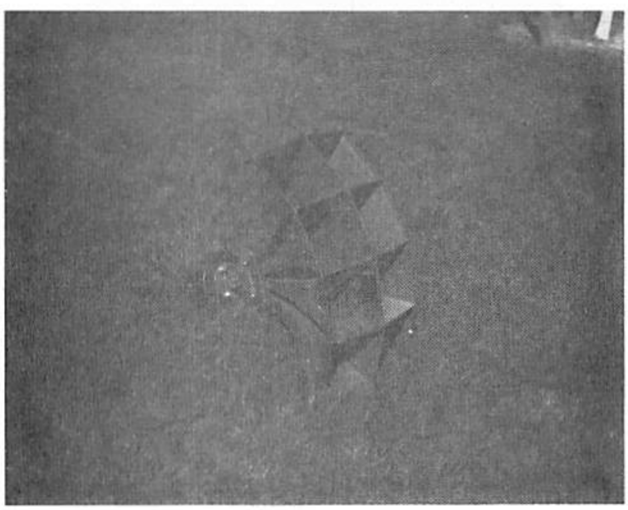

(b)

Figure 13. Transceivers used for the Tests at Logan Airport, Runway 22L
a) Altec Lansing 203B Horn; University ID60T Driver
b) Altec Lansing 805B Horn; Altec Lansing 291-16A Driver

Figure 14. Altec Lansing Multicellular Horn with Support Stand Against Fence.

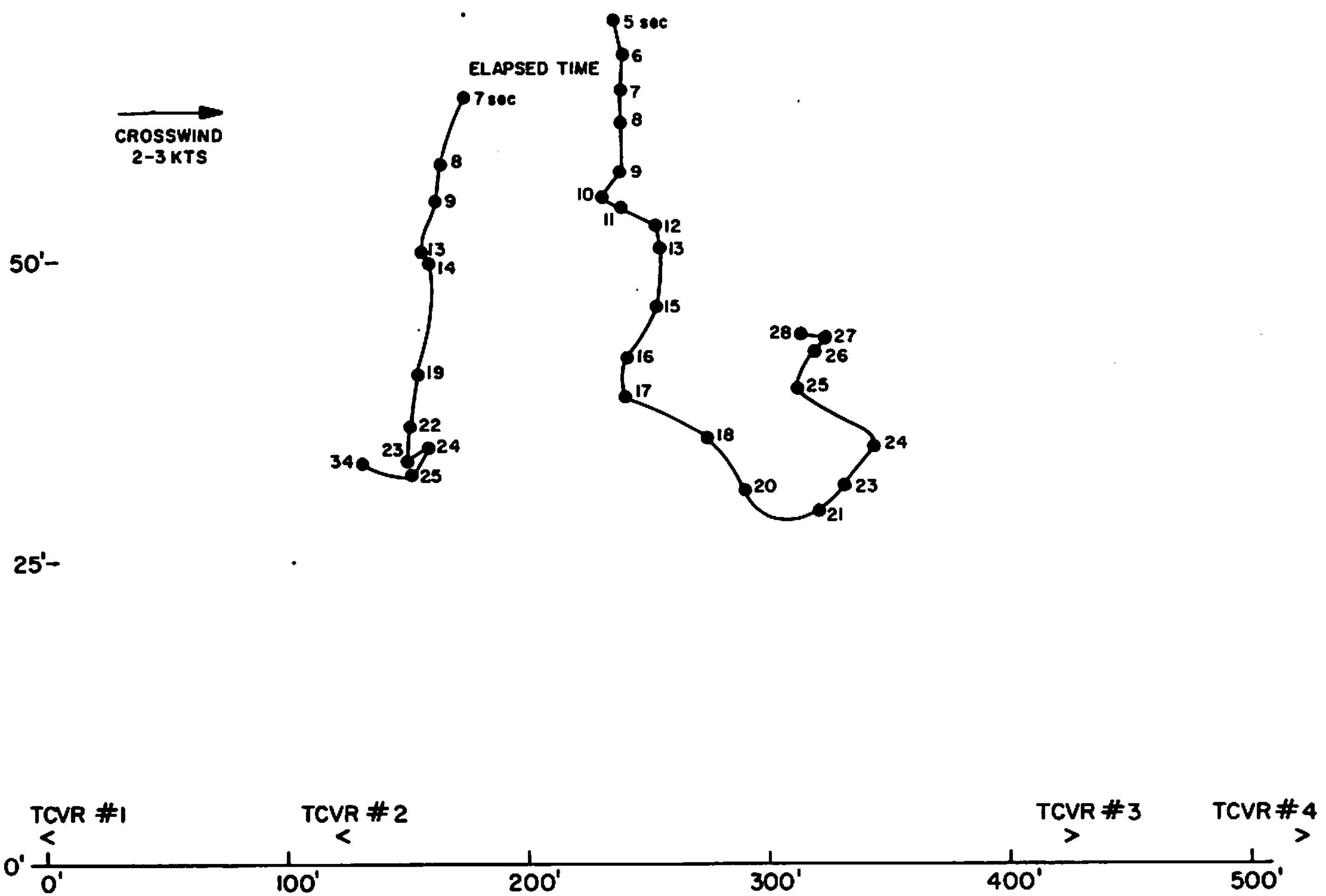

Figure 15. Vortex Tracks; Logan Airport 10/6/71; BAC-111: Wingspan ~ 90'; Local Time: 1540 Runway 22L. Note: Expanded Vertical Scale

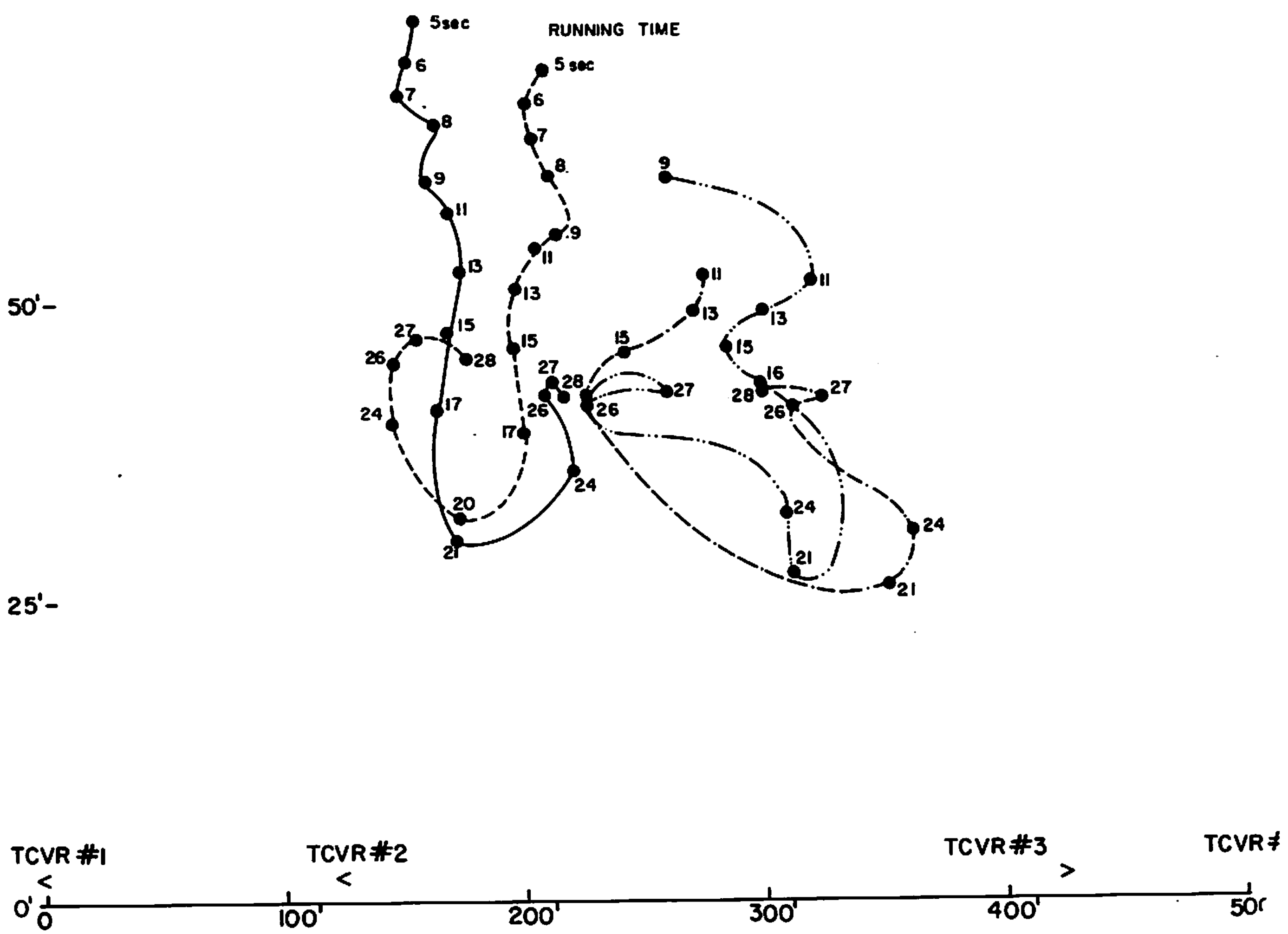

Figure 16. Right Vortex Track Using Each Combination of Receivers Separately. Run 35-16 BAC-111

TABLE 1. RUN #35-16 DOWNWIND VORTEX

Elapsed Time (Sec.)	Observed Time Delayed Signals (Milliseconds) 1,4 *	1,3	2,4	2,3
3			37	
4			27.5	
5		20	24	31
6		18.5	22	28
7		17	20.5	26
8		15.5	18.5	24.5
9	12	13	16	21
10	10	12.5	15.5	20
11	9	12.5	14.5	19.5
12	8	12	13	18
13	8	11	12	16.5
14	7			
15	7	9	10	13.5
16	6	7.5	9	11
17	4.5	6.5	7.5	10
18	4	5.5	5.5	8
19			5	6
20	3	4.5	4.2	6
21	2.5	5	4	5.5
22			4	5.5
23	3	6	4.5	7
24	3.5	7.5	5.5	9.5
25	4	8	7	10.5
26	6	9.5	7.5	12
27	6	10	8	13
28	6	9	7.5	12.5
29			7.5	11.5
30			7	11
31			7	10.5
32			5.5	

*1,4 implies the signal received in transceiver #1 which was transmitted by transceiver #4.

TABLE 2. RUN #35-16 UPWIND VORTEX

Elapsed Time (Sec.)	Observed Time Delayed Signals (Milliseconds) 3,2	4,2	3,1	4,1
5	45.5		22	18.5
6	42.5		19	16.5
7	38		17.5	14.5
8	35.5	30.5	15	12.5
9	33	29	14	11.5
10	31		12	10
11	30.5	26.5	12	10.5
12	30.5		12.5	10
13	29.5	27.5	12	9.5
14	28.5	27	11.5	10
15		26	11	9.5
16	25	25	9	8.5
17	23		8.5	7
18	22	8	8	7
19	21	20.5	7.5	7
20	20	18	7	
21	19.5	18	7	5.7
22	18	17.5	6	5.7
23	16	15.5	5.5	
24	15	14	5	
25	15	14	4.5	
26	15	14.5		
27	14	13.5	4.5	
28		12	3.5	
29		13.5	2.5	
30		14.5	2	
31				
32			2.5	
33			3.5	
34			5.5	5
35			7	5.5
36			6	5.7

2.3 TESTS AT J.F. KENNEDY INTERNATIONAL AIRPORT, APPROACH END OF RUNWAY 31R

2.3.1 Site Description

The site chosen for the sensor baseline at Kennedy Airport is located near the middle marker building at the approach end of Runway 31R (Figure 2). This site has the following desirable characteristics:

1. The mobile laboratory van can be driven right up to the building where there is an asphalt platform suitable for parking.
2. The aircraft are ordinarily 200' high when they pass over this spot.
3. The available land imposes few restrictions on the positioning of the sensors.
4. Supplementary power is available from the middle marker building. (It is desirable to run the tape recorders on external power because the frequency fluctuations of the generator in the van produce variations in the tape speed which are severe enough to degrade the data).
5. The runway is used frequently during the winter months.
6. The area is totally void of large obstacles which would perturb the natural behavior of the vortices.

The maximum height of an aircraft as it passed through the sensitive volume of the acoustic sensor was expected to be about 240' (the maximum height of the glide slope window at the middle marker). In this region the small angle approximations, Equations (2a)-(2d), can be used to obtain an expected maximum time delay: τ_m = 110 msec (assuming a maximum scattering angle of one radian). The shortest baseline with which it is possible to obtain a signal from a vortex in this region may then be calculated: L_m = 970' (880 msec).

The tests at Kennedy Airport were divided into two series:

Series 1. Those designed to track the vortices over very long lateral distances (2900 ft to the port side of the runway centerline, 1050 ft to the starboard side). (Section 2.3.2)

Series 2. Those designed to provide reliable vortex positions in the area relatively close to the runway centerline ($\pm$ 700 ft). (Section 2.3.3)

2.3.2 First Series of Tests: Long Range Tracking

The original test plan for instrumenting runway 31R is shown in Figure 17 (Set 1: TCVR 1, 2, 4, 5 or 6; Set 2: RCVR 1, 2, TMTR 1). The central baseline length of 970 msec (m=5 in Equation(1b) was chosen to satisfy the minimum distance requirement i.e., 880 msec. While remaining within the restriction of six channels for recording acoustic data, it was hoped that both vortices could be tracked near the runway centerline (using Set 1) and the port vortex out to 2500 ft., the current specification on parallel runway separation (using Set 2). It became obvious during the course of the experiments that this plan was overly ambitious, and Set 2 was never set up. The transceivers in Set 1 used on particular days are listed in Table 3. Note that the center microphone, originally used to position the speakers by acoustic time delay, was also used as a receiver during the data runs. TCVR #3 was added during the last day of operation with this system in an attempt to improve the vortex tracks near the runway centerline.

One difficulty that arises while trying to track vortices relatively near the ground with these long baselines is the rapid decrease in time delay as the vortex descends (Equation (2c)). As the vortex approaches its equilibrium height (30-70 ft), the time delays become excessively small (2-9 msec for the 1060 ft (970 msec) baseline) making accurate tracking very difficult, if not impossible.

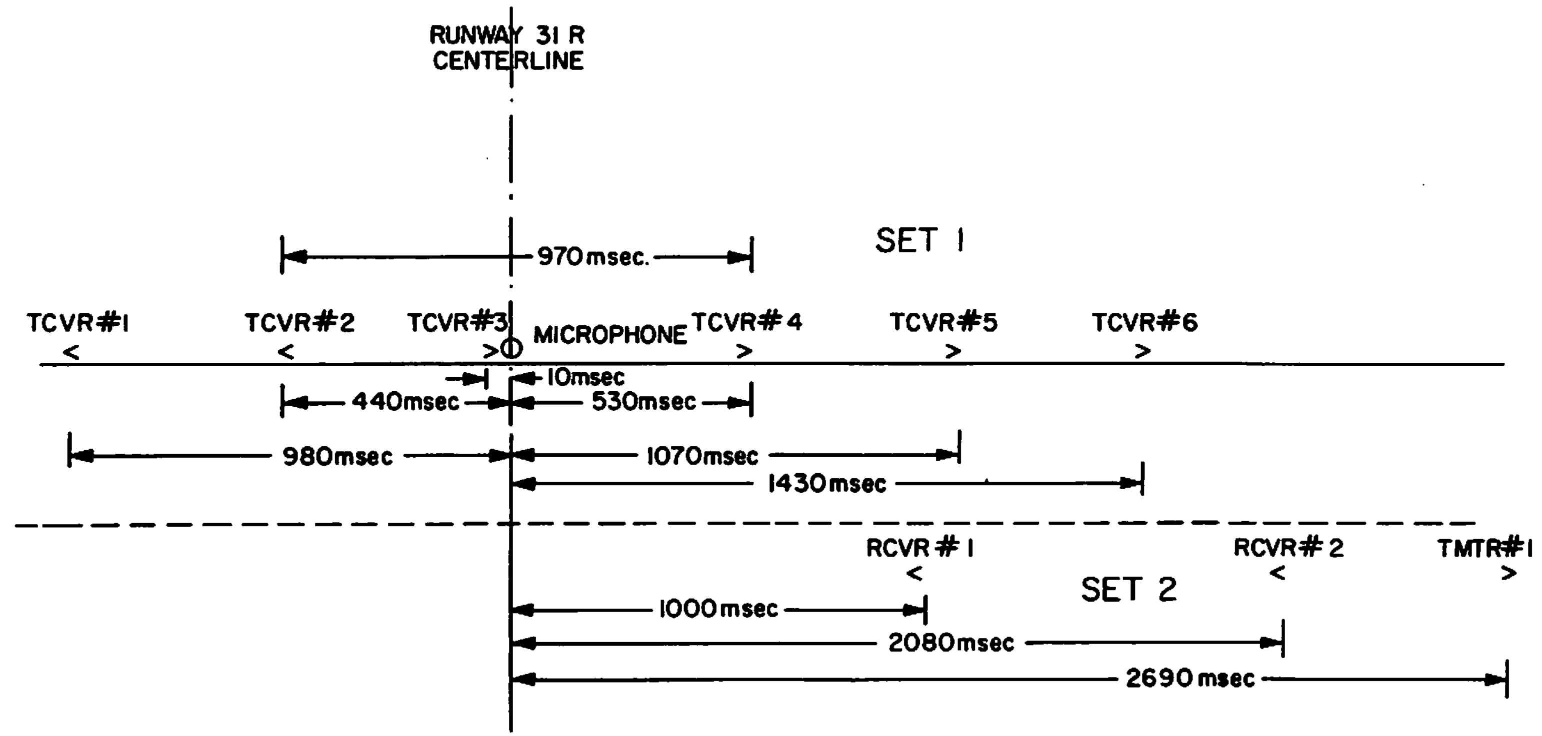

Figure 17. Sensor Positions for the Original Test Plan at Kennedy Airport. T=360 msec; τ_m=110 msec.; B=70 msec; T_1=970 msec; T_2=540 msec; m=5; n=2; q=1; p=1.
Note: All distances are normalized to c(the speed of sound)=1

TABLE 3. TRANSCEIVER USAGE DURING INITIAL TESTS AT KENNEDY AIRPORT

DATE	TCVR#1	TCVR#2	CENTER MIC.	TCVR#3	TCVR#4	TCVR#5	TCVR#6	RUNNING TIME	NUMBER OF AIRCRAFT OBSERVED
11/30/71	✓	✓	✓		✓		✓	14:55-16:21	32
12/1/71	✓	✓	✓		✓		✓	9:44-20:48	127
12/1/71	✓	✓	✓		✓	✓		12:34-17:43	106
1/3/72	✓	✓	✓		✓	✓		12:22-15:26	31
1/3/72	✓	✓	✓	✓	✓	✓		15:37-16:22	25

The initial tests were thus not very successful, since the vortices drifted downward fairly quickly to their equilibrium level relatively close to the ground. Also, the winds were fairly high (15-25KTS) during these tests (and probably very turbulent since we tested mostly during the late morning and afternoon), and the lifetimes of the vortices were fairly short. Some of the best acoustograms obtained with this arrangement are shown in Figure 18. Because of the poor quality of the data, no vortex tracks were computed.

With sufficient equipment the Kennedy 31R site would be very useful for long range tracking, if it were practical to keep personnel there to collect data during optimum wind conditions. Unfortunately, during normal operations, runway 31R is used mostly under conditions of brisk NW winds. More efficient use of testing time can be made at NAFEC where the flight times of the aircraft can be controlled (e.g., performing tests in the early morning hours, 5:00-8:00 A.M. when winds and turbulence are usually lowest).

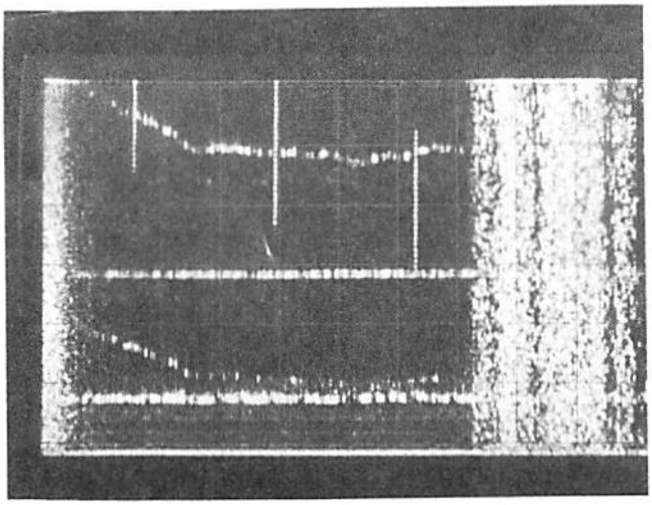

Run #35-5
B-727

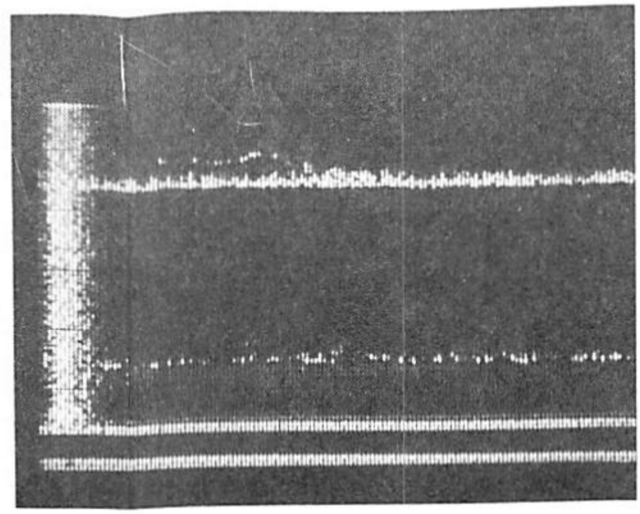

Run #37-19
B-727

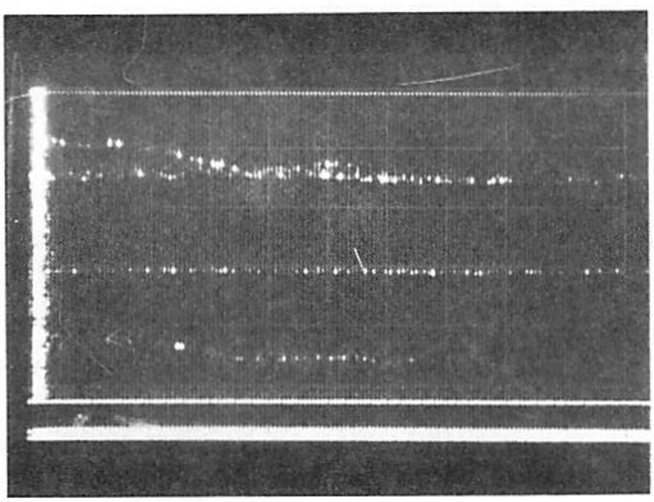

Run #38-54
B-727

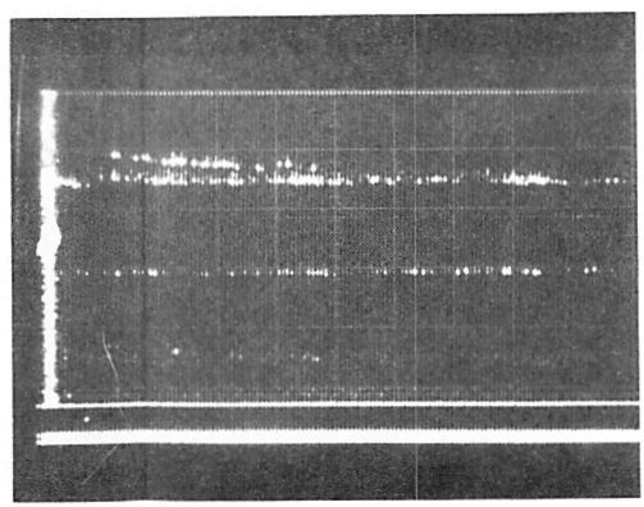

Run #39-29
B-727

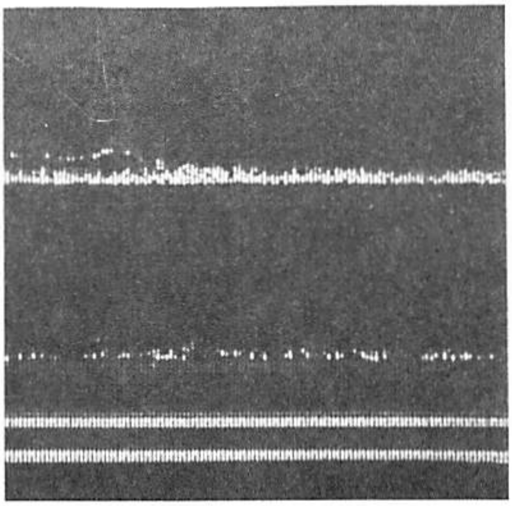

Run #37-19
B-727

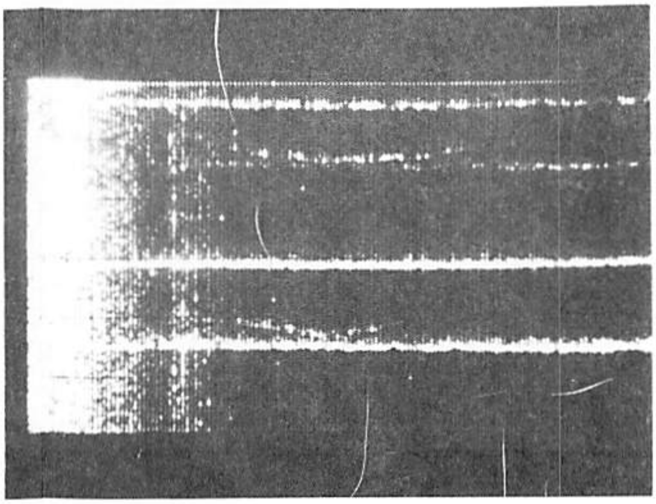

Run #38-34
B-747

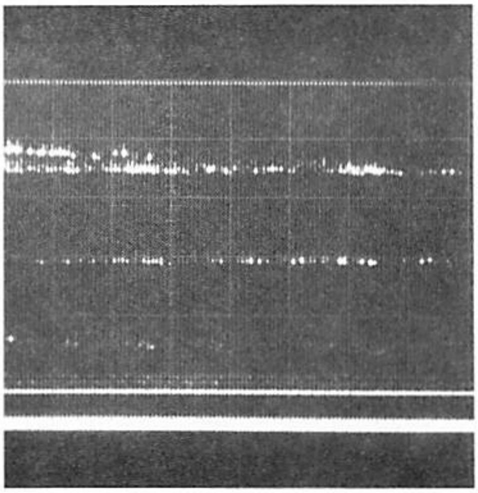

Run #39-29
B-727

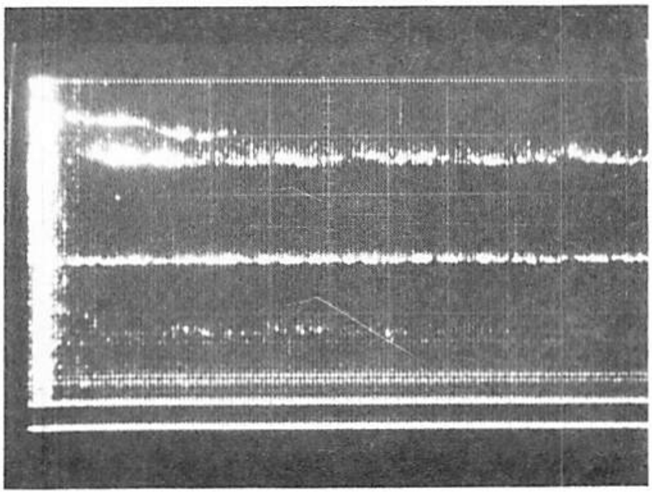

Run #39-44
B-727

Figure 18. Sample Acoustogram from the Initial Tests at Kennedy Airport

2.3.3 Second Series of Tests: Short Range Tracking

On January 5, 1972, the transceiver positions were changed to those indicated in Figure 19. The objective was to track the vortices as well as possible in the volume relatively near the runway centerline. This is an important region since a vortex which lingers there may present a hazard to following aircraft. Also, we hoped to obtain reliable tracks for the vortices as they passed over the pressure sensors so that it would be possible to compare the vortex locations indicated by each type of sensor. A good deal of redundancy in the acoustic data was obtained by placing three transceivers on either side of the runway. A photograph of the system, taken with a telephoto lens, is shown in Figure 20.

It was noticed during the first series of tests at Kennedy Airport that the altitudes of aircraft passing over the baseline were usually lower than expected. To compensate, the maximum expected time delay was reduced to τ_m = 100 msec. Also, since the amount of speaker ringing had been reduced, the value of B could be decreased to 50 msec. The integers q, p, and m (Eq. 1) were chosen as 2, 0, and 2 respectively so that a reasonable volume could be monitored.

Figure 19 shows the positions of ten transceivers. Only six of these were used in actual operation (limited by the number of channels on the tape recorder). The choice of speakers depended on the velocity of the crosswind. The three set-ups that were used are shown in Figure 21, where dotted lines indicate the general motion of the vortices. A listing of the speakers used during these tests is given in Table 4.

Vortex tracks obtained with this system are shown in Figures 22a and 23a. The sharp discontinuities in these tracks can be attributed to certain systematic errors, an example of which would be the interference of one vortex on the path of the signal from the other, as shown in Figure 24.

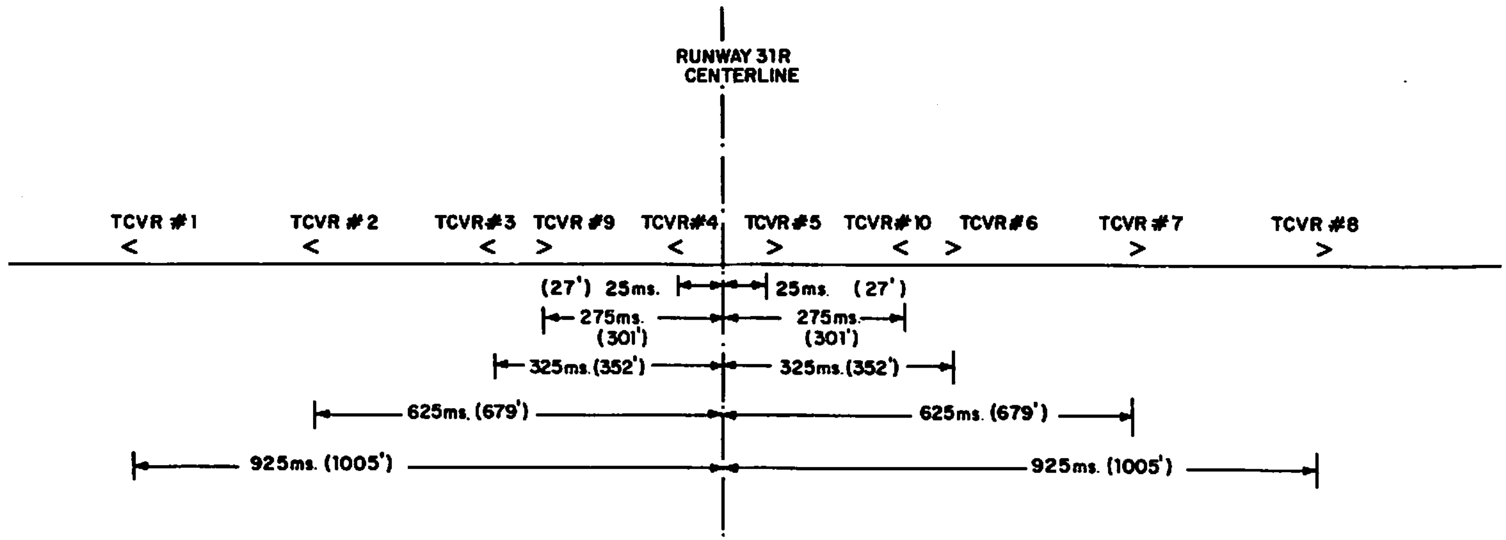

Figure 19. Transceiver Positions for the Second Series of Tests at Kennedy Airport.
T=450 msec; = 100 msec; B=50 msec; T=350 msec; T=300 msec; m=2; n=3, q=2; p=0
Note: All distances are normalized to c(the speed of sound)=1.

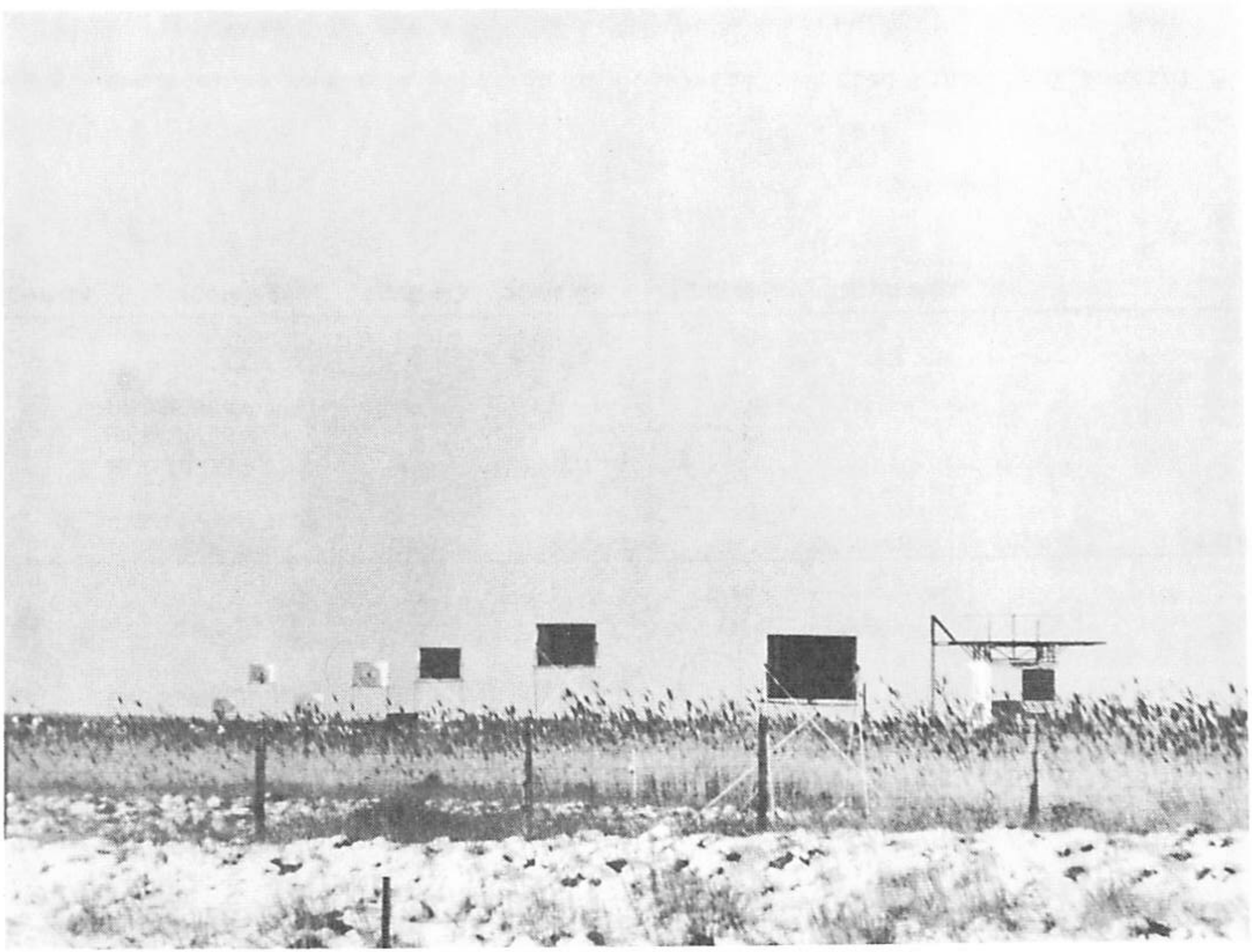

Figure 20. Sensor Positions for the Second Series of Tests at Kennedy Airport. Path of aircraft is from left to right, perpendicular to the sensor baseline. Middle Marker Building is at right.

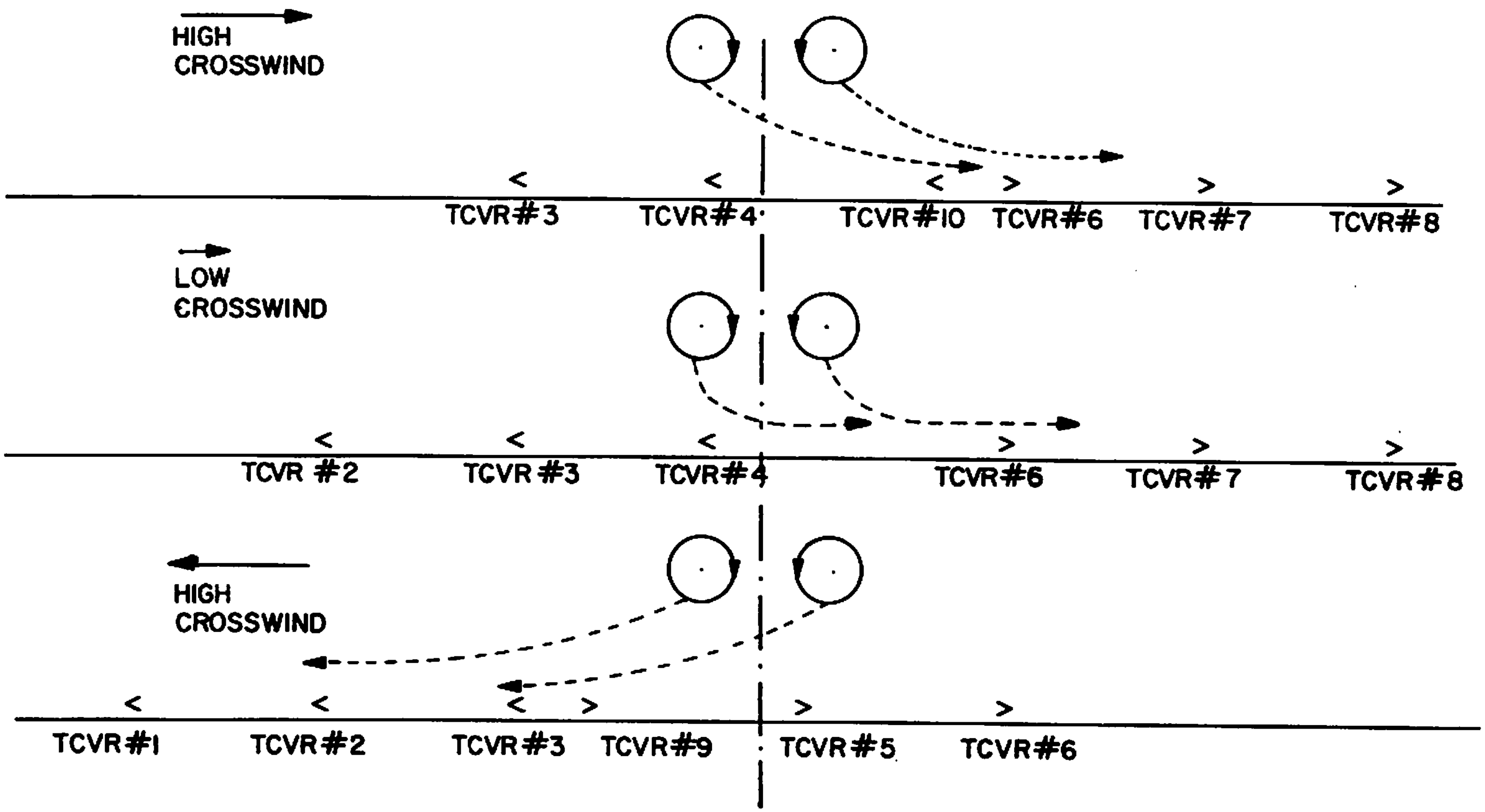

Figure 21. Transceiver use as a Function of Crosswind. Dotted Lines Show General Path of Vortices.

TABLE 4. TRANSCEIVER USAGE DURING THE SECOND SERIES OF TESTS AT KENNEDY AIRPORT

DATE	RUNNING TIME	NO. OF RUNS	TCVR #1	TCVR #2	TCVR #3	TCVR #4	TCVR #5	TCVR #6	TCVR #7	TCVR #8	TCVR #9	TCVR #10
1/4/72	14:43-21:00	138		✓	✓	✓		✓	✓	✓		
2/8/72	11:42-12:06	6		✓	✓	✓		✓	✓	✓		
2/8/72	12:10-16:54	67	✓	✓	✓		✓	✓	✓			
2/8/72	16:55-20:09	70	✓	✓	✓		✓	✓			✓	
2/8/72	20:11-21:17	22	✓	✓	✓		✓	✓	✓			
2/9/72	9:24-10:26	12	✓	✓	✓		✓	✓	✓			
2/9/72	10:30-11:42	9		✓	✓	✓		✓	✓	✓		
2/9/72	11:49-13:10	16	✓	✓	✓		✓	✓	✓			
2/9/72	13:13-15:15	34	✓	✓	✓		✓	✓			✓	
2/9/72	15:18-15:27	4	✓	✓	✓		✓	✓	✓			
2/9/72	15:33 15:54	8		✓	✓	✓		✓	✓	✓		
2/10/72	20:53-21:15	10		✓	✓	✓		✓	✓	✓		
2/10/72	21:21-23:00	36			✓	✓		✓	✓	✓		✓
2/11/72	10:23-12:15	16			✓	✓		✓	✓	✓		✓

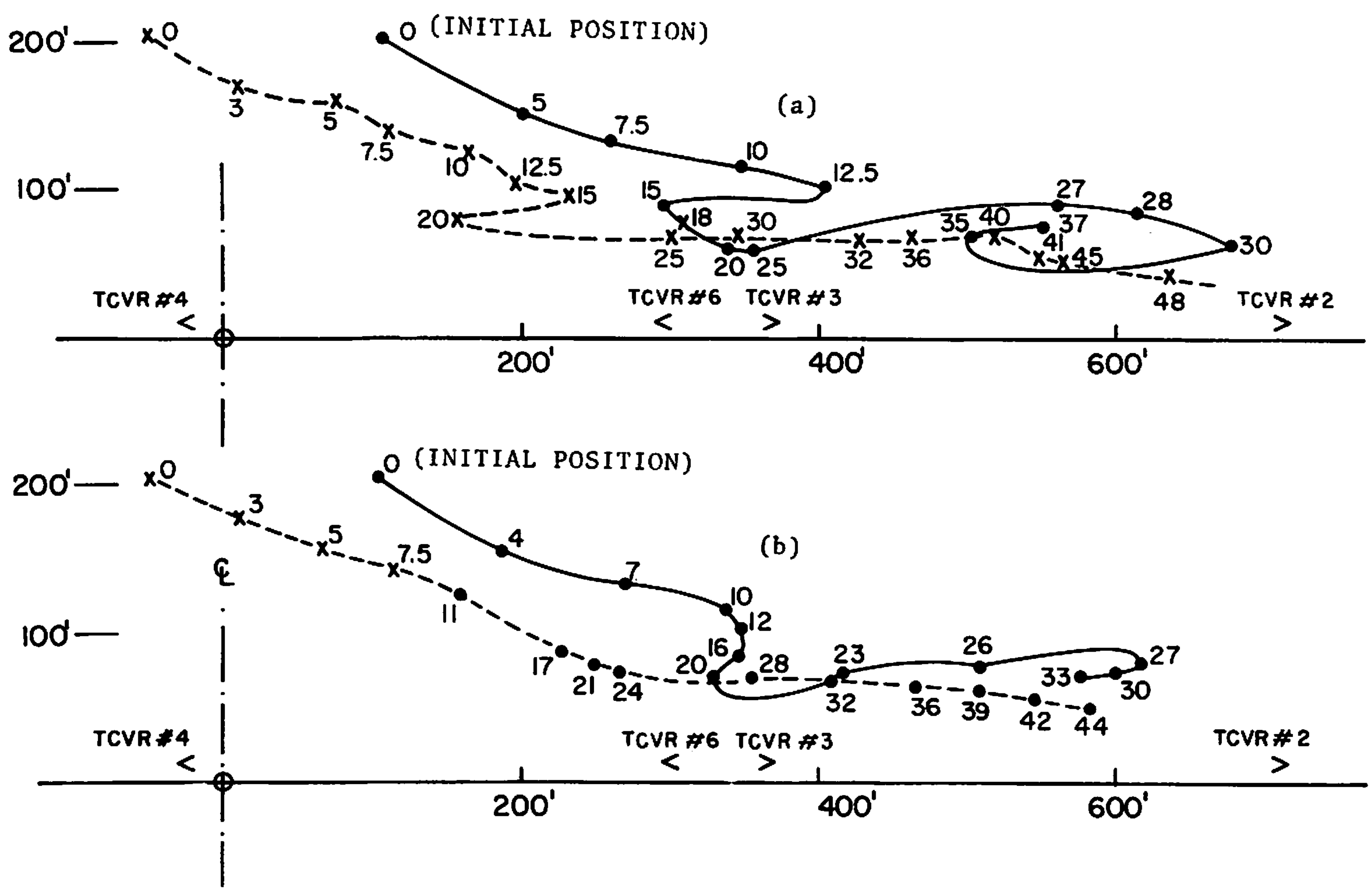

Figure 22. Vortex tracks Run#46-41; Kennedy Airport 2/9/72; B-747; Wingspan - 196' Local Time: 1429; Runway 31R; Initial position obtained by photograph of aircraft a) unaveraged data b) 3-point averaged data

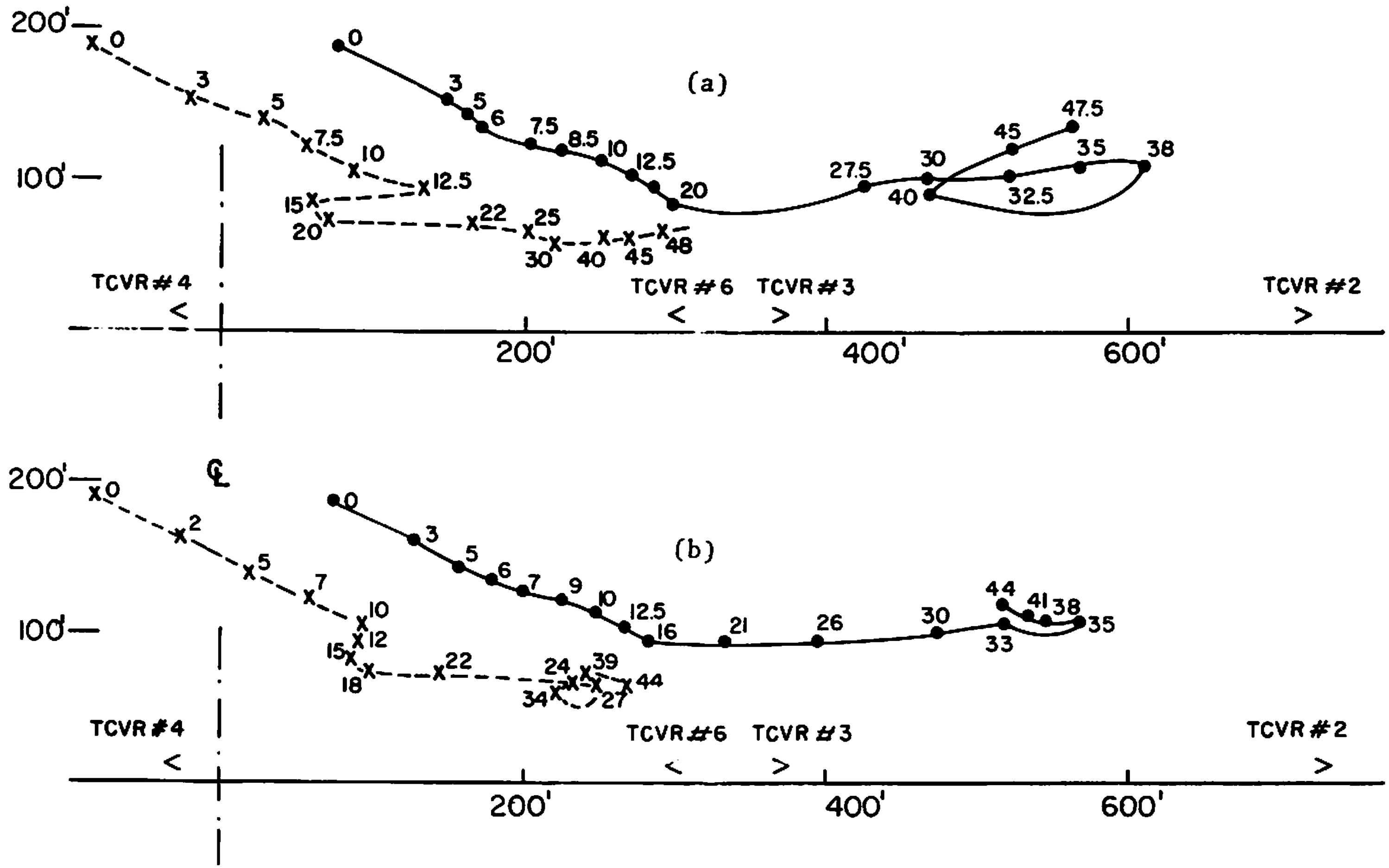

Figure 23. Vortex Tracks Run #46-46; Kennedy Airport 2/9/72; B-747: Wingspan - 196' Local Time: 1451; Runway 31R. Initial position obtained by photograph of aircraft
a) unaveraged data
b) 3-point averaged data

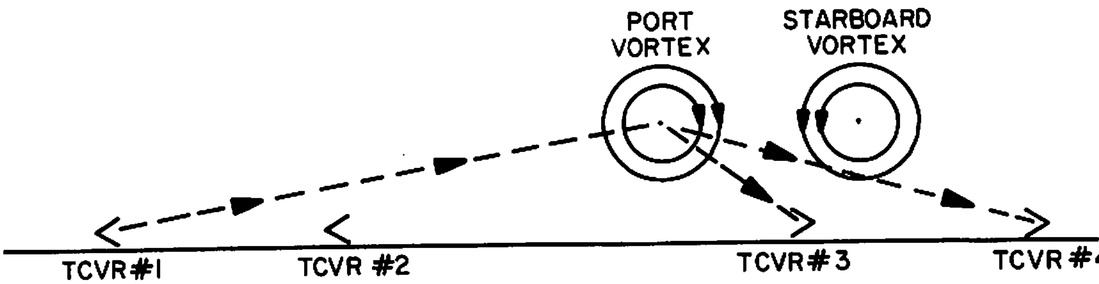

Figure 24. Example of Vortex Interference. The starboard vortex influences the signal from the port vortex to transceiver #4 much more than to transceiver #3.

As can be seen from the observed time delayed signals of Tables 5, 6,7, and 8, these discontinuities occur whenever the time delays from a different set of speakers are added to the position calculations. These systematic errors are reduced somewhat by using the average of three consecutive data points as shown in Figures 22b and 23b.

A judicious choice of speakers can also help to reduce this systematic error. Suppose the vortices are positioned as shown in Figure 24, and the time delayed pulses transmitted by TCVRS #1 and 2 are both observed in TCVRS #3 and 4. There is then the possibility of four independent calculations of the position of the port vortex. Since the starboard vortex can interfere with the time delayed signals received in TCVR #4, the position of the port vortex may best be calculated using TCVRS #1 and 2 as transmitters and TCVR #3 as a receiver. While the starboard vortex does not interfere with these signals, the redundancy of the system is lost. On the other hand, the first order interference effects caused by the other vortex are well understood in theory and could be included in a more comprehensive data analysis program.

A variety of aircraft types was observed during these tests. The numbers of each are listed in Table 9. It should be noted that the pulsed acoustic radar has significantly different sensitivity to vortices generated by different aircraft (see Report No. DOT-TSC-FAA-72-2, p.9). Since the sensor depends upon the deflection of an acoustic ray by the vortex core, it is sensitive to the type of core. In fact, the maximum scattering angle θ_m can be shown

TABLE 5. RUN #46-41 UPWIND VORTEX

Observed Time-Delayed Signals (in msec)

Elapsed Time (sec.)	3,6*	2,6	1,6	3,5	2,5	1,5	3,4	2,4	1,4
0									
3				64	49	43.5			
5				59	41	36			
7.5				48	31.3	27			
10				41.5	24	20			
12.5				34	17	14.5			
15				32	14.5	11			
18				33	10.3	5			
20					9	4		20.5	17.3
25					7.3			14	9
30					6.5			11.5	7.5
32					7			11.5	6.8
36		21	15					10	
40		15	10					9	
41		13.3	8					8.5	
45		10.8						8	
48		9.3						8	

*The notation m,n implies a time delayed signal received in speaker #m which was transmitted by speaker #n.

TABLE 6. RUN #46-41 DOWNWIND VORTEX

Observed Time-Delayed Signals (in msec)

Elapsed Time (sec.)	6,3	6,2	6,1	5,3	5,2	5,1	4,3	4,2	4,1
5					35.5	29		60	
7.5					28	21		44	36
10					22.5	16		32	24
12.5					18	10.5		22.5	17.5
15				39	16	8		20	12
20		42	30	33	13.5			15.5	6
25		38	18	36.5	18			19.5	
27		40	17		21			22	
28		42	16					26	
30			14					33	2.5
35			15						8
37			16.5						10

TABLE 7. RUN #46-46 UPWIND VORTEX

Observed Time-Delayed Signals (in msec)

Elapsed Time (sec.)	3,6	2,6	1,6	3,5	2,5	1,5	3,4	2,4	1,4
3				56	45	41			
5				46.5	35	32			
7.5				35.5	26	23.5			
10				29	20	18.8			
12.5				23.3	15	14			
15				20	13	11	43		
20				16.5	9.5	7.5	32		
22				15	9	7	27	18	16
25				11.5			18		
28				9.5			16.5		
30				9			16.5		
35				9.5			16		
40				14			19		
45				16.5			22		
48							26	11	

TABLE 8. RUN #46-46 DOWNWIND VORTEX

Observed Time-Delayed Signals (in msec)

Elapsed Time (sec.)	6,3	6,2	6,1	5,3	5,2	5,1	4,3	4,2	4,1
3				53	42	38			
5				43.5	32	29			
6				32.5	23	20.5			
7.5				26	17	15.8			
8.5				20.3	12	11			
10				17	10	8	40		
12.5				13.5	6.5	4.5	29		
15				12	6	4	24	15	13
20				11.5	5	4	18	11	10
27.5			12	9.5			16.5	9.5	8
30				9			16.5	9	7
32.5									
35				9.5	3.5		16	9.8	8.3
38									
40				14	4.5		19	10	8.3
45				16.5	5		22	10.5	8.3
47.5					6.5		26	11	

to be proportional to the maximum circulation divided by the core radius. According to the observed scattering angles, we can define two types of vortices:

1. The "tight core" vortex where very high velocities are found in a relatively small core. Our system is very sensitive to this type.

2. The "soft core" vortex where the velocities are more spread out in a larger core. Our system is less sensitive to this type.

A subjective analysis of a large number of acoustograms leads to the conclusion that the former type of vortex is produced by three types of aircraft in *landing configuration:*

1. "clean wing" types with no wing mounted engines (viz. B-727, DC-9, BAC-111, VC-10, etc.).

2. Aircraft with wing mounted engines located relatively near the fuselage. e.g., B-737, DC-10.

3. Propeller driven aircraft (e.g., DC-7, Electra, C-130, P3V).

Aircraft which appear to produce the "soft core" vortex are the "dirty wing" variety (i.e., at least one engine mounted relatively far out on the wing, e.g., B-707, DC-8). Although the B-747 has wing-mounted engines, the maximum scattering angles observed from its vortices are only slightly smaller than those from "tight core" vortices. It should also be pointed out that the data indicate that the maximum observed scattering angles are larger for the DC-8 than for the B-707.

To illustrate the sensitivity of the acoustic sensor system to the vortices from these various aircraft, sample acoustograms obtained from tests on three different days are presented in Figures 25 to 39. Most figures represent an arbitrary choice of nine runs for the day and for the type of aircraft indicated. For comparison purposes transceiver #4 or #5 was used to monitor the downwind vortex in each case. The general wind velocity can be obtained from the Kennedy Summary (Table 9). The consistency of the acoustograms obtained for the same type of aircraft should be noted.

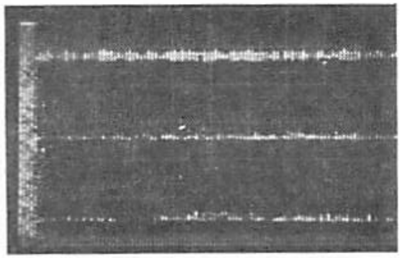

43-7

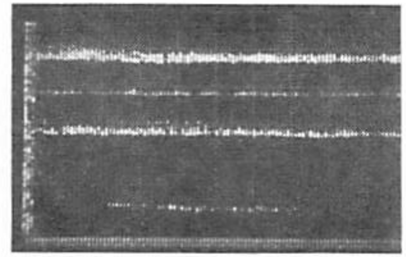

43-34

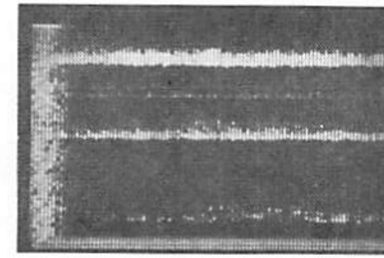

43-51

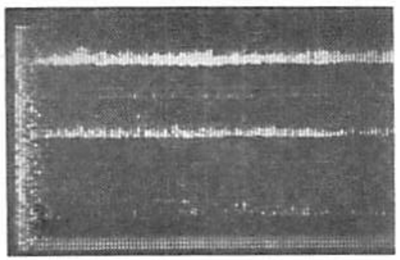

44-11

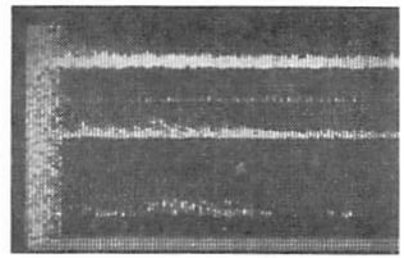

44-26

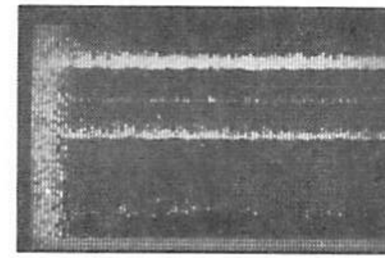

44-29

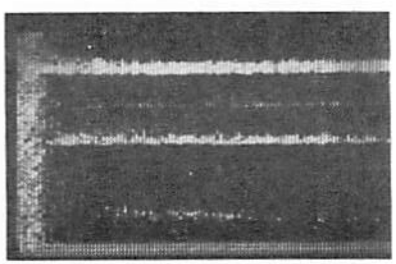

44-32

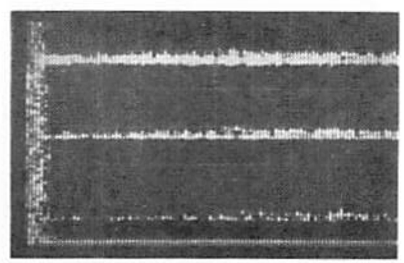

45-14

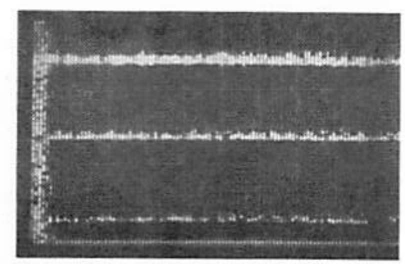

45-21

Figure 25. B-707 Acoustograms
2/8/72 Transceiver #5

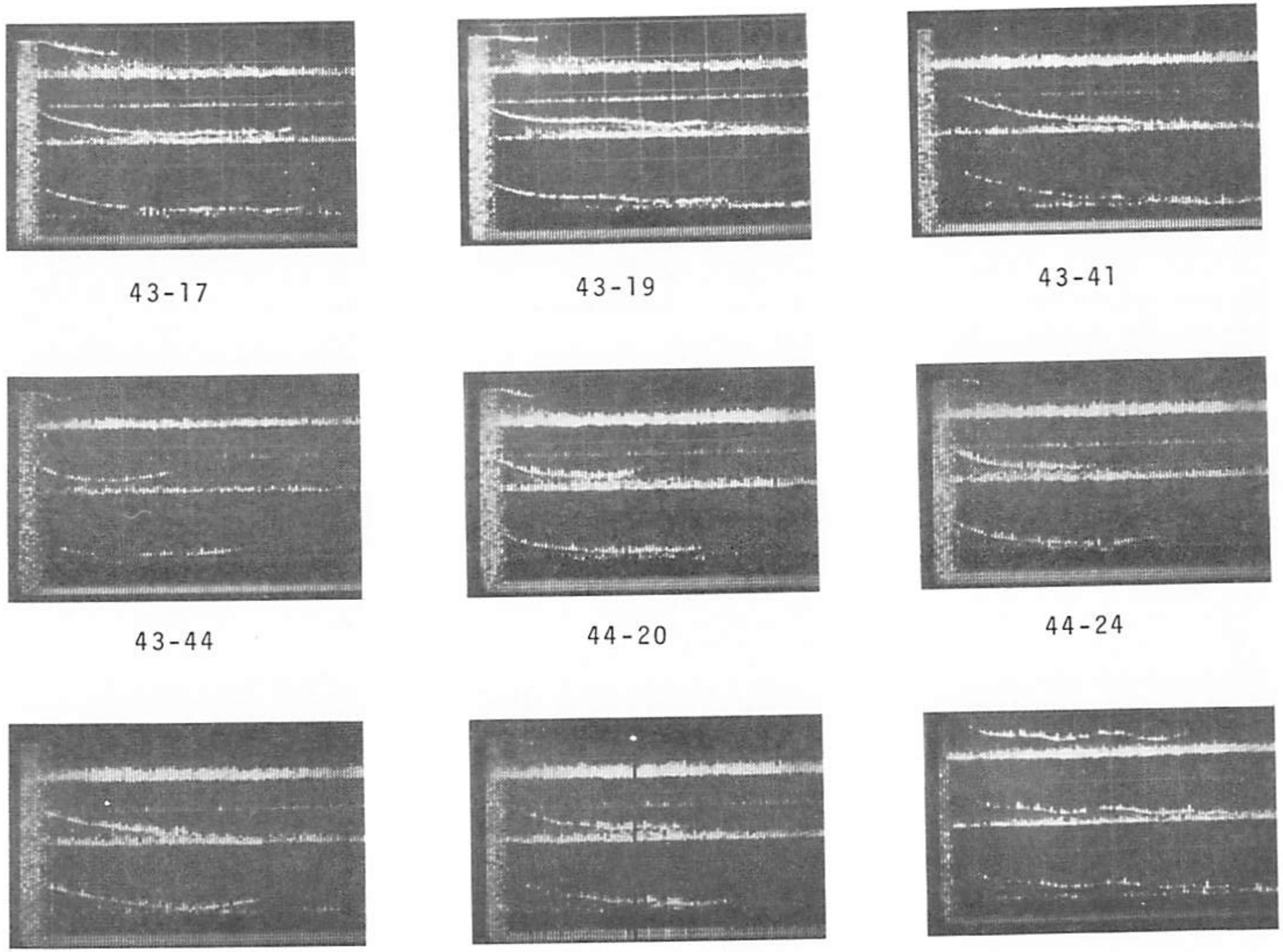

43-17 43-19 43-41

43-44 44-20 44-24

44-31 44-37 45-3

Figure 26. B-727 Acoustograms
2/8/72 Transceiver #5

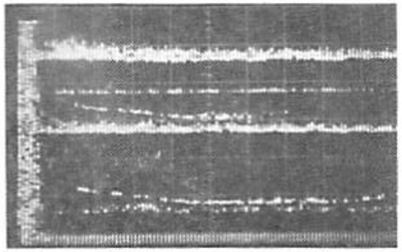

43-11

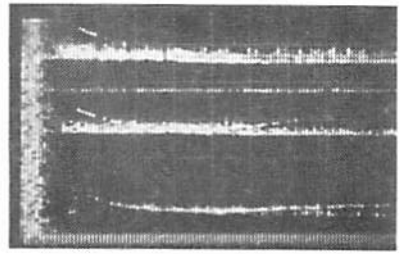

43-20

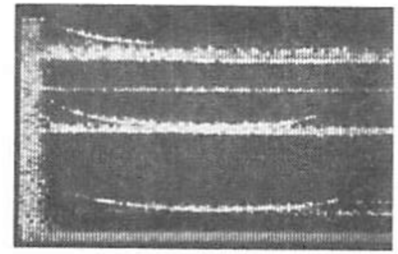

43-30

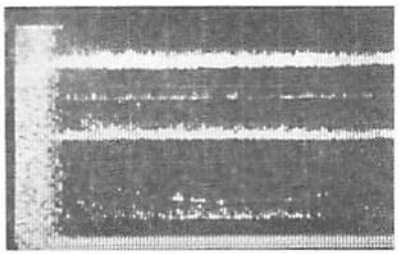

43-49

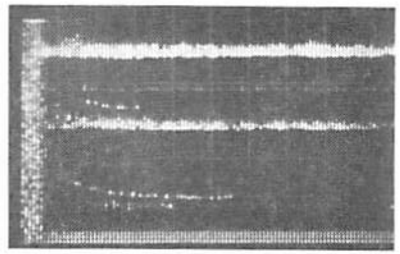

44-7

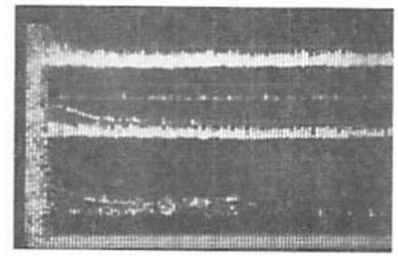

44-22

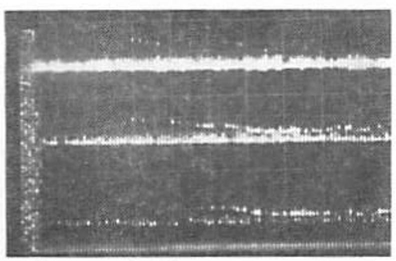

45-6

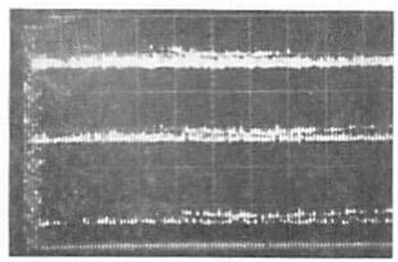

45-19

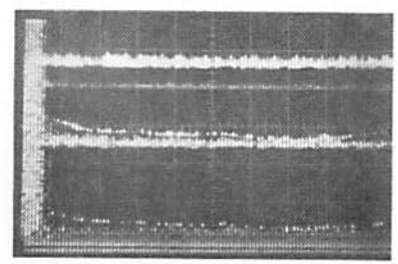

45-25

Figure 27. B-747 Acoustograms
2/8/72 Transceiver #5

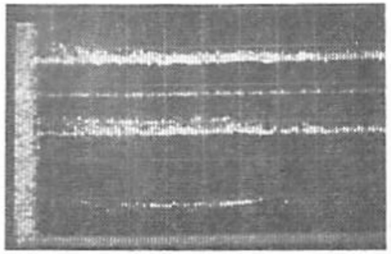

43-14

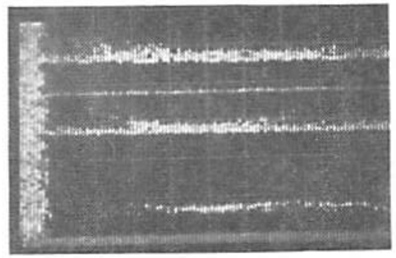

43-16

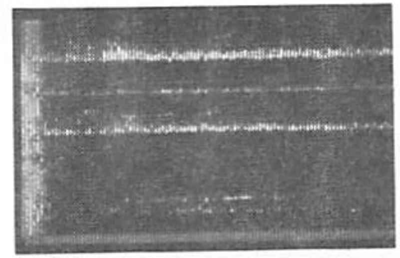

43-28

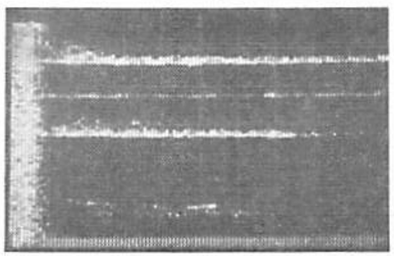

43-32

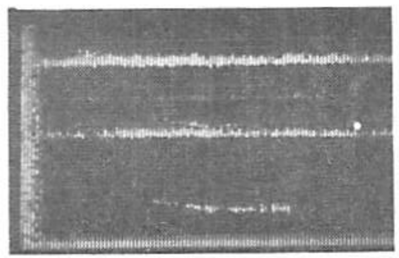

43-45

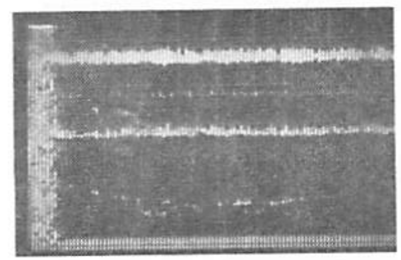

43-55

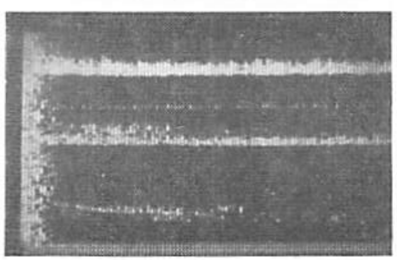

44-36

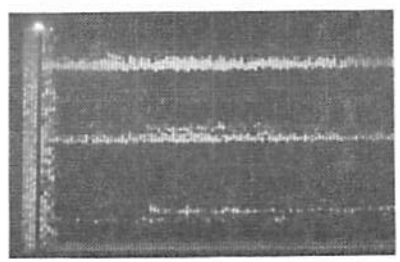

44-71

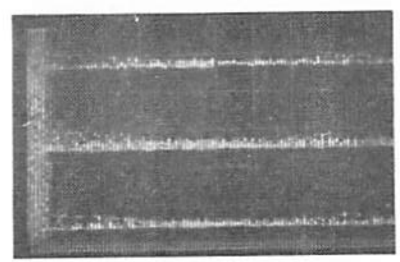

45-28

Figure 28. DC-8 Acoustograms
2/8/72 Transceiver #5

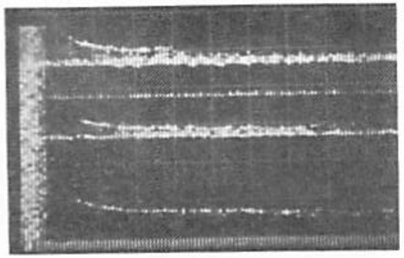

43-12

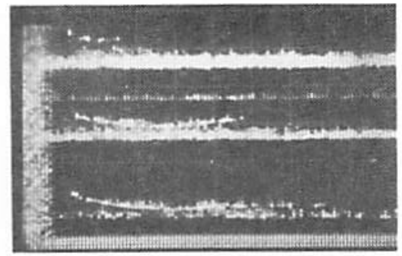

43-48

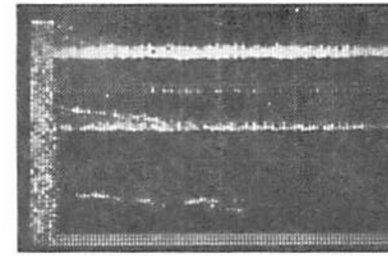

44-8

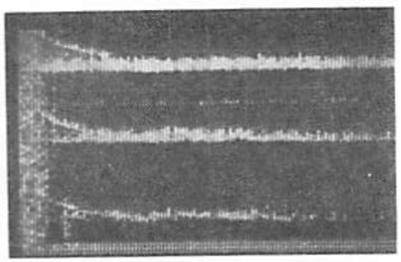

44-49

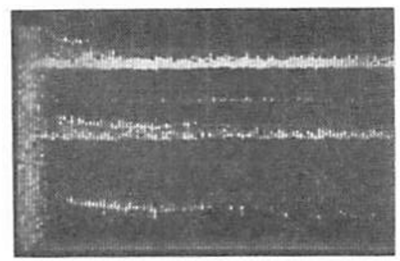

44-58

DC-9

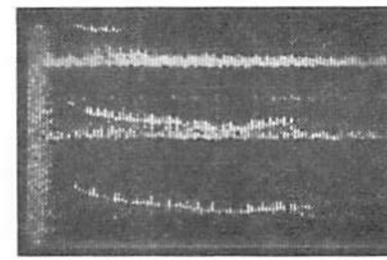

44-70

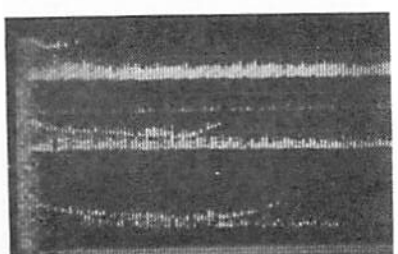

44-39

DC-10

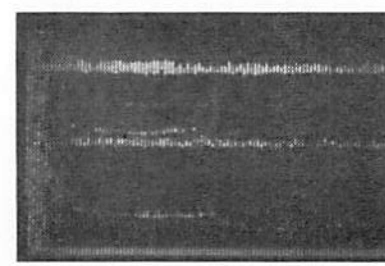

43-43

VC-10

Figure 29. DC-9,DC-10,VC-10, Acoustograms
2/8/72 Transceiver #5

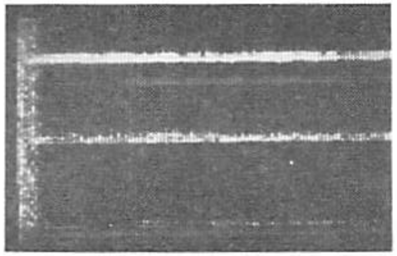

45-39

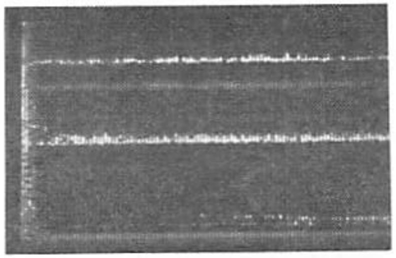

45-42

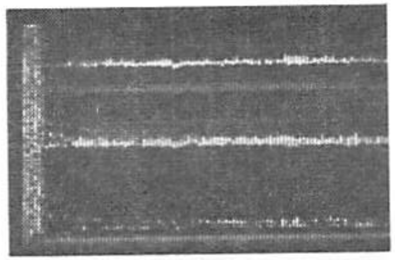

45-46

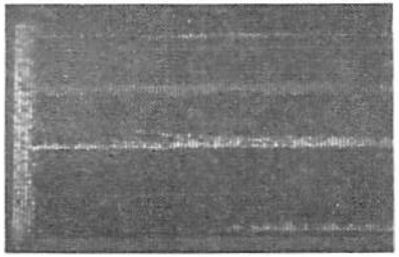

45-51

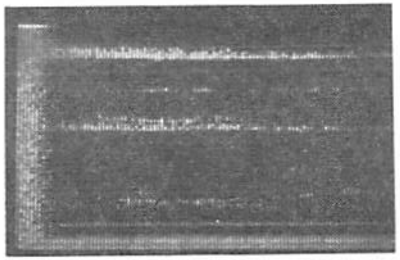

46-22

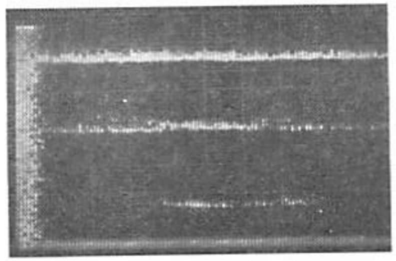

46-34

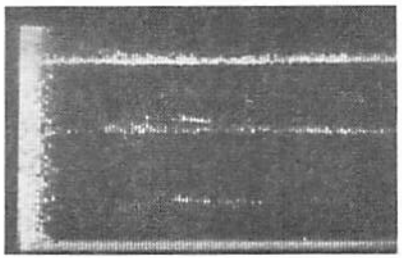

46-39

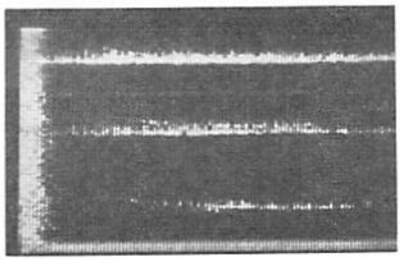

46-47

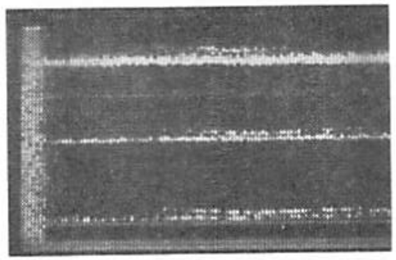

46-58

Figure 30. B-707 Acoustograms
2/9/72 Transceiver #5

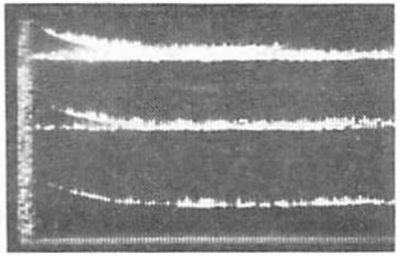

46-7

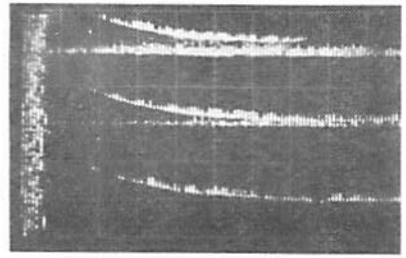

46-12

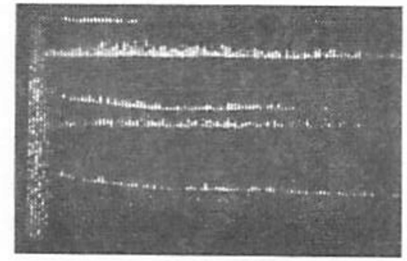

46-15

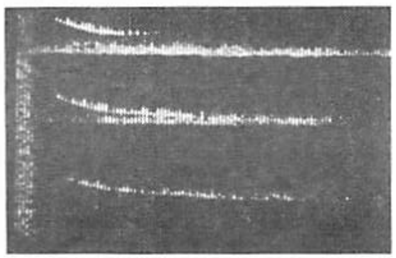

46-16

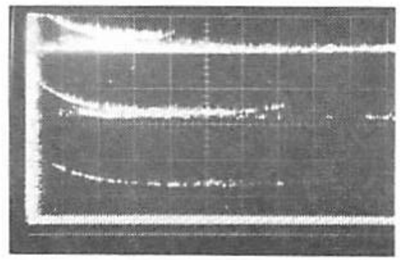

46-31

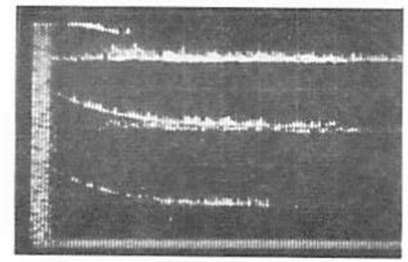

46-32

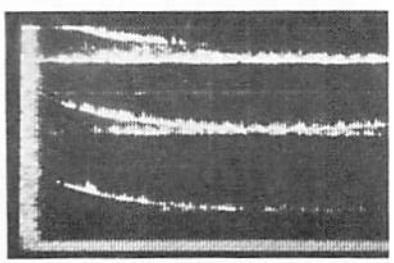

46-48

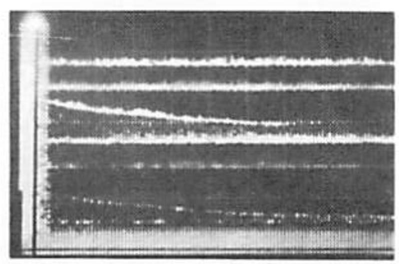

46-54

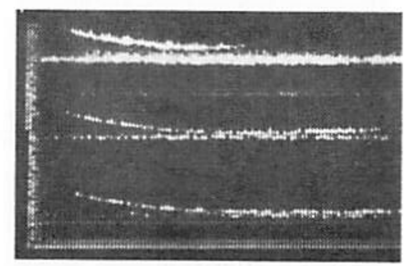

46-61

Figure 31. B-727 Acoustograms
2/9/72 Transceiver #5

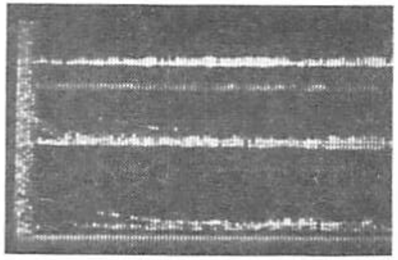

45-44

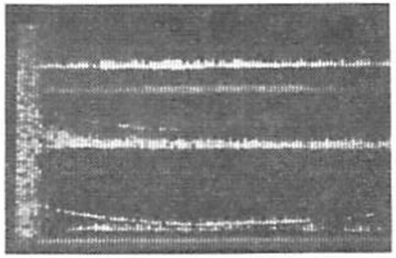

45-45

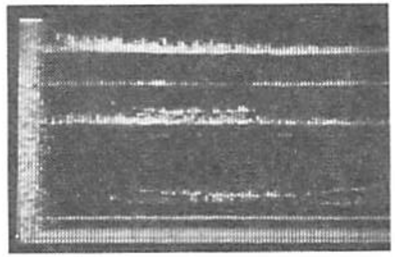

46-21

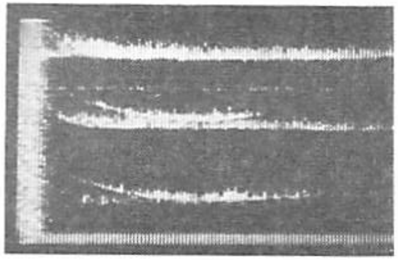

46-24

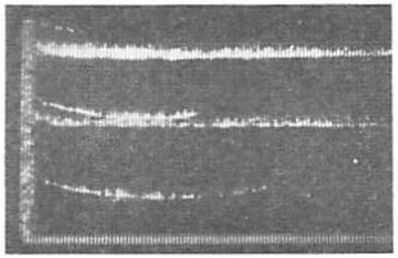

46-25

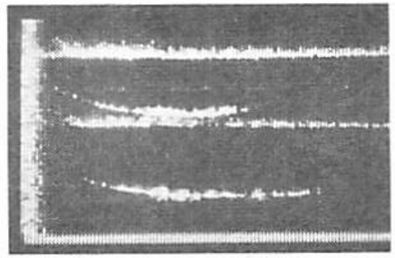

46-41

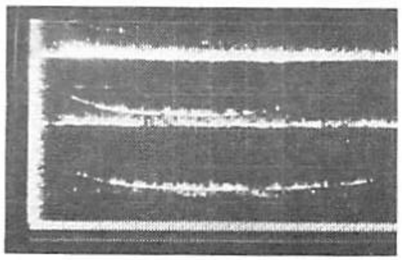

46-46

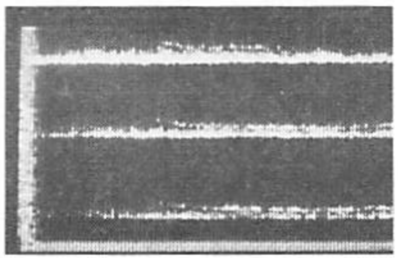

46-50

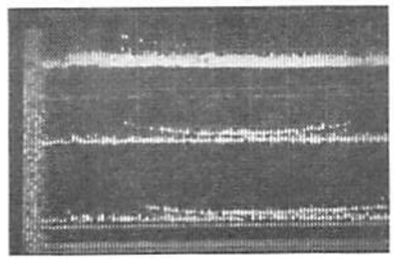

47-4

Figure 32. B-747 Acoustograms
2/9/72 Transceiver #5

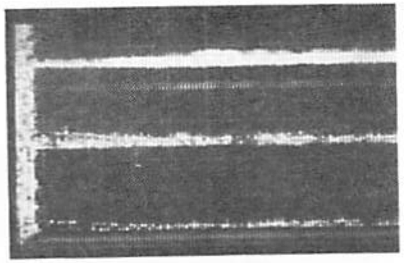

45-40

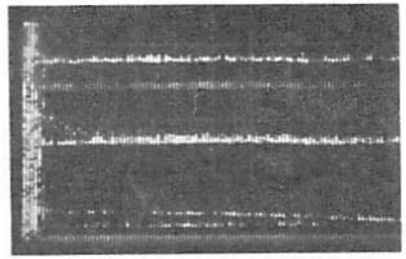

45-49

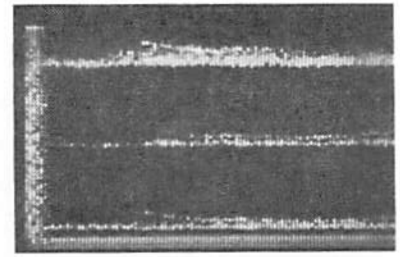

45-54

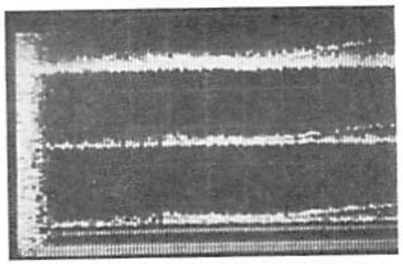

45-57

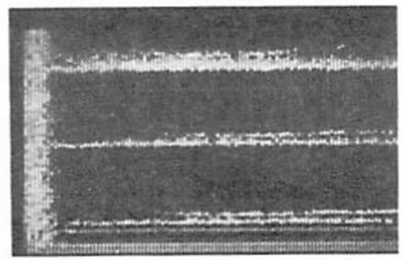

45-58

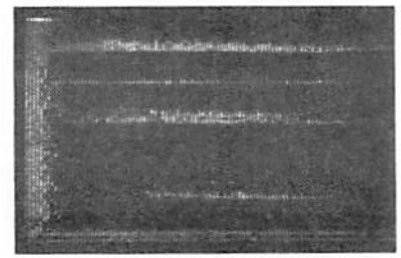

46-20

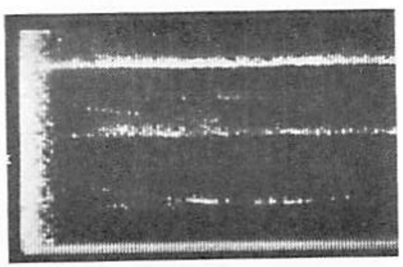

46-38

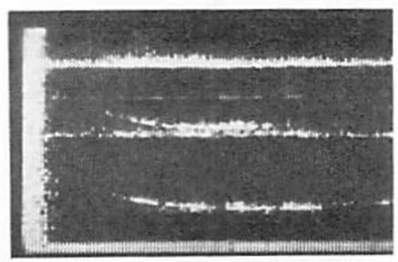

46-45

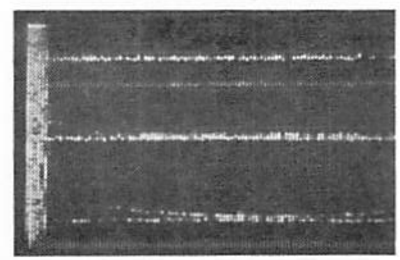

46-56

Figure 33. DC-8 Acoustograms
2/9/72 Transceiver #5

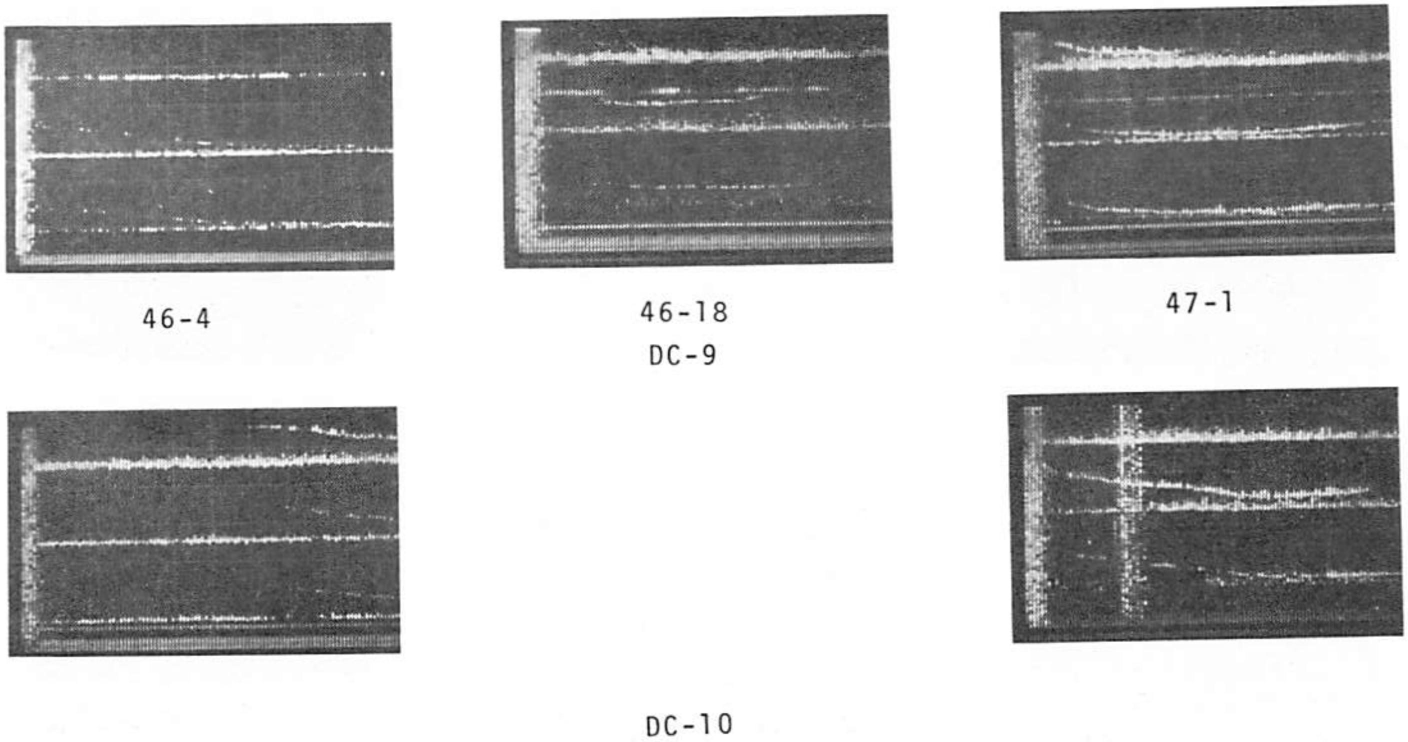

Figure 34. DC-9, DC-10 Acoustograms
2/9/72 Transceiver #5

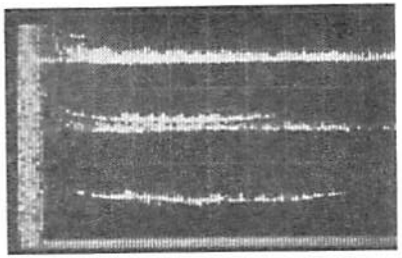

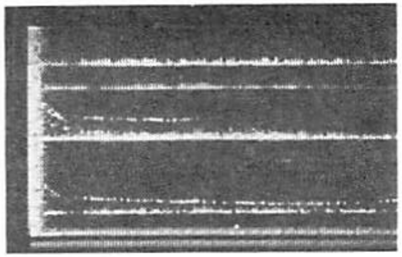

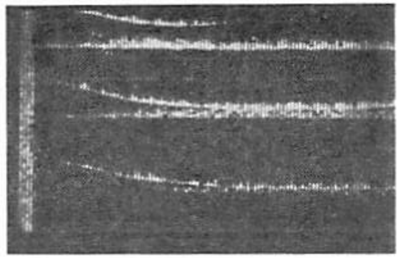

46-35 — VC-10 — 46-55

46-11
C-130

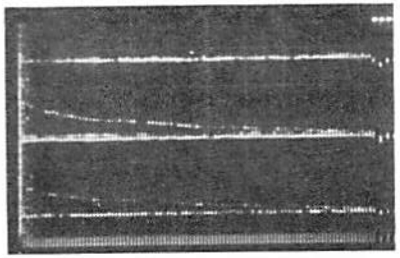

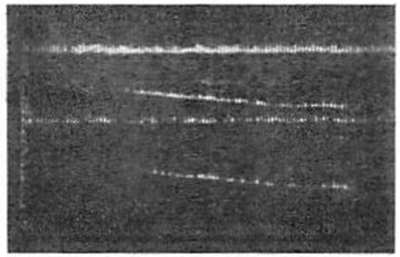

46-3
BUSINESS JET

46-13
DEHAVILLAND

Figure 35. VC-10, Business Jet, DeHavilland Acoustograms
2/9/72 Transceiver #5

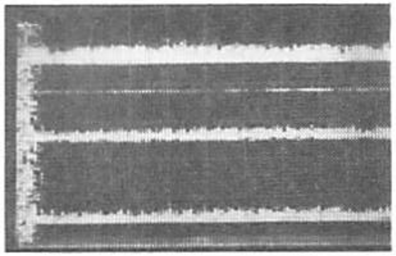

47-6

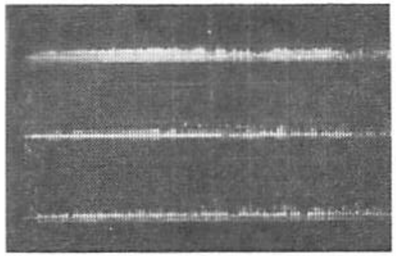

47-14

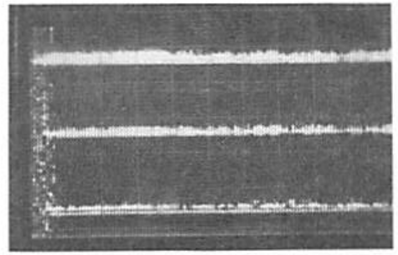

47-27

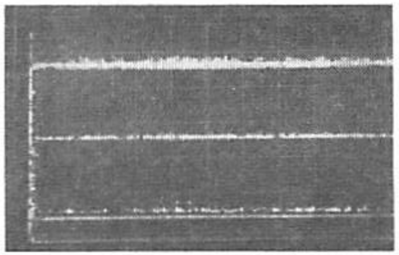

47-34

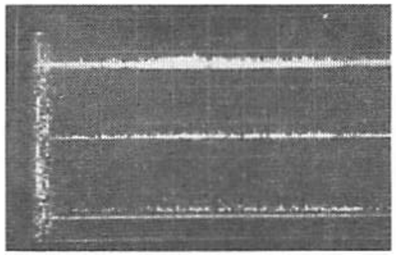

47-36

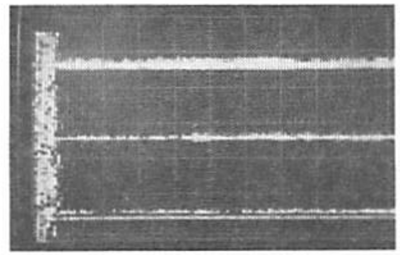

47-42

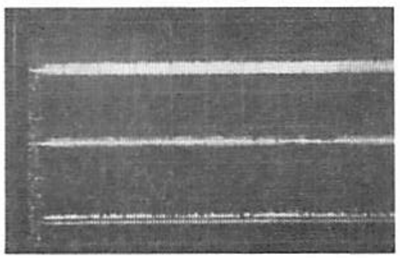

47-45

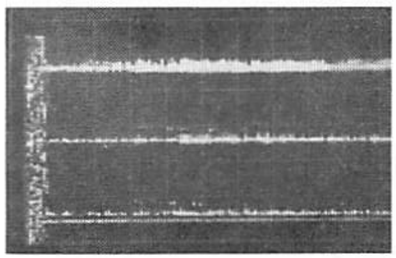

47-49

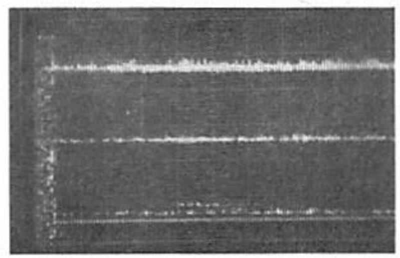

47-50

Figure 36. B-707 Acoustograms
2/10/72 Transceiver #4

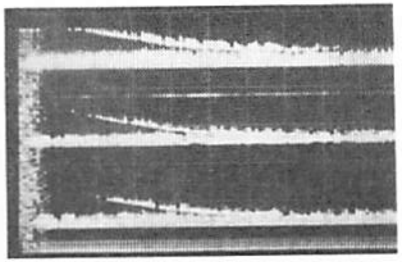

47-9

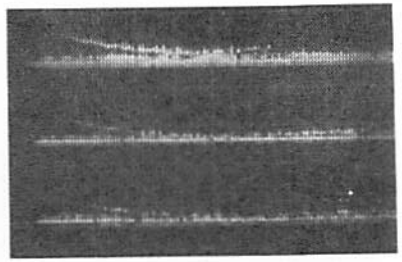

47-13

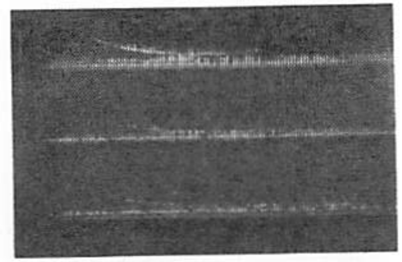

47-17

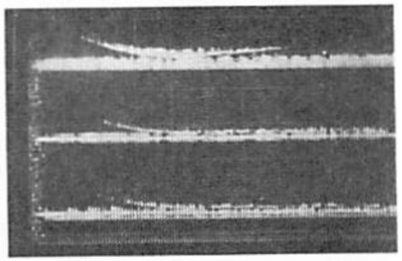

47-21

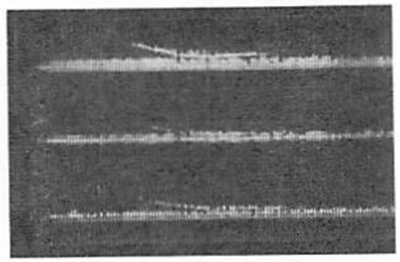

47-23

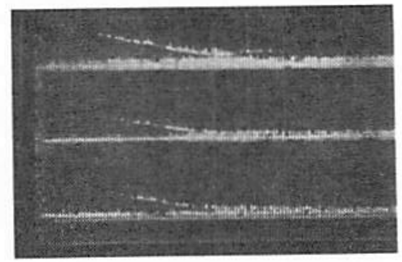

47-26

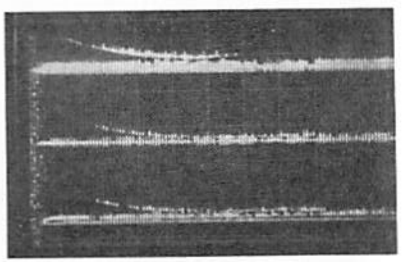

47-30

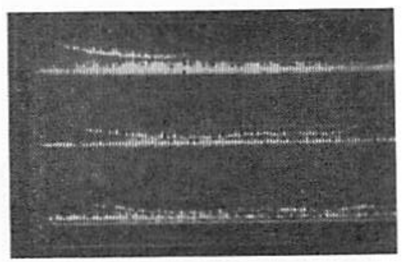

47-33

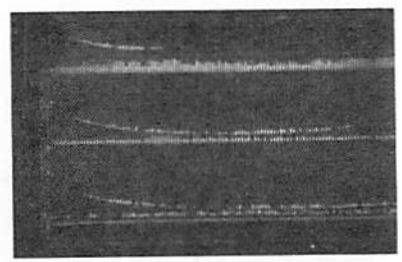

47-37

Figure 37. B-727 Acoustograms
2/10/72 Transceiver #4

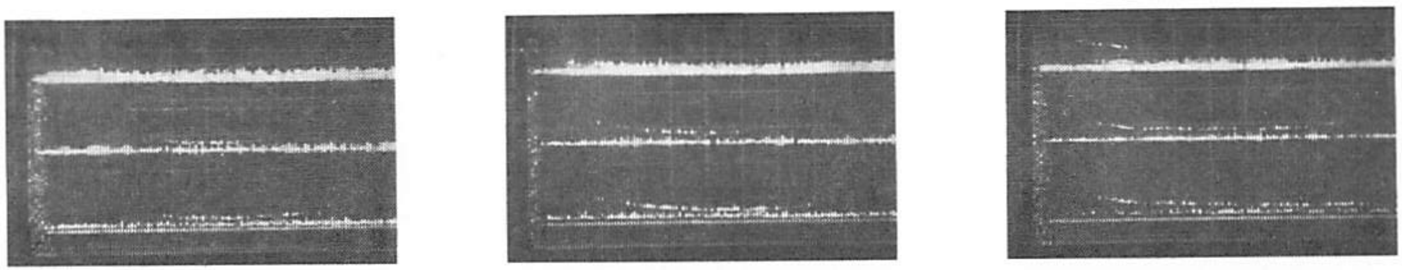

47-28 47-32 47-40

B-747 DC-9

Figure 38. B-747 Acoustograms
2/10/72 Transceiver #4

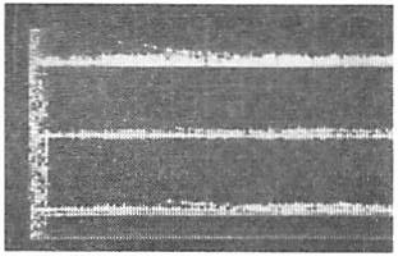

47-19

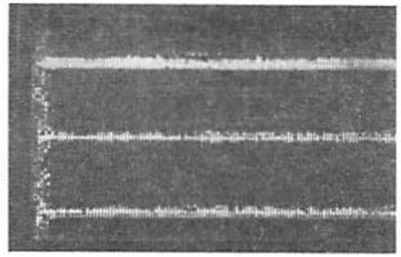

47-22

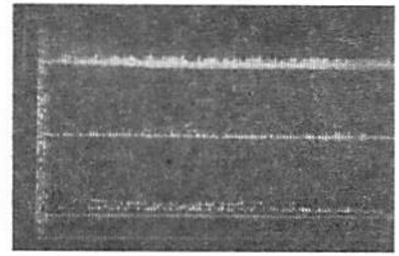

47-35

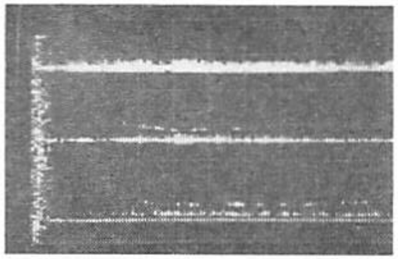

47-38

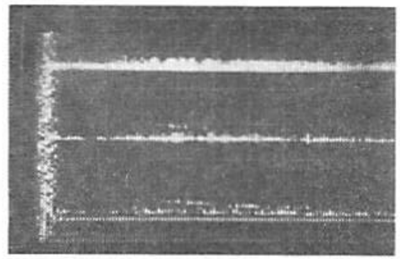

47-39

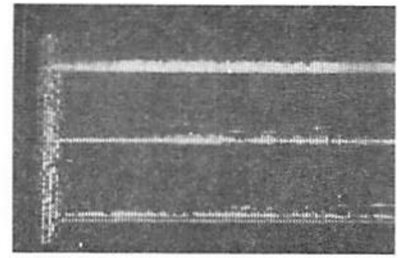

47-44

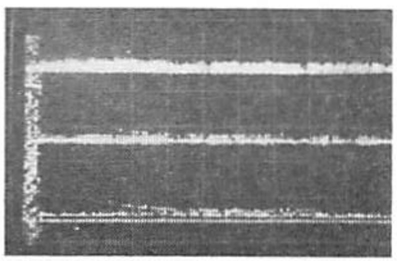

47-46

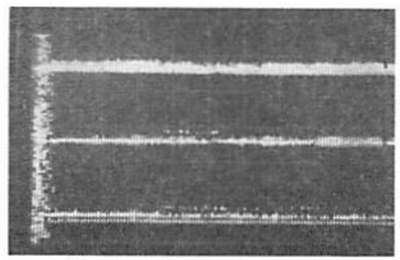

47-47

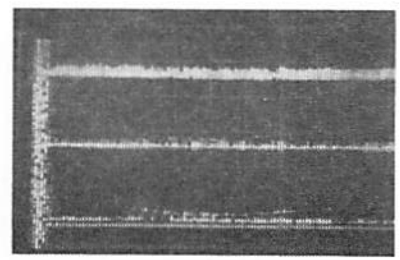

47-48

Figure 39. DC-8 Acoustograms
2/10/72 Transceiver #4

TABLE 9. KENNEDY TEST SUMMARY

DATE	RUNNING TIME	GENERAL WIND CONDITIONS	TYPES OF AIRCRAFT OBSERVED							
			DC-8	BAC-111 DC-9	727	DC-10	B-707	B-747	VC-10	OTHER
11/30/71	1430-1621	320°-340° @ 20-30KTS	4	2	4	0	13	4	1	1
12/1/71	944-2048	330°-360° @ 15-20KTS	23	10	26	0	47	25	2	0
12/16/71	1234-1743	280°-300° @ 15-22KTS	24	8	22	1	33	22	2	1
1/3/72	1222-1622	270°-280° @ 10-12KTS	4	4	12	2	22	12	1	2
1/5/72	1443-2100	340°-010° @ 10-12KTS	20	12	29	1	42	29	2	4
2/8/72	1140-2117	260°-300° @ 15-18KTS	32	10	35	2	53	33	1	1
2/9/72	924-1554	0°-020° @ 5-6KTS 240°-310° @ 8-12KTS	18	2	19	2	28	21	2	5
2/10/72	2053-2300	320°-360° @ 8-10KTS	16	1	12	0	14	12	0	1
2/11/72	1023-1215	340°-020° @ 6-10KTS	1	3	4	1	6	4	0	1
TOTAL			142	52	163	9	258	124	11	16

3.0 PRESSURE SENSOR SYSTEM

The basic use for a pressure sensor array is to track wake vortices which have descended into ground effect. Such tracking may be necessary at airports with parallel or intersecting runways. The tests reported here were designed to determine the feasibility of tracking vortices by this method and to try to obtain some data on the distance a vortex can drift in ground effect before dissipating.

The pressure sensor tests were conducted almost exclusively at Kennedy Airport. Six differential sensors of the type shown in Figure 40 (Ball Engineering Model 100D) were deployed along the baseline (Figure 2) on posts five feet high. Nine posts were set

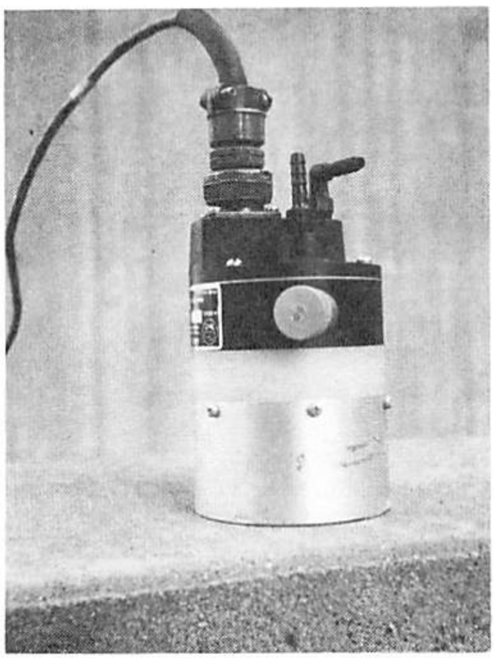

Figure 40. Ball Engineering Differential Pressure Sensor (3" Diameter)

out at the locations listed in Table 10. The sensors were placed on six of these posts, selected according to the ambient wind conditions. For most tests the six pressure sensor signals were recorded on six fm channels (0-312 Hz bandwidth at 1.75 i.p.s.) of a seven channel instrumentation tape recorder. The seventh was used to record comments and aircraft arrival time markers similar to those recorded on the acoustic radar tapes. In addition, two of the six sensor signals were recorded on a two-channel strip chart recorder for immediate observation. The pressure data tapes were subsequently played back and displayed on a multichannel (up to eight) strip chart recorder. (See Figure 47 for a sample record.)

TABLE 10. PRESSURE SENSOR POST LOCATIONS

Identification Number	Position (ft)
P7	840
P8	635
P9	420
P10	215
P11	0
P12	-220
P13	-430
P14	-635
P15	-890

3.1 HISTORICAL DEVELOPMENT

The single differential pressure sensor used in the July 1971 tests at NAFEC was a precision laboratory instrument which required complex electronics.[3] An array of pressure sensors should consist of inexpensive sensors with self-contained electronics, whose accuracy need not be better than $\pm 10\%$. For this purpose Ball Engineering Variometers, used commercially as rate of climb indicators in gliders, have proved to be generally reliable. Some problems with zero stability have been experienced, and operation under cold, wet conditions without careful waterproofing was found to be unreliable.

The sensitivity required for a pressure sensor depends upon the speed of the winds being sensed. The two are related by Bernoulli's principle,[4]

$$\Delta p = \frac{1}{2} \rho v^2,$$

where Δp is the pressure change, ρ is the air density and v is the wind speed. One can show that the ground wind produced by a vortex which has descended into ground effect is four times the free descent rate of the vortex pair (about 8 ft/sec for a B-747). Thus, the maximum velocity to be measured is at least 32 ft/sec, which corresponds to a pressure of 0.25 inches of water (at sea level, 0°C). Inadvertently, the first Ball Engineering sensors were ordered with a full scale sensitivity of $\pm$ .05 inches of water. Consequently, until the sensitivity could be reduced, external means were used to reduce the pressure applied to the sensor.

The technique adopted in the July 1971 tests was to block one orifice of the pressure sensor and measure the wind induced pressure with the other, which pointed generally in the vertical direction. Changes in atmospheric pressure required occasional unstopping of the blocked orifice to keep the sensor on scale. Sample data obtained with this scheme are shown in Figure 41. The need for pressure equalization was eliminated with the arrangement shown in Figure 42. The pressure in the reference port P responds to slow barometric pressure changes but not to rapid vortex induced pressure changes because of the time constant R_2C_2. The sensor therefore detects only the desired rapid changes in pressure at port S. The purpose of the additional capillary R_1 is to reduce the sensitivity of the sensor. Unfortunately, the response speed is also reduced because of the volume C_1 and the change in volume produced by diaphram motion in the sensor. The time constant $(R_1+R_2)C_2$ was about 40 sec and the ratio R_1/R_2 about eight.

Figure 43 shows some data taken with this arrangement. The movement of vortices across the array is evident. In some cases both vortices are detected by the second sensor P13 and are recorded as a double peak. The identification of which vortex appears in the first sensor P12 is uncertain for this sensor

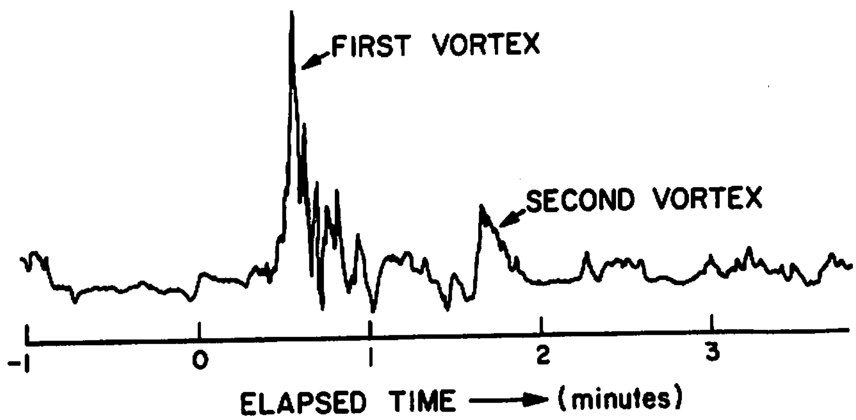

Figure 41. Pressure Data Run 12, 7/31/71, B-747. The Aircraft Arrived at Time Zero

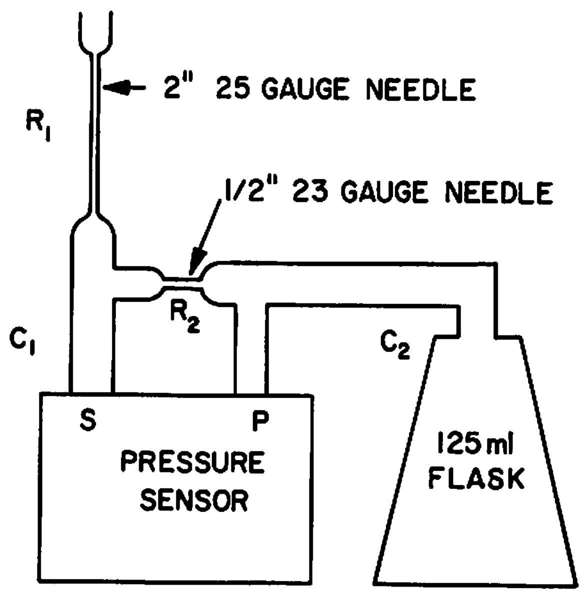

Figure 42. Pressure Sensor with Auxiliary Apparatus to Reduce Sensitivity and Eliminate Response to Barometric Changes.

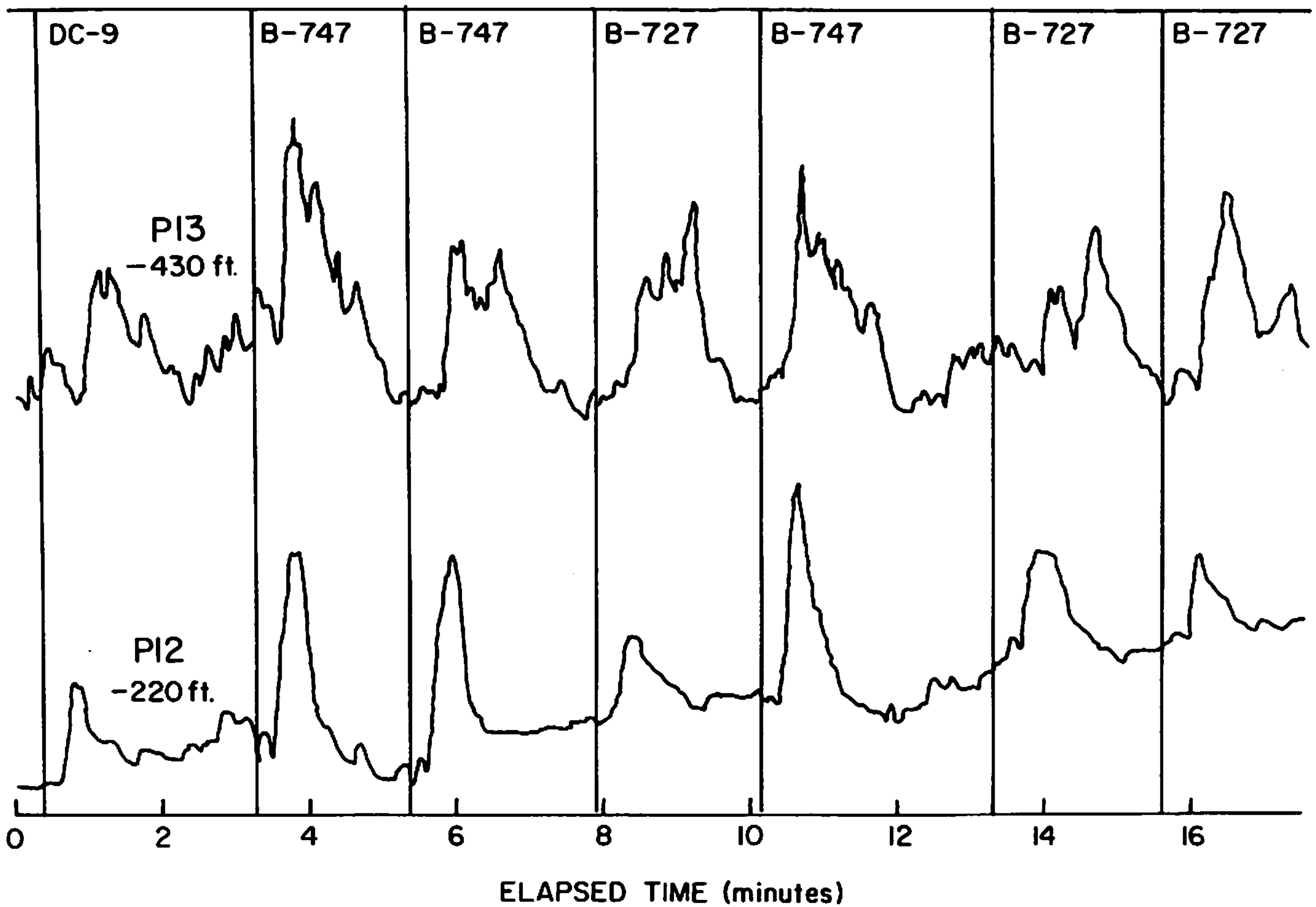

Figure 43. Pressure Data Taken on 12/16/71, 1647-1702 Local Time, Runs 39-26 Through 39-32. The measured wind at 13 ft altitude was approximately 23 mph at 300° (Magnetic). The data have been copied from the original strip charts. The vertical lines indicate the arrival time of the aircraft at the sensor baseline.

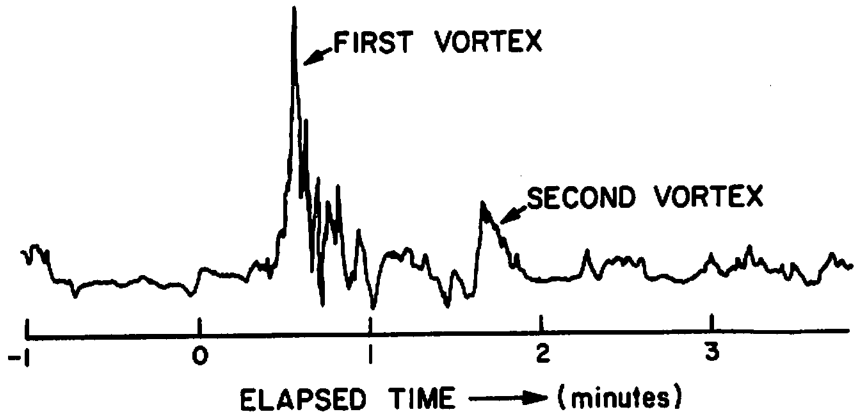

Figure 41. Pressure Data Run 12, 7/31/71, B-747. The Aircraft Arrived at Time Zero

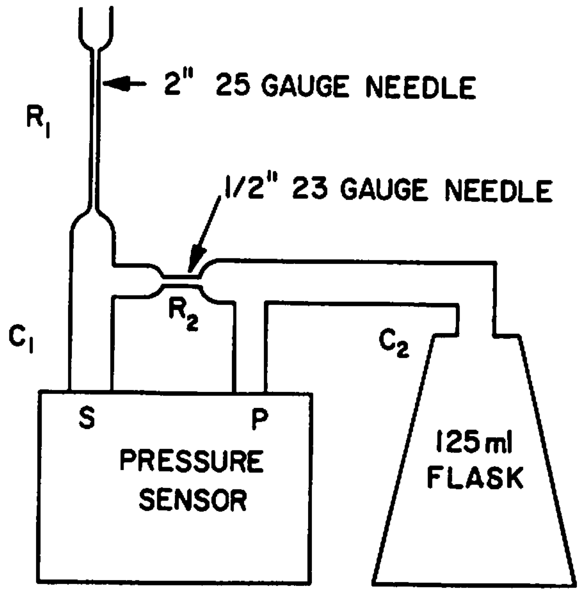

Figure 42. Pressure Sensor with Auxiliary Apparatus to Reduce Sensitivity and Eliminate Response to Barometric Changes.

mainly upon wind speed. The sensor thus shows the desired sensitivity to transverse winds and relatively much less sensitivity to the longitudinal ambient wind.

The first experimental arrangement using 120° dual Pitot tubes is shown in Figure 47. The capillaries reduce the sensor sensitivity as before and also serve to limit the speed of response. Data taken with this arrangement are shown in Figure 48. The two vortices produce signals of opposite sign as they pass over a pressure sensor (see sensor P-9 particularly), tracing a characteristic "S" shaped curve. The down wind vortex (upward signal) can be tracked all the way across the 800 ft array in some cases. The arrangement shown in Figure 47 (with $C_1 \neq C_2$) results in the

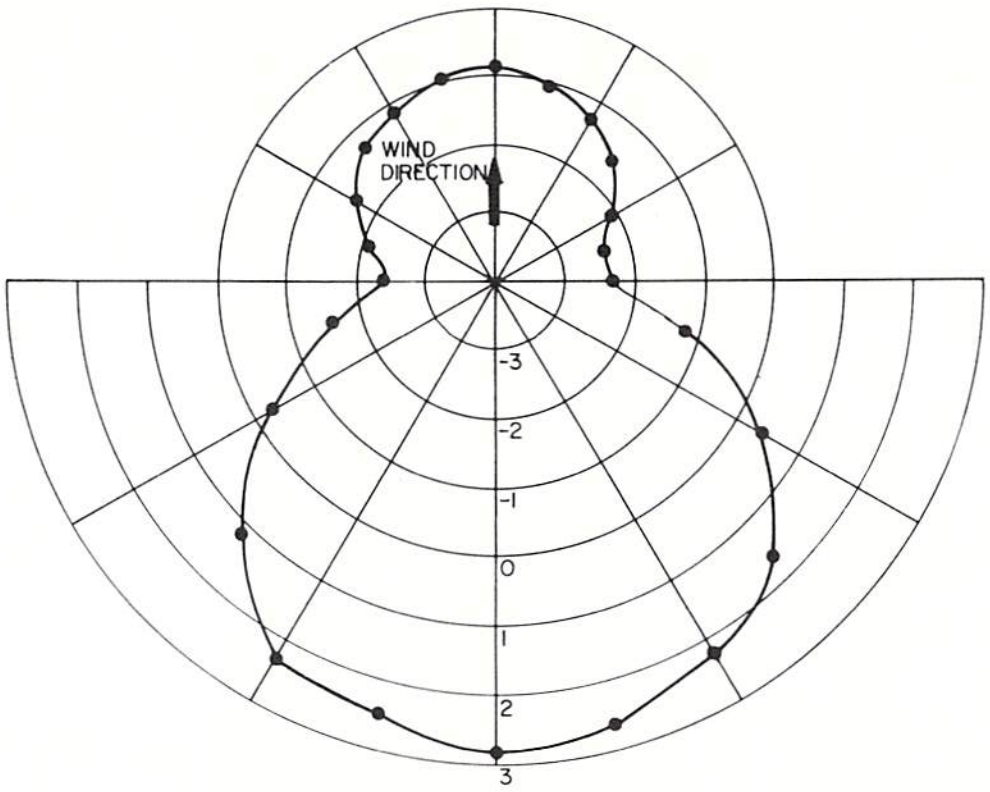

Figure 44. Polar Plot of Pitot Tube Pressure as a Function of Wind Direction. (The tube used to produce this plot had a diameter roughly 1/3 of that used in the field tests.)

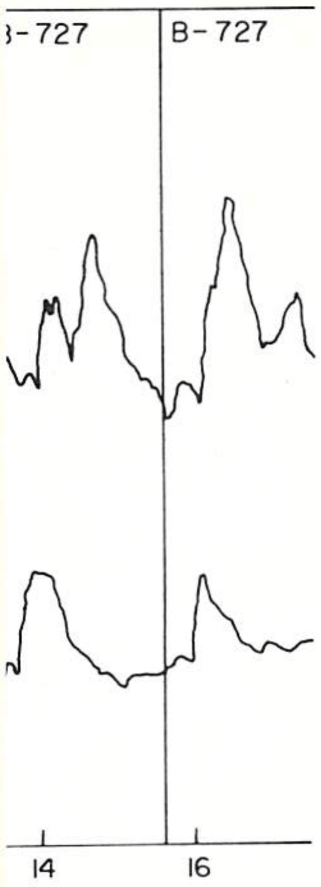

Runs 39-26 Through
mately 23 mph at 300°
l strip charts. The
t at the sensor baseline.

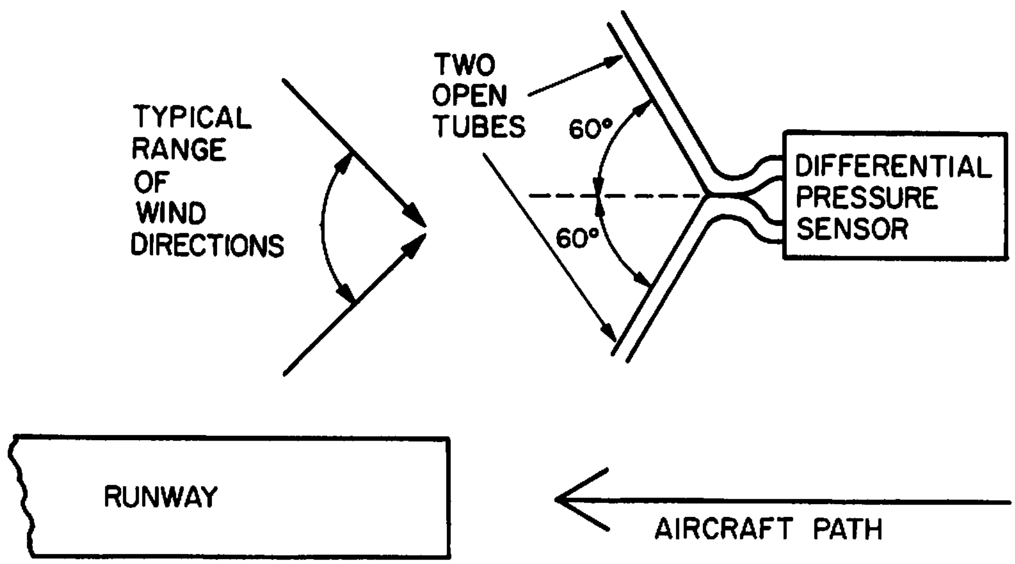

Figure 45. 120° Dual Pitot Tube Pressure Head Arrangement.

Figure 46. 120° Dual Pitot Tube Installed at Kennedy 31R Middle Marker. (The Tubes are Made of 1/4" Copper Tubing.)

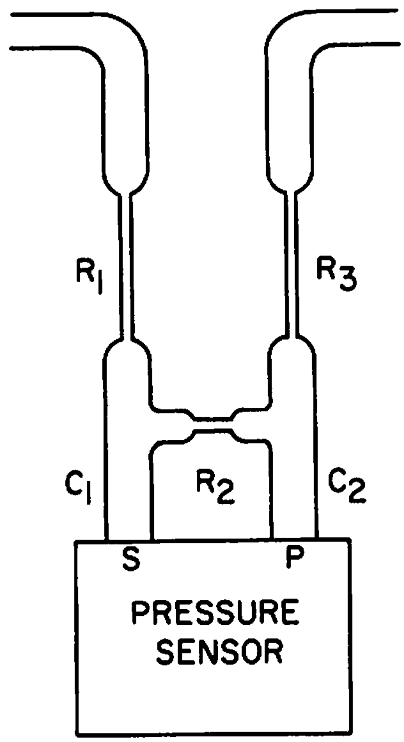

Figure 47. Pressure Sensor with 120° Dual Pitot Tubes and Reduced Sensitivity. R_1 and R_3 are 2" long 23 gauge needles. R_2 is a 1/2" long 23 gauge needle

detection of the ambient pressure change associated with aircraft passage overhead. This effect produces narrow pips in the center-line sensor P11, especially for B-747 runs.

The final week of pressure sensor testing was conducted with sensor sensitivity reduced to a full scale value of $\pm$ 0.5 inches of water. The original value of $\pm$ 0.05 inches of water was reduced by installing a thicker diaphram (.001" replacing .00025") and changing the position of the inductors which sense the diaphram location. A full scale pressure of 0.5 inches of water is sufficient to measure a 32 ft/sec cross wind with a dual Pitot tube sensor since the two tubes experience comparable but opposite pressure changes of 0.25 inches of water or less (Figure 44). The reduction of the intrinsic sensitivity of the sensor makes it possible to retain the full speed of response of the sensor, which was

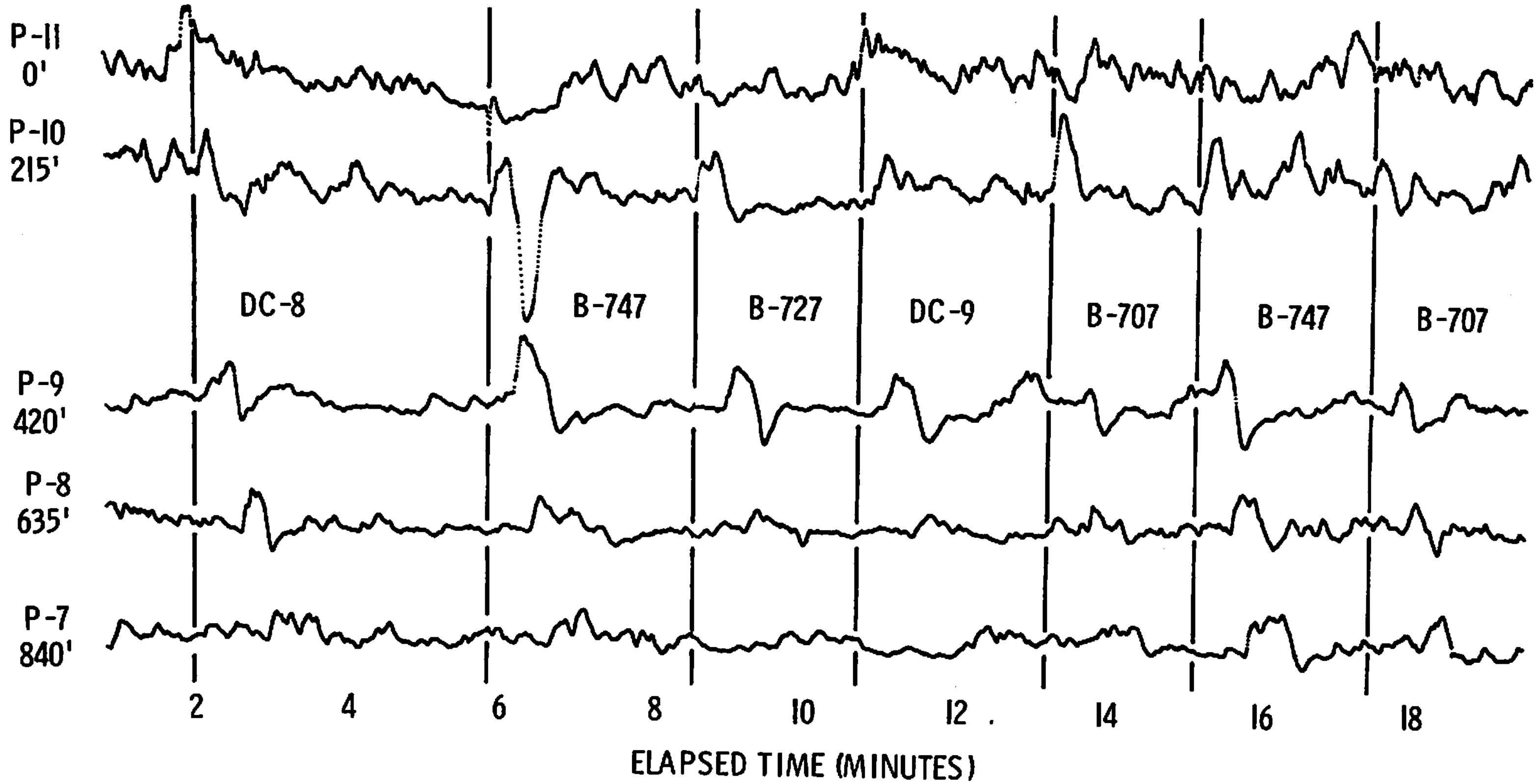

Figure 48. Pressure Data Taken on 1/5/72, 1908-1925 Local Time. The measured wind (13 ft) was 13 mph at 010°. The wind reported by the Kennedy Tower was 15 Kts at 360°. The vertical lines indicate the arrival time of the aircraft.

limited to a 0.1 sec time constant by electronic filtering. Some pressure data recorded with this full bandwidth are shown in Figure 49. Figures 50 and 51 show the effects of smoothing the data with 0.5 and 1.5 second time constants. All further pressure data presented in this report were recorded with a 0.5 second time constant.

A basic requirement for the analysis of pressure data is a convenient, compact means of simultaneously displaying the outputs of many pressure sensors. This requirement has been met by a Brush Model 816 Recorder which uses a single pen to display up to eight multiplexed channels at a maximum total sampling rate of 16 per second. The type of record produced by this recorder is shown in Figure 52 which includes the two runs shown in Figure 50. The discontinuous nature of the recording is evident at points where the signal is changing rapidly.

3.2 TYPICAL RESULTS

Experimental pressure data taken under a variety of conditions are shown in Figures 53 to 61 and are presented in chronological order. When available, the data include the wind measured by an anemometer on the van at 13 ft altitude, "Measured Wind", measured at 12 ft altitude, 7000 ft from the van. The wind direction is given with respect to magnetic north. Data were taken whenever runway 31R (i.e., 310° magnetic heading) was being used for landings. When the wind direction is less than 310°, the vortices tend to drift to the left (Figure 2), i.e., toward the higher number pressure sensors, P11 being at the centerline (Table 10). When the wind direction is greater than 310°, the vortices tend to drift in the opposite direction, i.e. toward lower numbered pressure sensors.

3.3 DISCUSSION OF RESULTS

The discussion here is based on the pressure data of Section 3.2 and is therefore qualitative since the altitude and arrival time of the vortices at each sensor cannot be determined from the pressure data alone. All quantitative discussions will be deferred

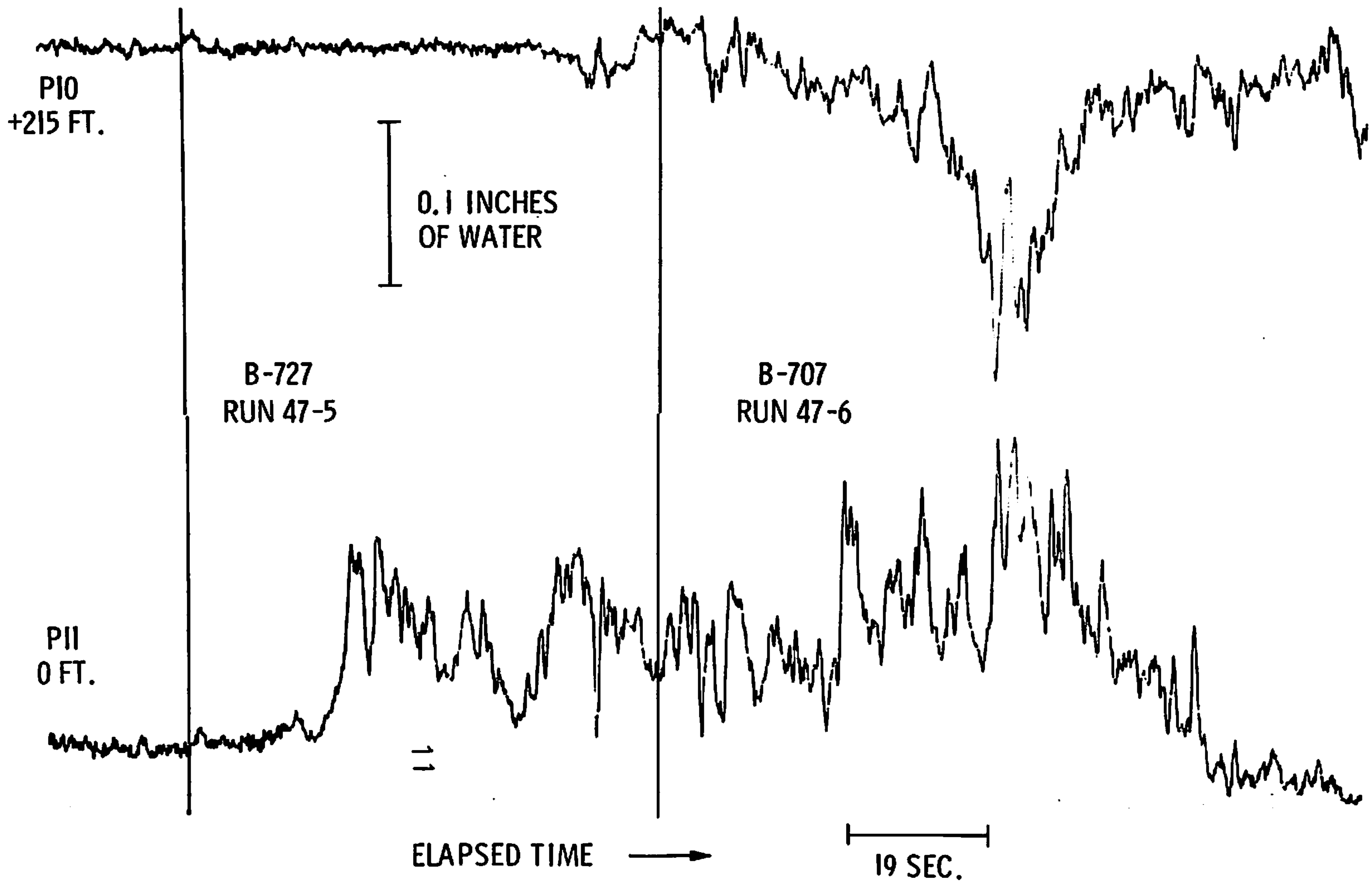

Figure 49. Pressure Data Taken on 2/10/72, 2053-2056 Local Time. The signals were filtered with a four pole 5Hz high pass filter. The measured wind (13 Ft) was 2 mph. The Kennedy Tower reported a wind of 3Kts at 320°.

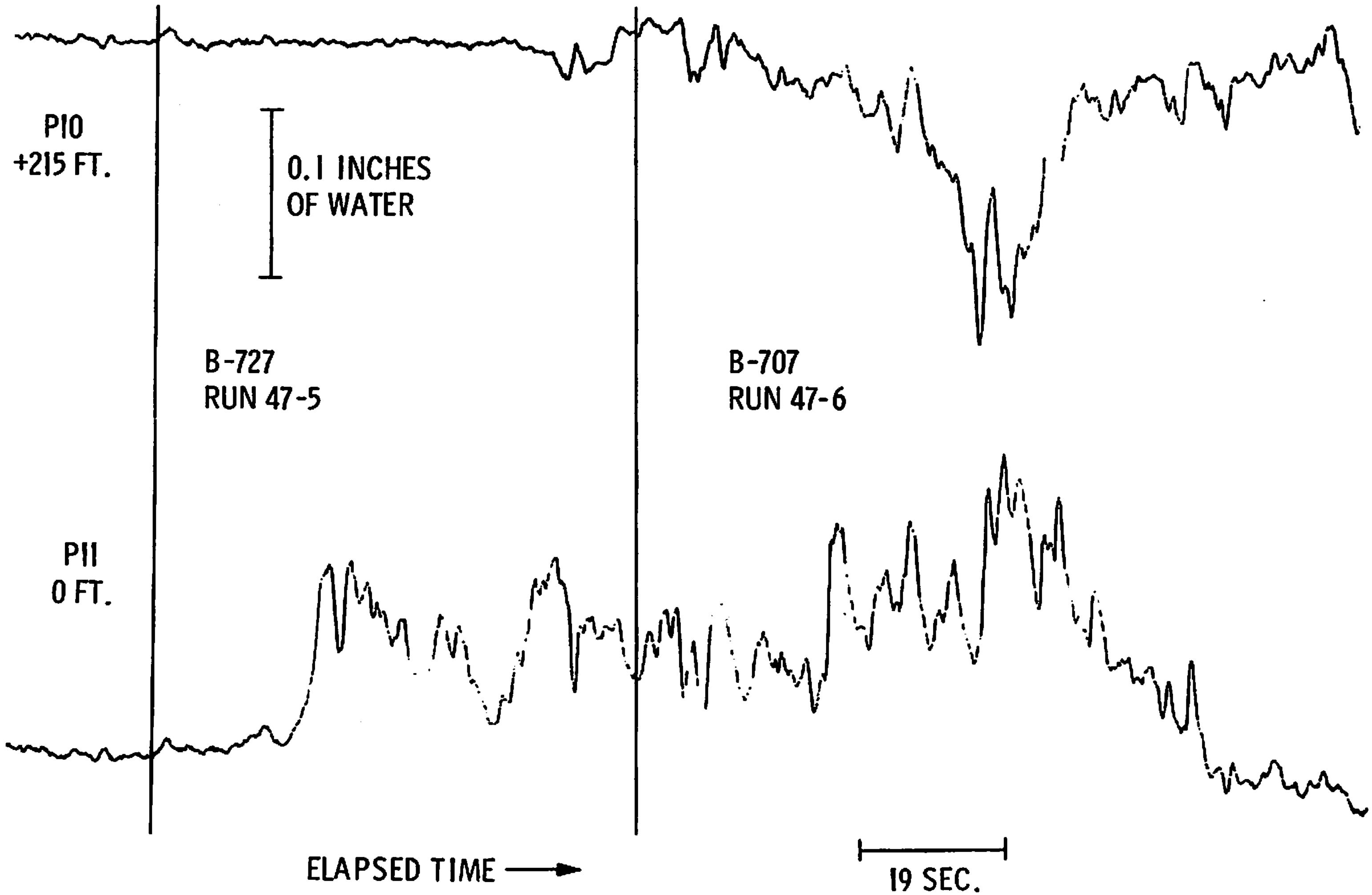

Figure 50. Data Shown in Figure 49 Filtered with a 0.5 Second Time Constant

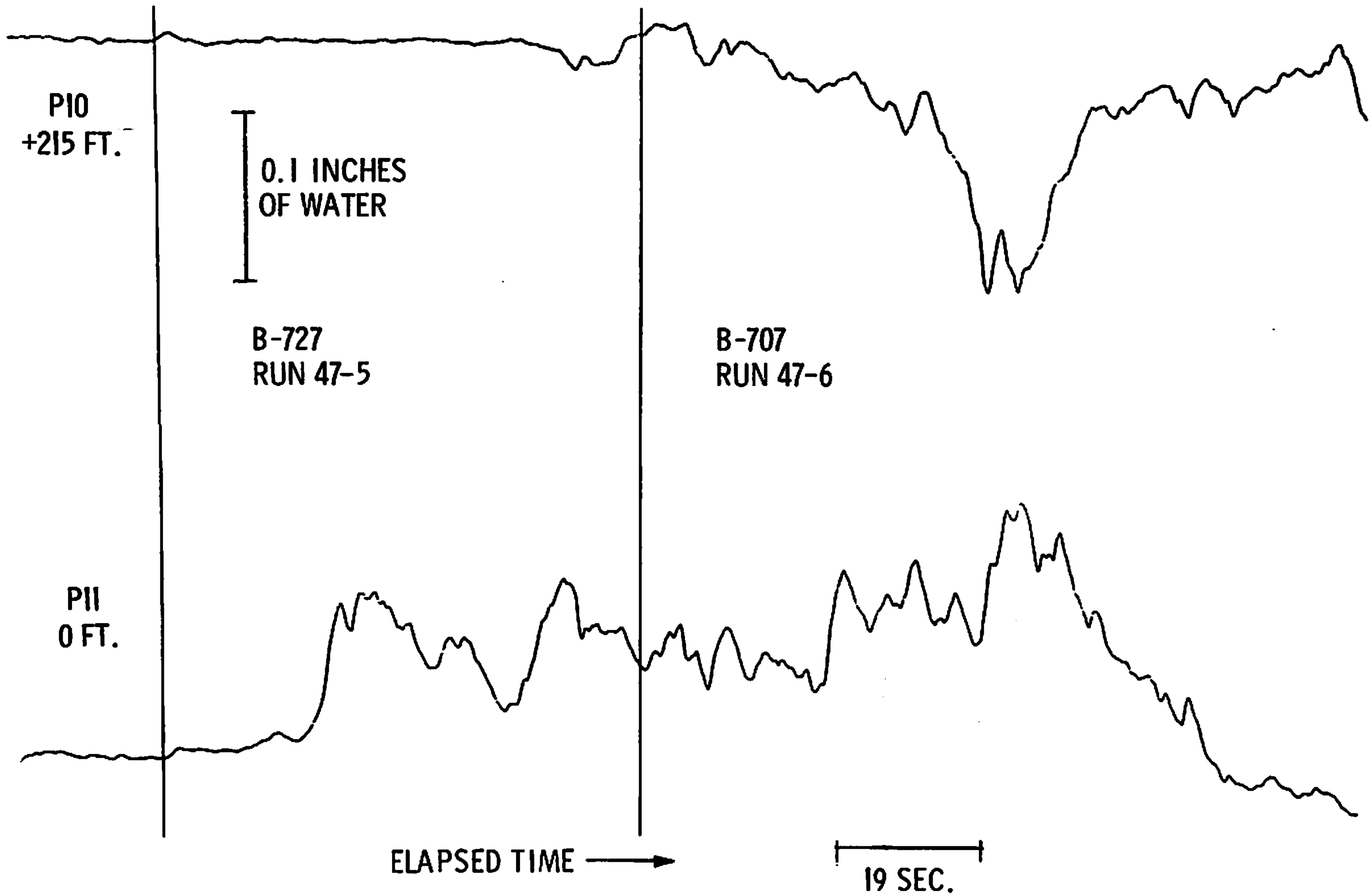

Figure 51. Data Shown in Figure 49 Filtered with a 1.5 Second Time Constant.

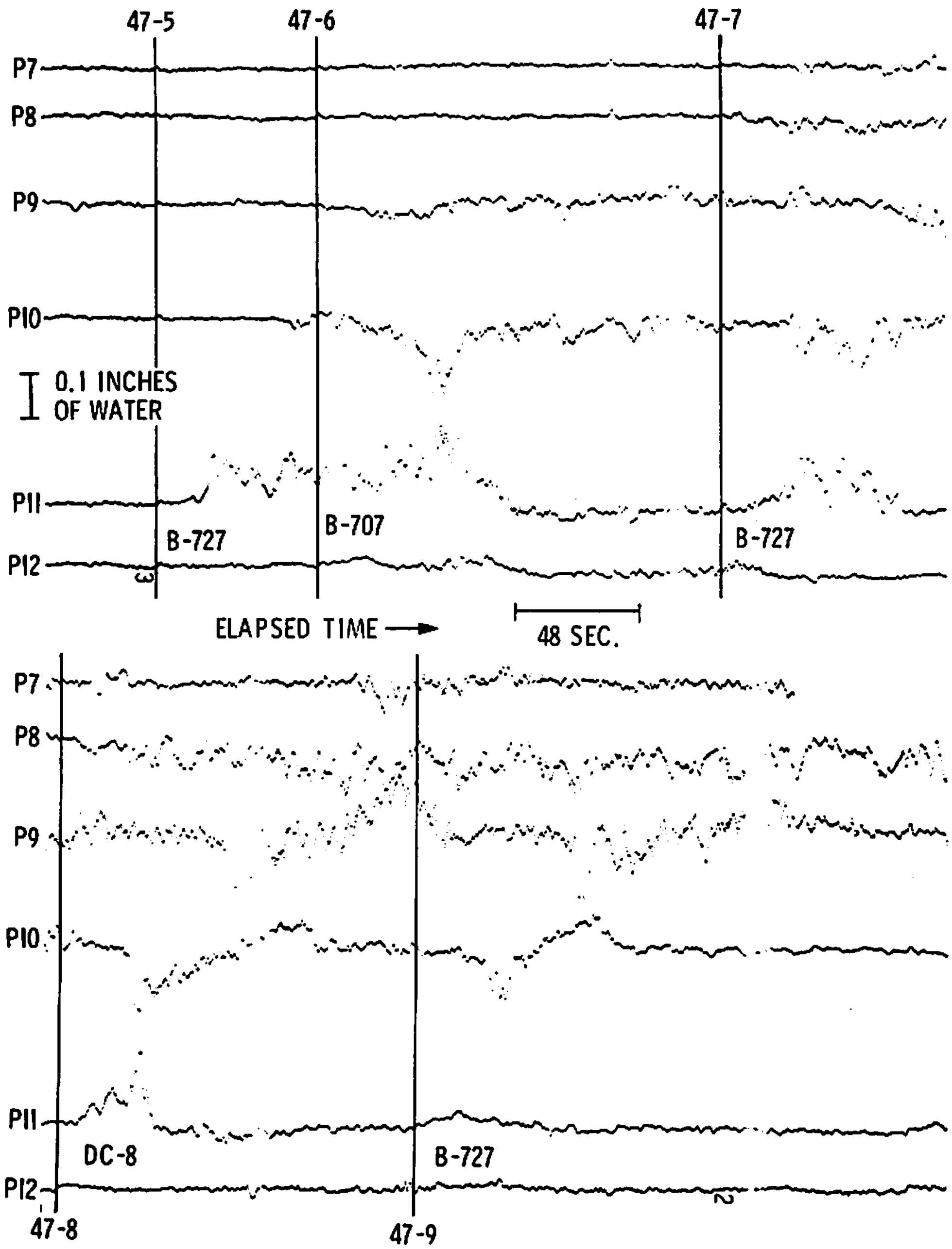

Figure 52. Pressure Data Taken on 2/10/72, 2052-2102 Local Time. The data from six pressure sensors is plotted at a rate of 16 samples per second (i.e., 2-2/3 samples per channel per second). The signals are filtered with a 0.5 second time constant. The measured wind (13 ft) was 7 mph after the first two runs. The Kennedy Tower reported winds in the range 5-8Kts at 310°-350°.

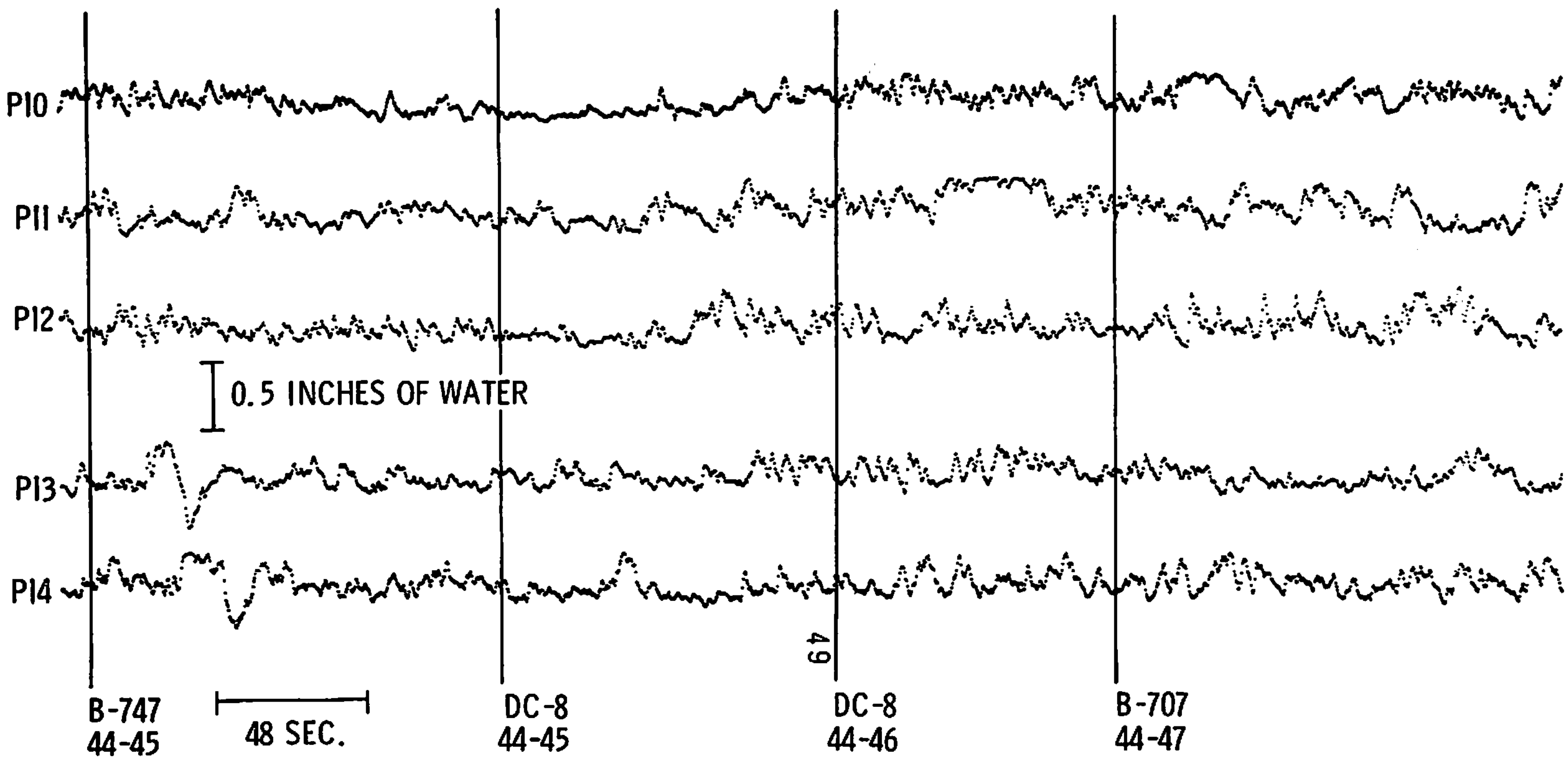

Figure 53. Pressure Data, 2/8/72, 1809-1815 Local Time, Runs 44-45 Through 45-48. Measured Wind = 19 mph @ 270°, Tower Wind = 20 Kts @ 270°.

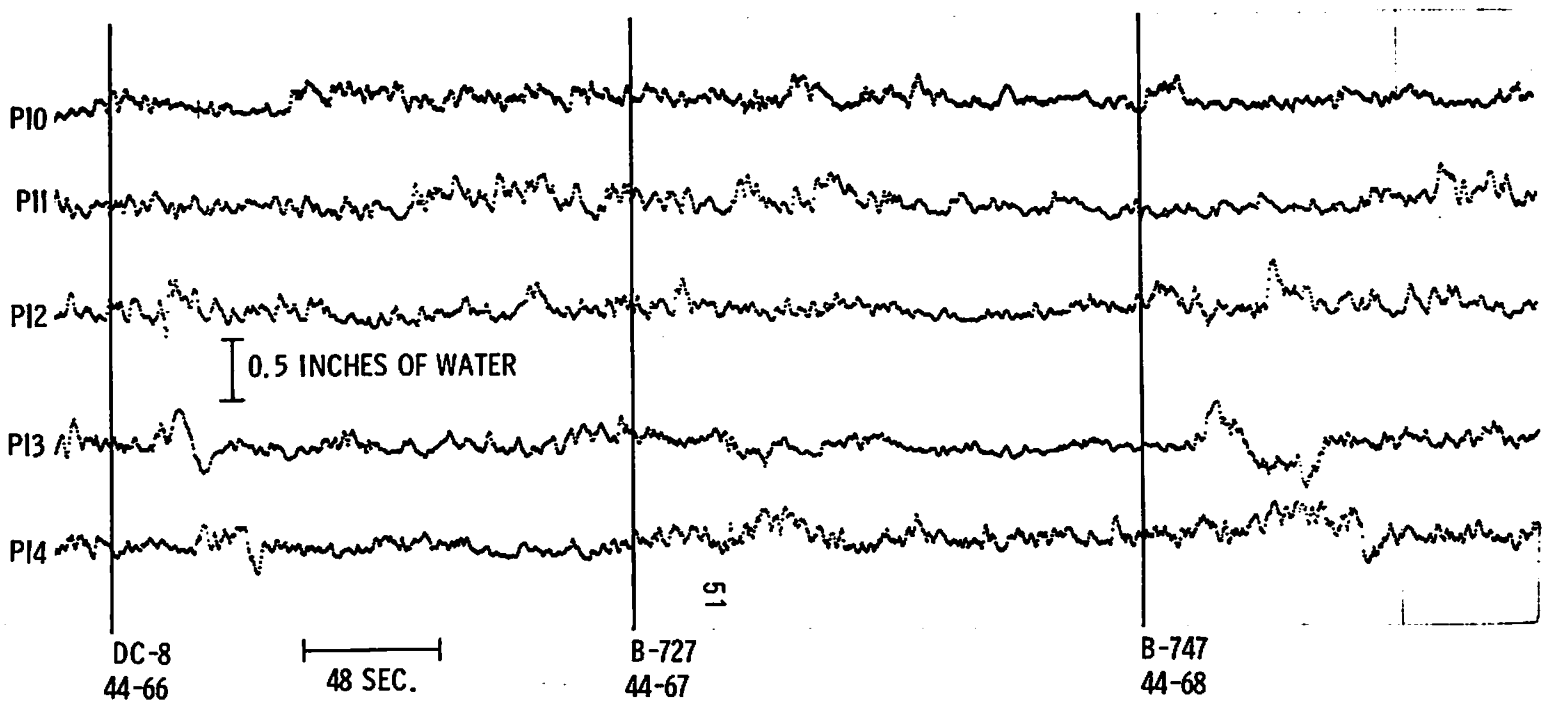

Figure 54. Pressure Data, 2/8/72, 1915-1922 Local Time, Runs 44-66 Through 44-68. Measured Wind = 16 mph @ 270°, Tower Wind = 16 Kts @ 280°.

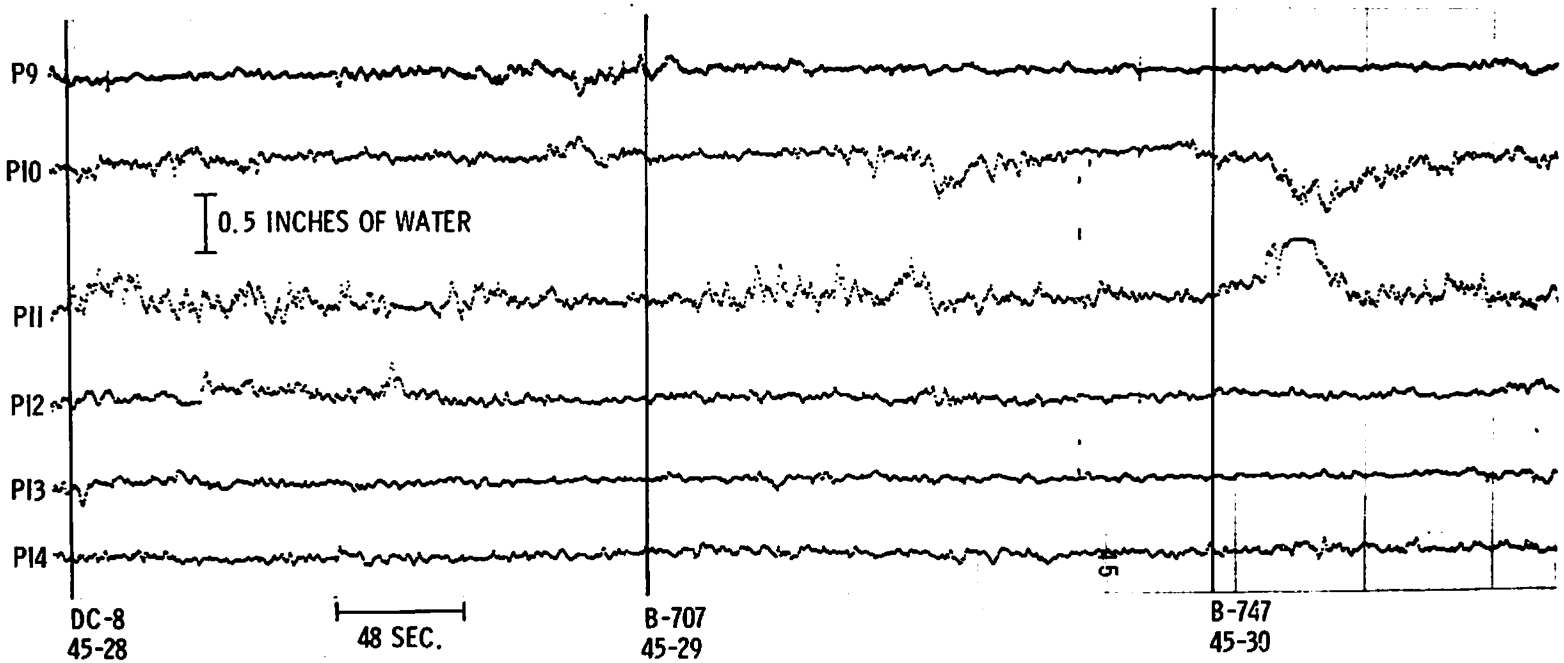

Figure 55. Pressure Data, 2/8/72, 2045-2052 Local Time, Runs 45-28 Through 45-30. Measured Wind = 19 mph @ 310°, Tower Wind = 15 Kts @ 290°320°. Note, the P11 signal on run 45-30 has been clipped by overdriving the tape recorder.

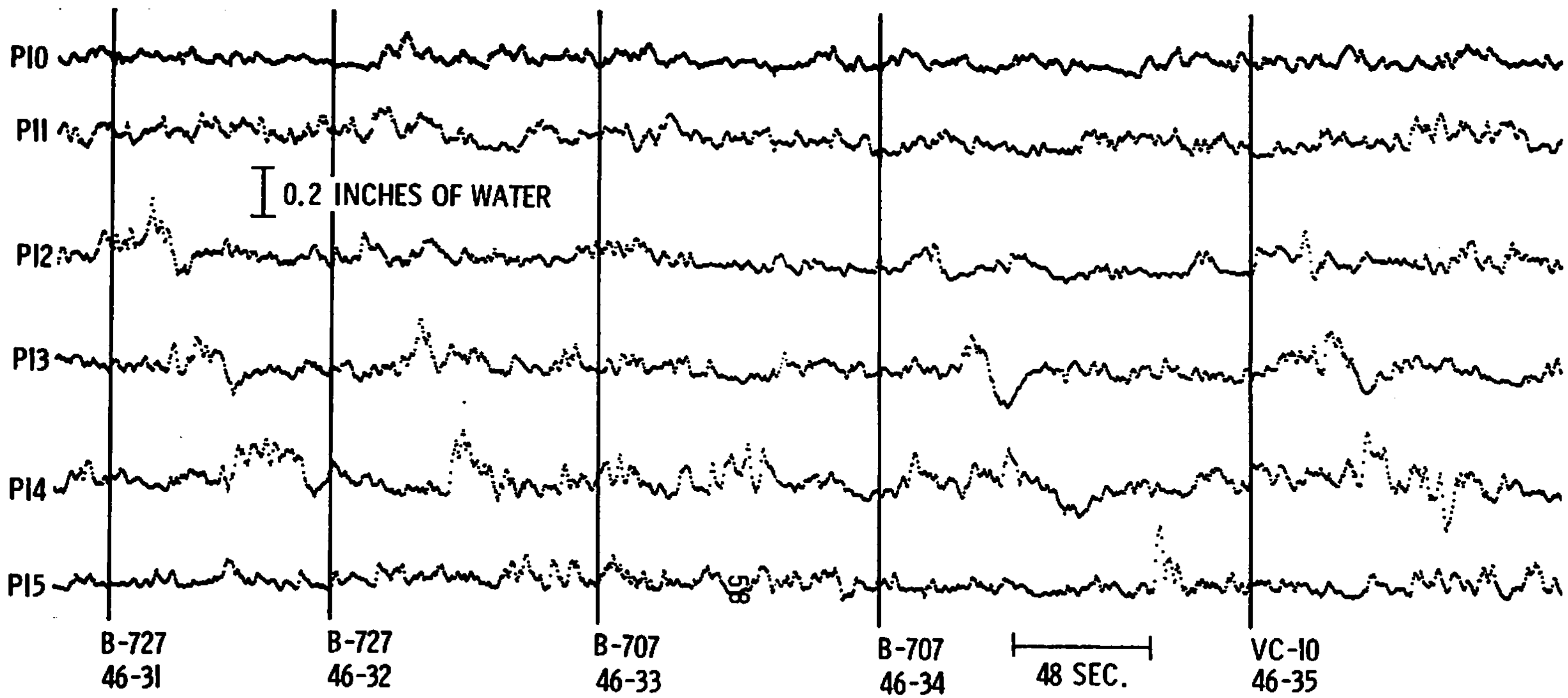

Figure 56. Pressure Data, 2/9/72, 1359-1408 Local Time, Runs 46-31 Through 46-35. Measured Wind - 11 mph @ 260°, Tower Wind 10 Kts @ 260°.

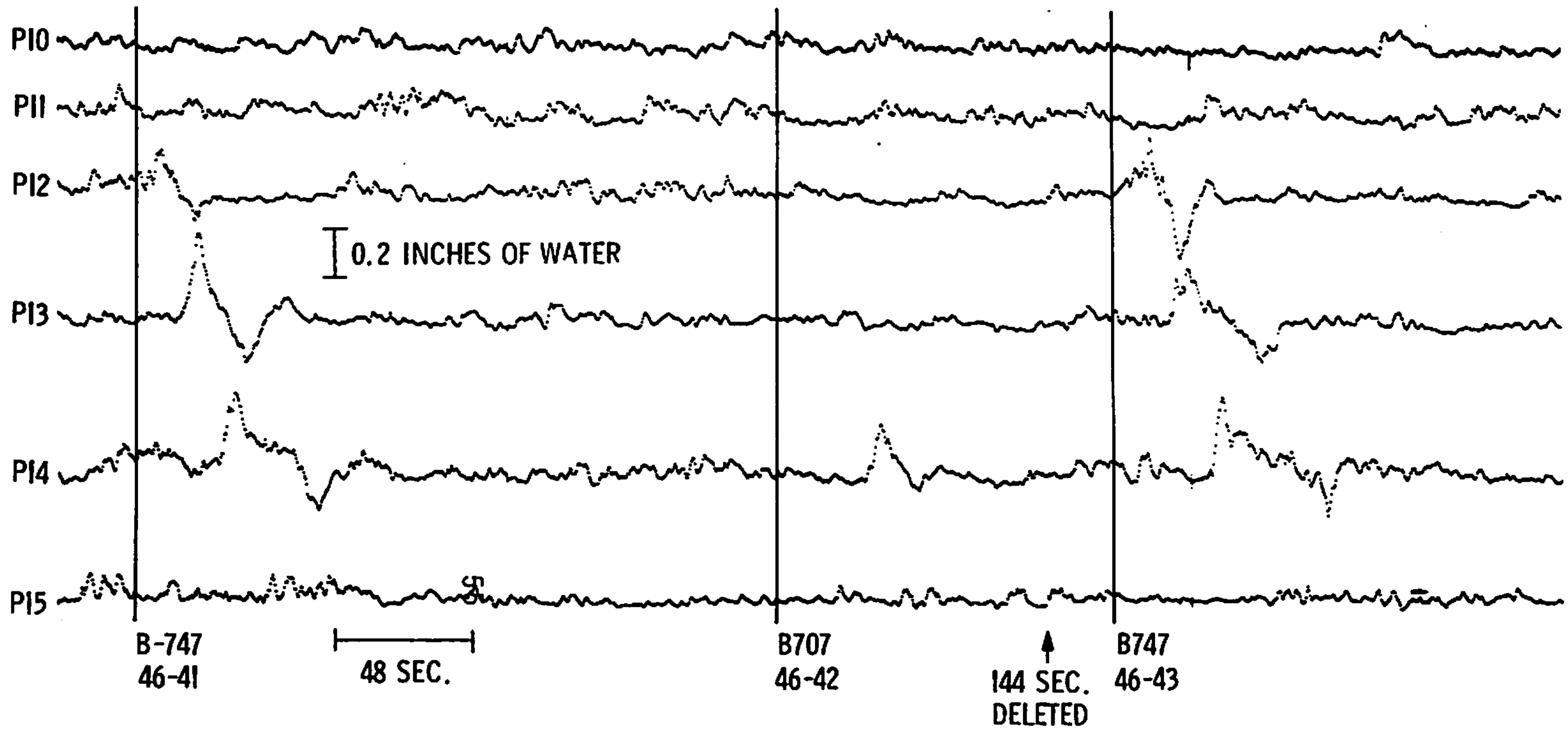

Figure 57. Pressure Data, 2/9/72, 1429-1439 Local Time, Runs 46-41 Through 46-43. Measured Wind = 11 mph @ 240°, Tower Wind = 9 Kts @ 250°.

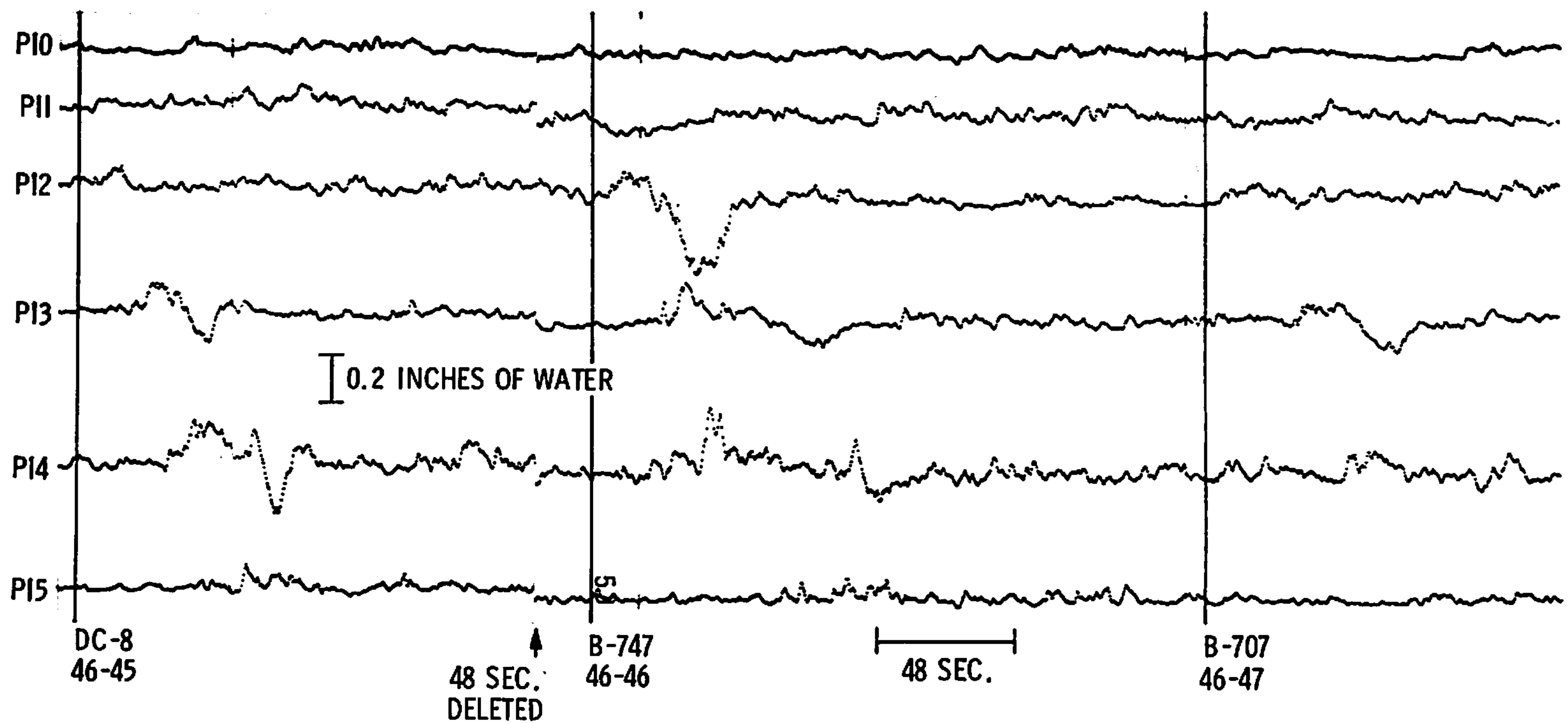

Figure 58. Pressure Data, 2/9/72, 1447-1455 Local Time, Runs 46-45 Through 46-47. Measured Wind = 8 mph @ 260°, Tower Wind = 8 Kts @ 260°.

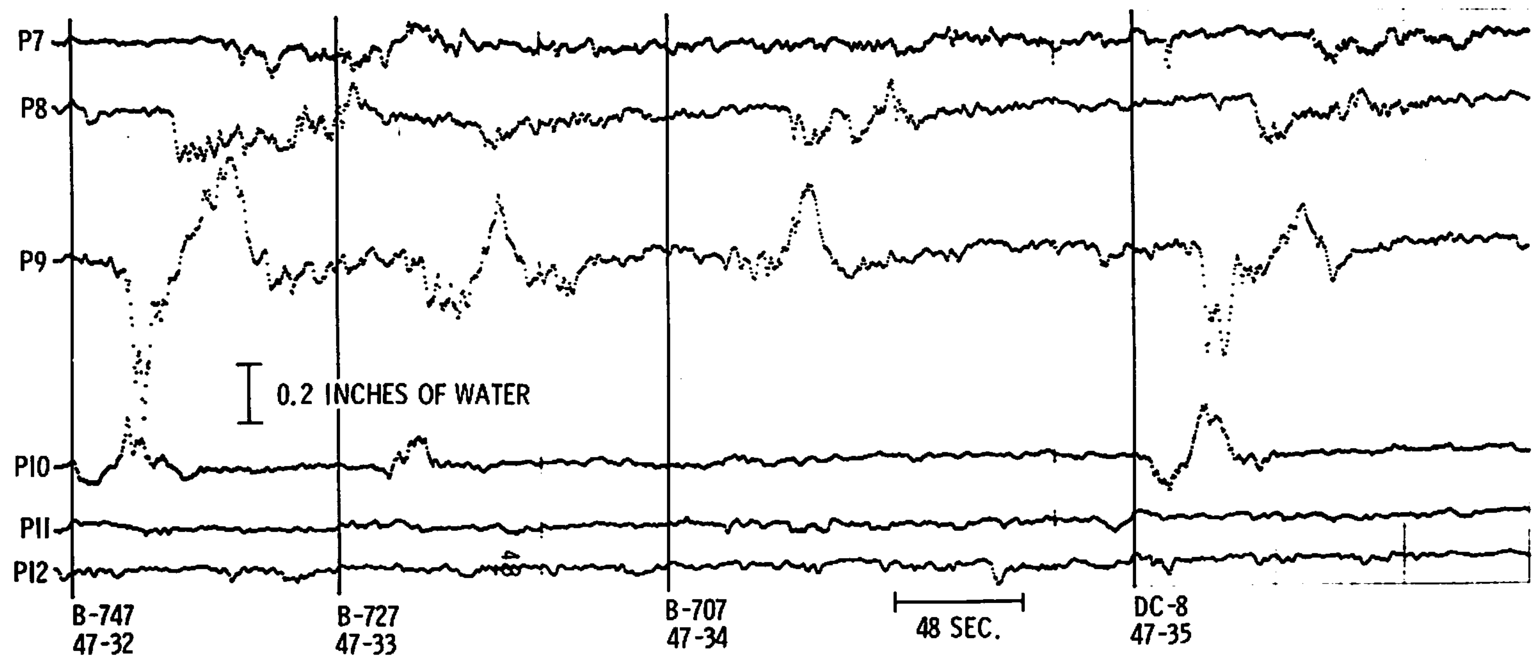

Figure 59. Pressure Data, 2/10/72, 2212-2220 Local Time, Runs 47-32 Through 47-35.
Measured Wind = 6 mph @ 340°

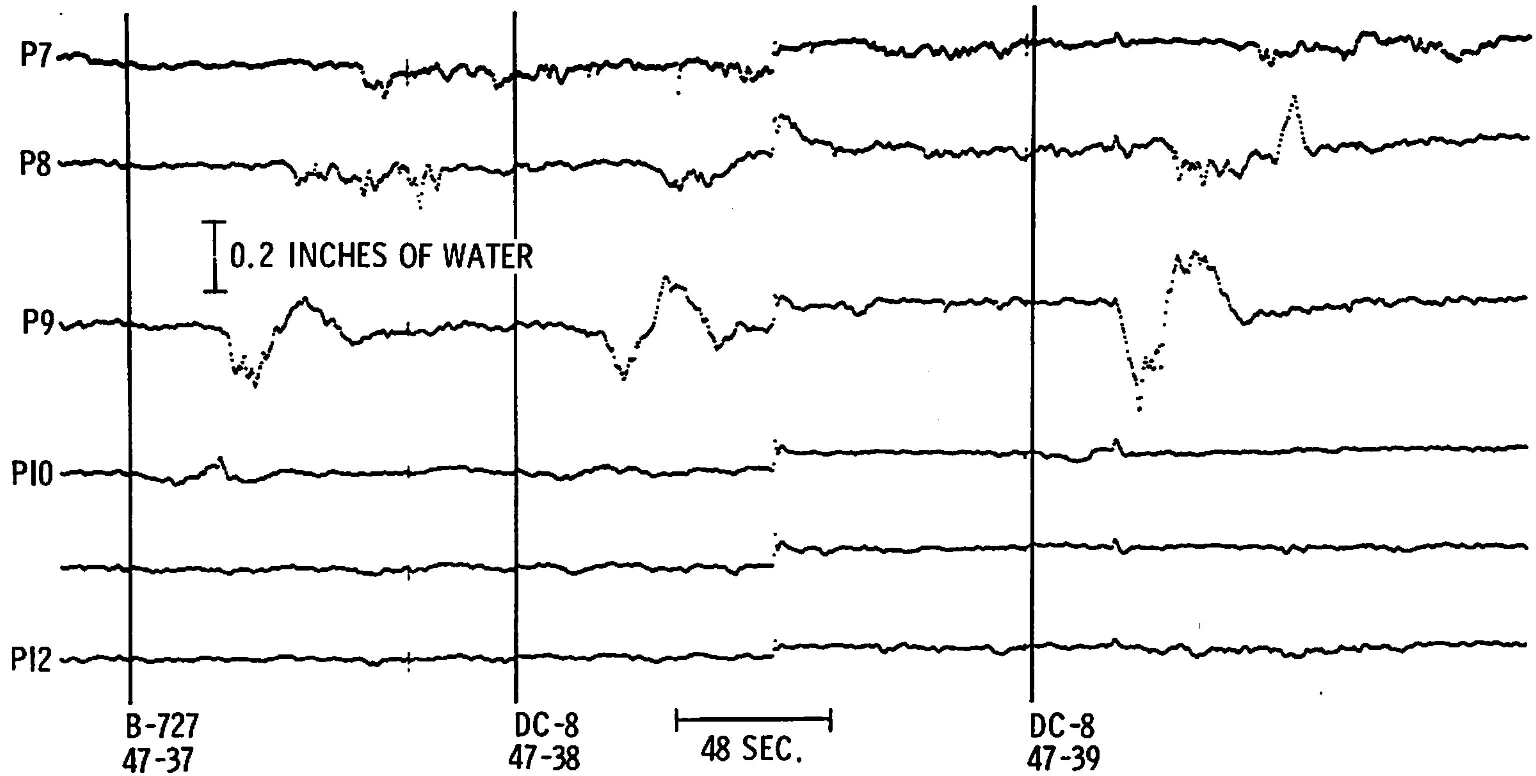

Figure 60. Pressure Data, 2/10/72, 2225-2232 Local Time, Runs 47-37 Through 47-39. Measured Wind = 6 mph @ 360°, Tower Wind = 8 Kts @ 010°

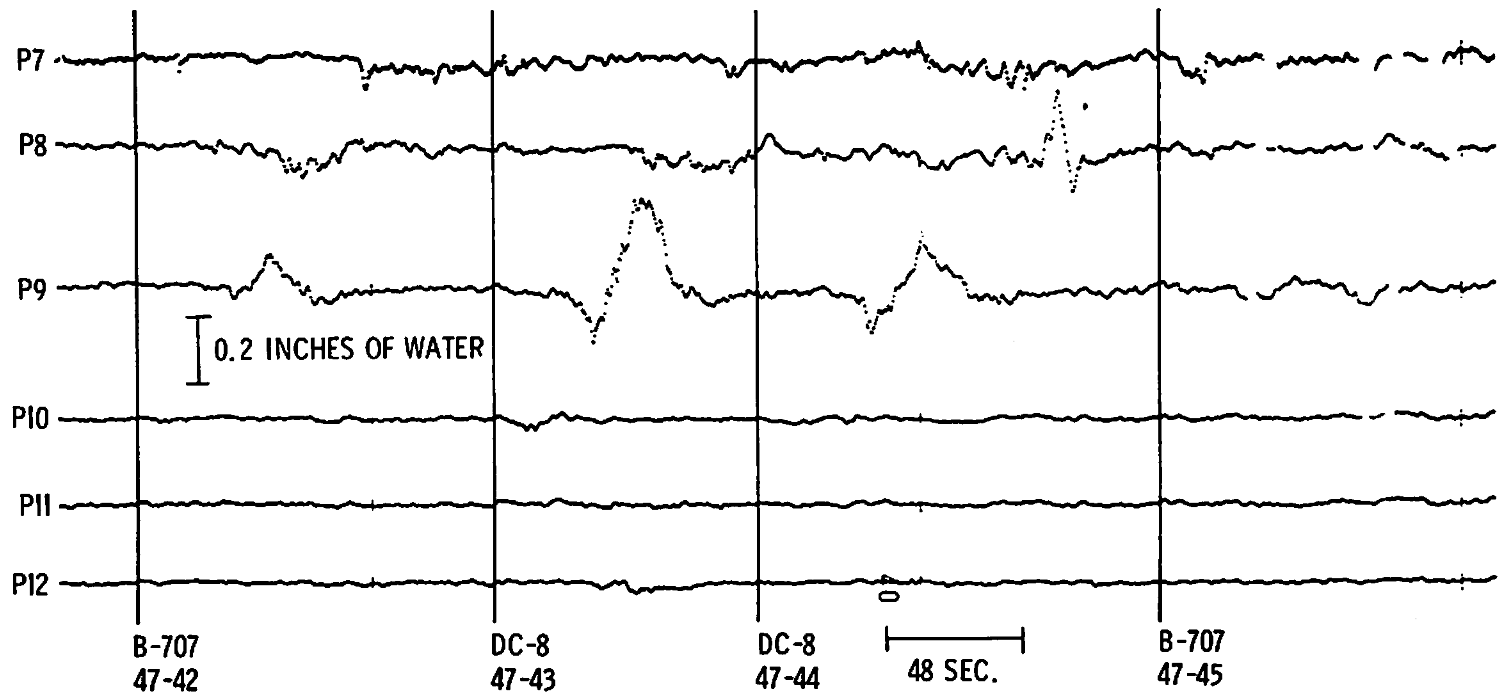

Figure 61. Pressure Data, 2/10/72, 2238-2246 Local Time, Runs 47-42 Through 47-45. Measured Wind = 5 mph @ 350°, Tower Wind = 8 Kts @ 360°

to Section 4.0 where the pressure sensor data will be compared to vortex tracks determined by the acoustic radar.

The ambient wind strongly affects both the vortex signals and the noise in the observed pressure data. The noise level depends upon atmospheric turbulence, which generally increases with wind intensity (compare Figures 53 and 60, for example). A vortex can be detected only when the wind produced by the vortex at the sensor is larger than the fluctuations in the ambient wind. Under some conditions (Figure 53), the noise levels are so high that only vortices from the B-747 can be identified. On the other hand, when the ambient winds are very low (Figures 52,60,61,62) the observed noise is due to the intrinsic turbulence of the vortex in ground effect.

Under specific wind conditions the best vortex signals generally appear at a particular pressure sensor. This effect results from the two requirements for vortex detection by a ground based sensor:

a. The vortex must be low enough to produce an observable wind at the ground, and

b. The vortex must not have dissipated before it reaches the sensor.

The first appearance of the vortex signal can be estimated by the following simple calculation. The altitude of the aircraft at the 31R middle marker is usually 175-200 ft. At a typical descent rate of 7 ft/sec a vortex takes 20 sec to drop to 60 ft from 200 ft. If the transverse wind component is 15 ft/sec (as in Figure 53), the vortex will have travelled 300 ft horizontally in that time. This is consistent with the fact that the "400 ft" sensors (P9 and P13) produced the best vortex signals in the presence of a strong cross wind (see Figures 53,56,57,60, 61). As a vortex begins to dissipate, the pressure signals deteriorate. This effect can be seen in the P8 and P7 signals of Figure 59. The absence of identifiable vortex signals in P15 (Figures 56 and 57) may not be due to dissipation alone since the region between sensors P14 and P15 contains a large patch of tall marsh reeds (8 feet high) which undoubtedly affected the wind near the ground.

The horizontal motion of a wake vortex in ground effect is not solely a function of the ambient cross wind but is also influenced by interaction with the ground. This effect increases the speed of the down-wind vortex and decreases the speed of the up-wind vortex. The vortex separation increases with time as can be seen clearly in Runs 46-41 and 46-43 in Figure 57, and Run 47-35 in Figure 59. If the cross wind is small enough, the vortices should propagate in opposite directions. This situation occurred for only a very small fraction of the total number of runs. Data from two such occasions are shown in Figures 52 (the first three runs) and 55. In the first case the ambient wind was low and in the second the wind was high but blowing directly down the runway. In neither case did the vortices last long enough for the signals to appear in more than one pressure sensor.

The data shown in Figure 52 deserve further comment, Run 47-5 was the first aircraft to land on runway 31R after a runway change. Before the aircraft arrived, the wind was very calm. The wind and turbulence increased significantly after the first two aircraft passed. Figure 52 shows the propagation of increased turbulence along the sensor baseline. It is not clear whether the aircraft or a coincidental increase in ambient wind is responsible for this turbulence.

The shape of the vortex signals observed by the pressure sensors is quite variable. Often the signals are slowly rising symmetrical peaks as one might expect. Sometimes however, the first vortex signal has a sharp leading edge and a long trailing edge (e.g., Run 47-8, P10 in Figure 52 and Run 46-43, P14 in Figure 57). Often the second (up-wind) vortex signal is followed by a signal of the same polarity as the first vortex (e.g., Runs 46-41, 43, P13 in Figure 57). The shape and magnitude of the vortex signal results from the detailed interaction of the vortex with the boundary layer of the atmosphere at the earth's surface. We have not had the resources to investigate the theory of this interaction except to construct a model calculation of the effect of wind shear on vortex trajectories.[5]

4.0 COMPARISON OF VORTEX POSITIONS OBTAINED FROM ACOUSTIC AND PRESSURE DATA

The nature of the information obtained from the two sensing systems is quite different. The acoustic system determines the position coordinates, $x(t)$ and $h(t)$ of the vortex core as a function of time. One would expect that the maximum pressure signal would occur at the time t_m when the vortex core is directly above the sensor. In this case the horizontal vortex location is $x_i(t_m)$, and one point is obtained for each sensor which detects the vortex. The relevant comparison in this section is therefore between $x(t)$ and $x_i(t_m)$.

Knowing the aircraft parameters and the height $h(t=t_m)$, one can also predict the magnitude of the pressure signal, or conversely use this magnitude to determine a height $h_i(t_m)$. Such comparisons give rough agreement but are probably of limited value for the present data. Quantative evaluation of the pressure data is intrinsically limited by the nonlinear nature of sensor response to transverse velocities. For transverse wind velocities much smaller than the longitudinal velocity the response is linear. For transverse velocities larger than the longitudinal velocity the response is quadratic. Since the transition between the two responses depends upon the ambient wind, a universal response curve cannot be constructed. A detailed quantative analysis of the data also requires a knowledge of the zero response level, which is difficult to determine because of zero offsets in the pressure sensor, the signal amplifier and the tape recorder. We conclude that it is more reasonable to regard the pressure sensor data from the point of view of vortex detection rather than vortex measurement.

Figures 62-69 compare the vortex positions $x(t)$ calculated from the acoustic data with the positions $x_i(t_m)$ obtained from the pressure data. Only a few comparison tests are presented since it is presently a very laborious and tedious task to reduce the acoustic data to obtain these vortex tracks. This problem will be resolved by the use of a mini-computer for the data analysis.

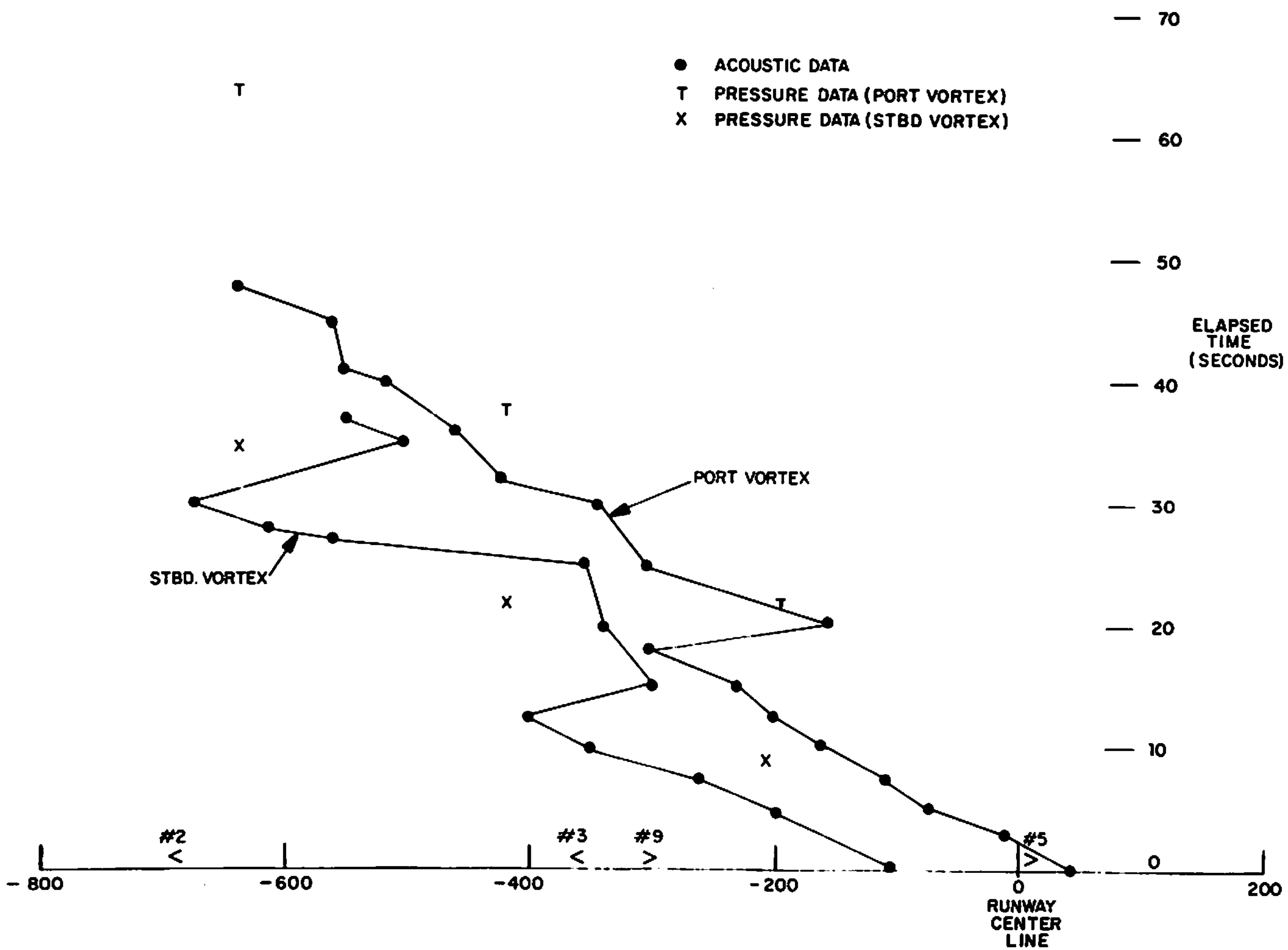

Figure 62: Comparison of vortex lateral position calculated with the data from acoustic sensors and pressure sensors. Numbers on horizontal scale indicate transceiver locations. Run #46-41; B-747; Kennedy Airport 2/9/72; Middle marker of Runway 31R; Local time: 1429; Configuration: landing.

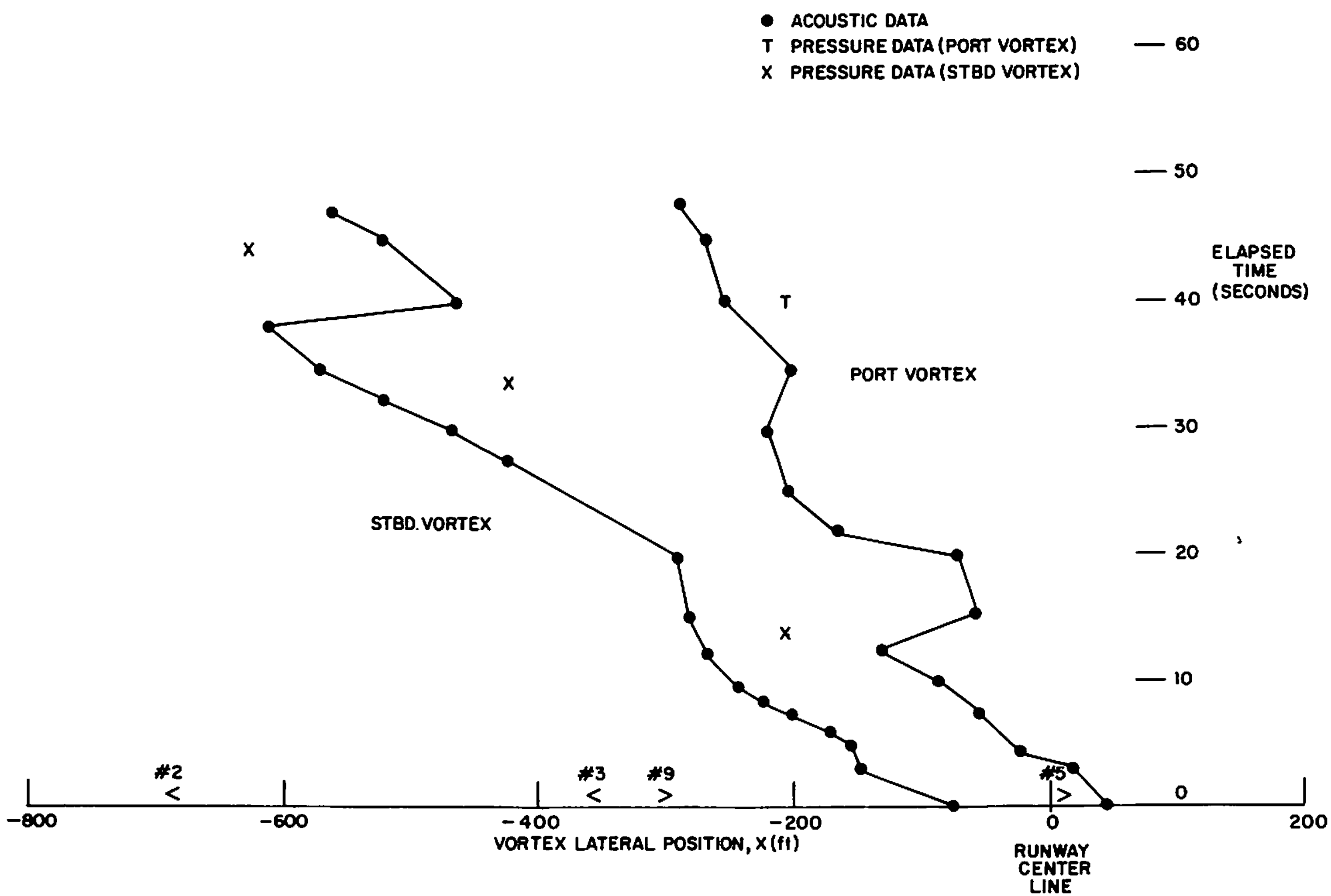

Figure 63. Comparison of vortex lateral position calculated with the data from acoustic sensors and pressure sensors. Numbers on horizontal scale indicate transceiver locations. Run #46-46 B-747; Kennedy Airport 2/9/72; Middle marker of Runway 31R; Local time: 1450; Configuration: landing.

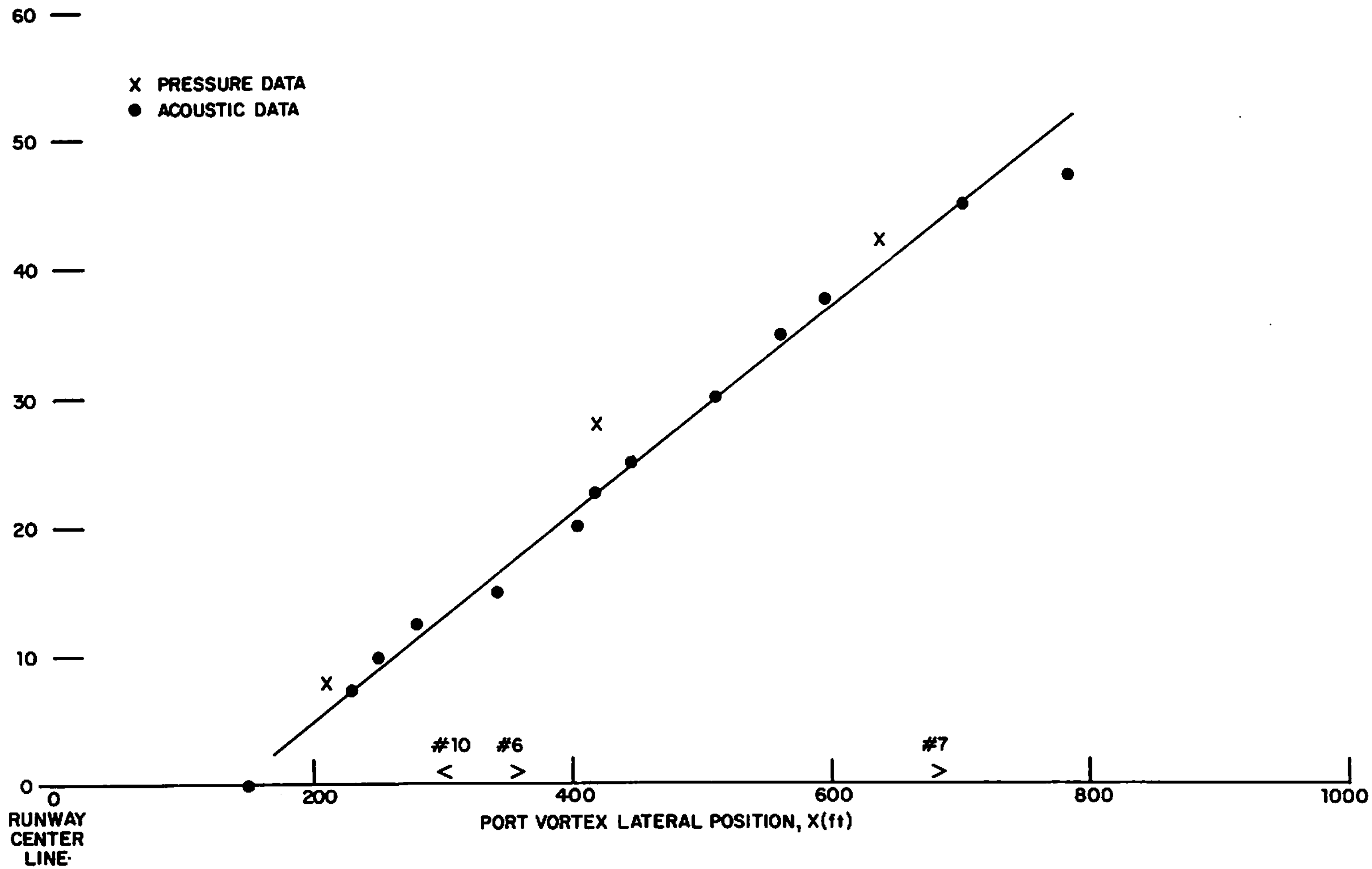

Figure 64. Comparison of port vortex lateral position calculated with the data from acoustic sensors and pressure sensors. Numbers on horizontal scale indicate transceiver position. Run #47-32 B-747; Kennedy Airport 2/10/72 Middle marker of Runway 31R; Local time: 1012; Configuration: landing

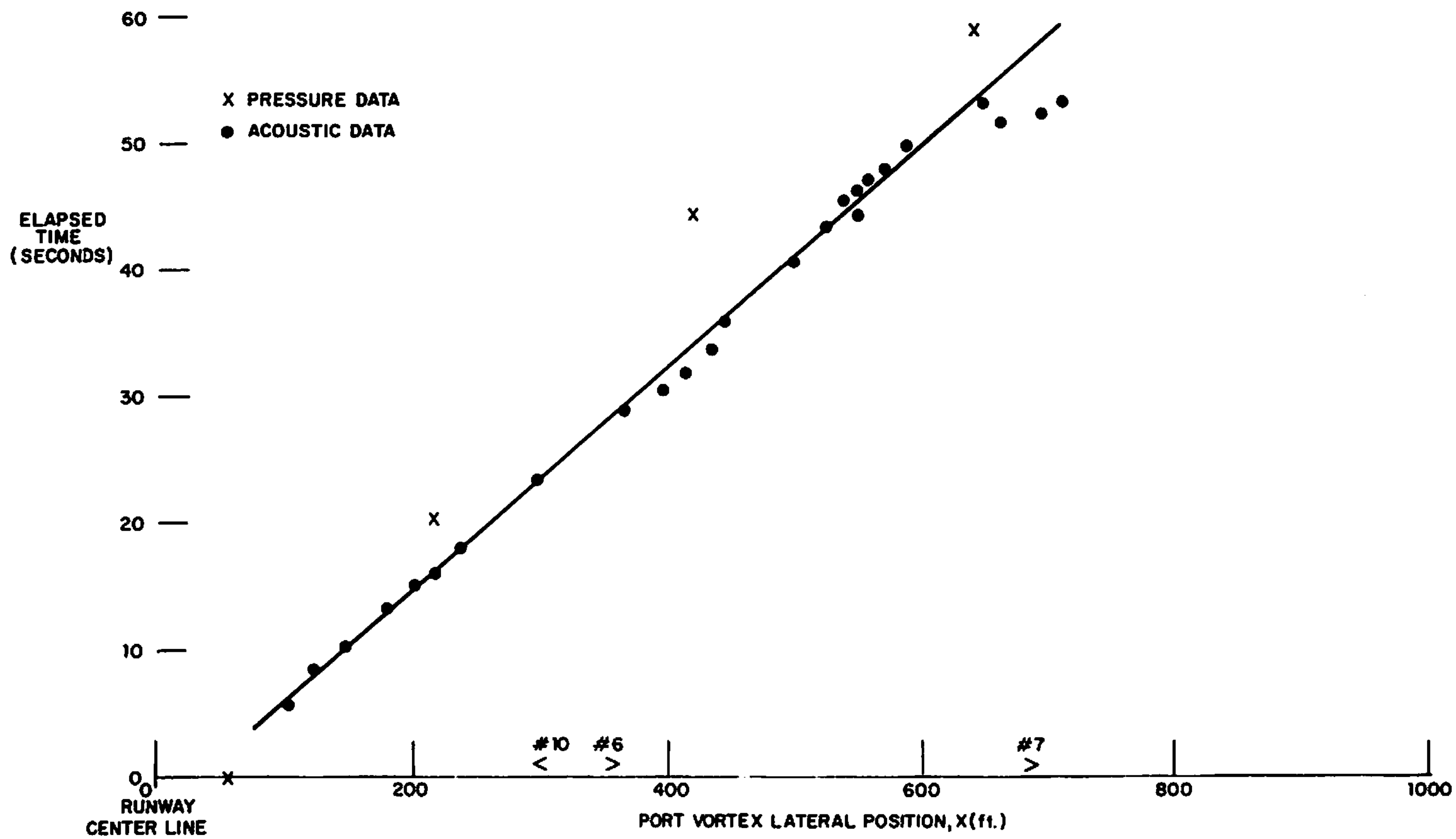

Figure 65. Comparison of port vortex lateral position calculated with the data from acoustic sensors and pressure sensors. Numbers on horizontal scale indicate transceiver positions. Run #47-33 B-727; Kennedy Airport 2/10/72; Middle marker of Runway 31R; Local time: 1013

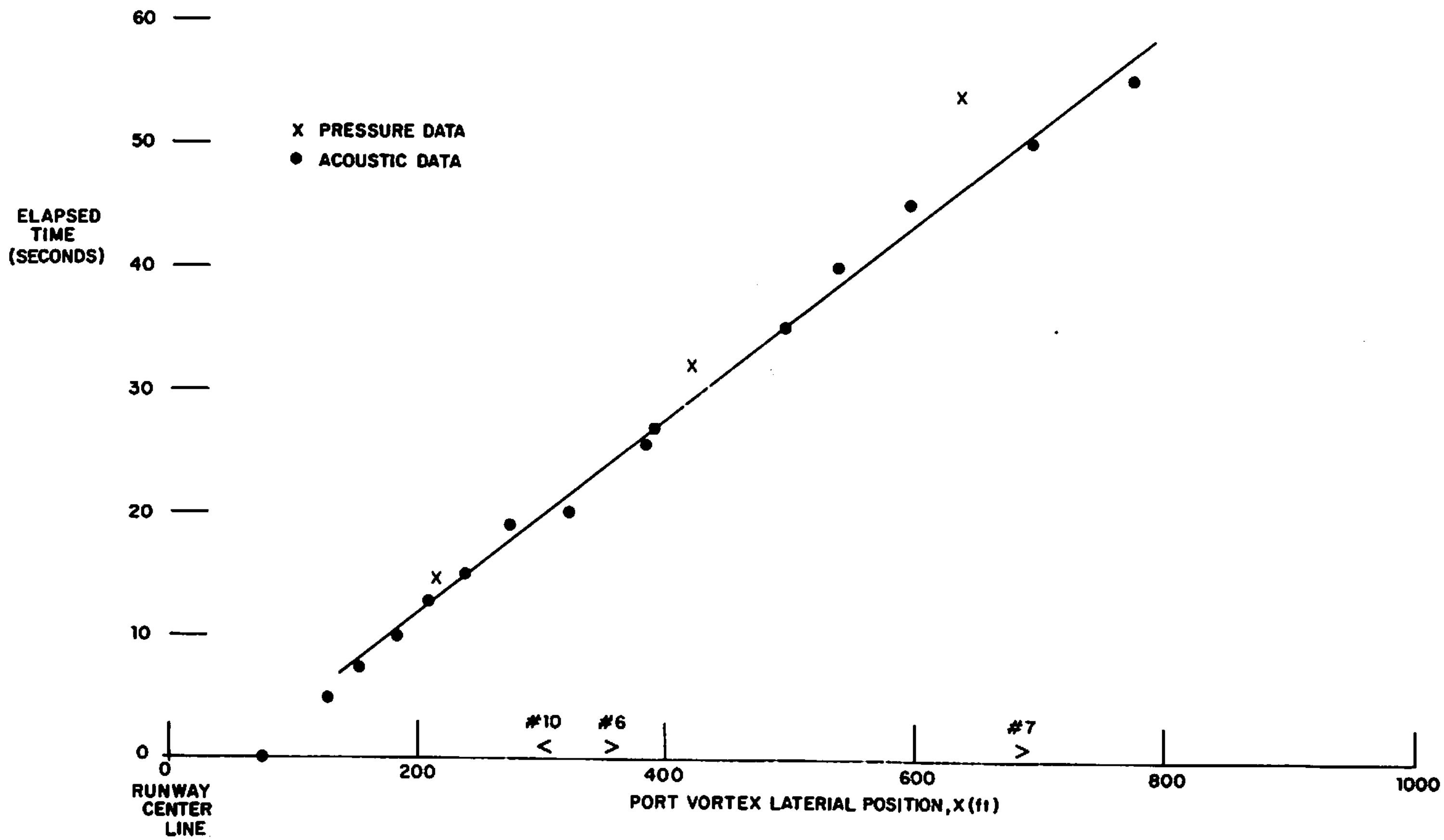

Figure 66. Comparison of port vortex lateral position calculated with the data from acoustic sensors and pressure sensors. Numbers on horizontal scale indicate transceiver positions. Run #47-37 B-727; Kennedy Airport 2/10/72; Middle marker of Runway 31R; Local Time: 1025; Configuration: landing

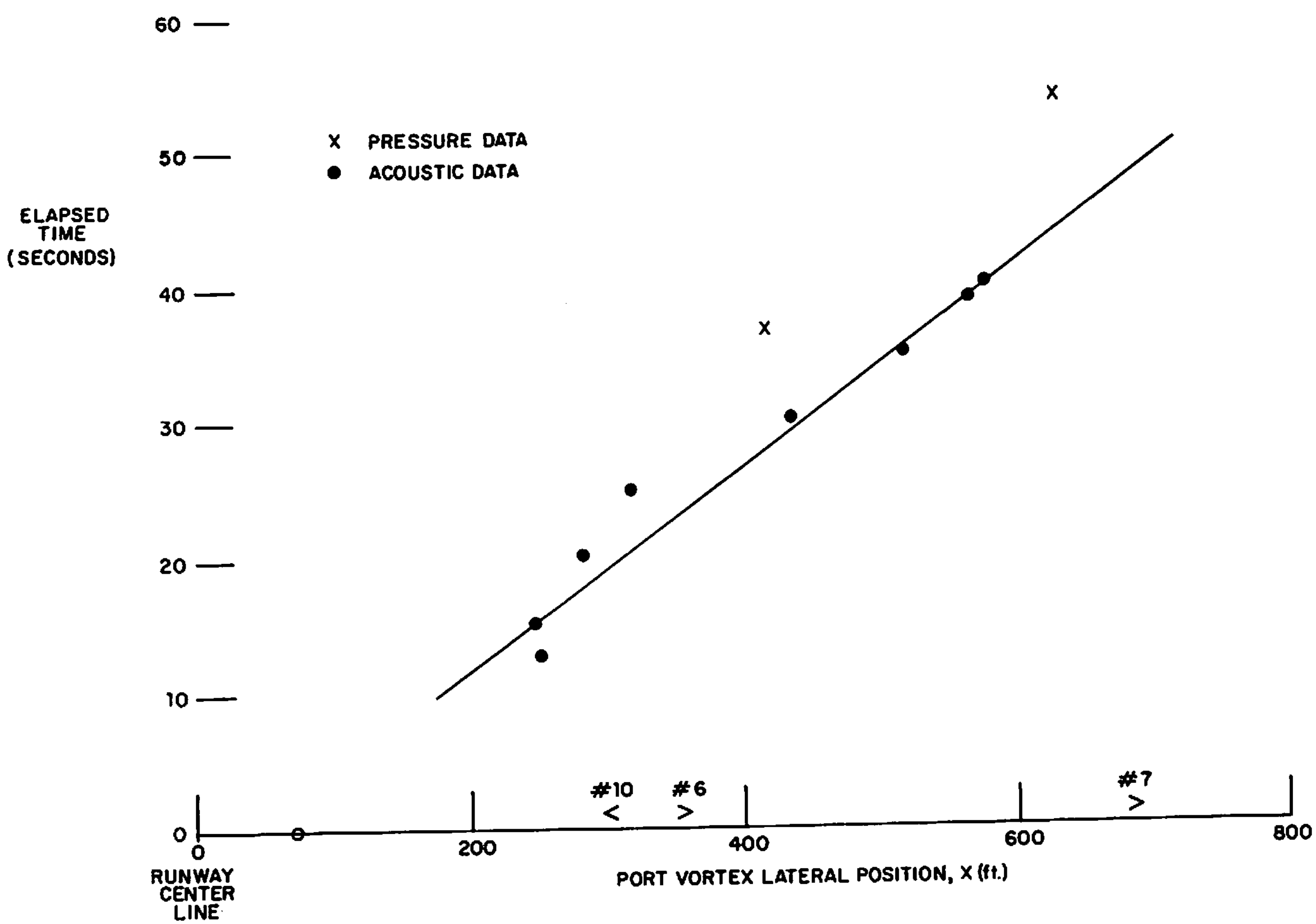

Figure 67. Comparison of port vortex lateral position calculated with the data from acoustic sensors and pressure sensors. Numbers on horizontal scale indicate transceiver positions. Run #47-38 DC-8; Kennedy Airport 2/10/72; Middle marker of Runway 31R; Local time: 1028; Configuration: landing

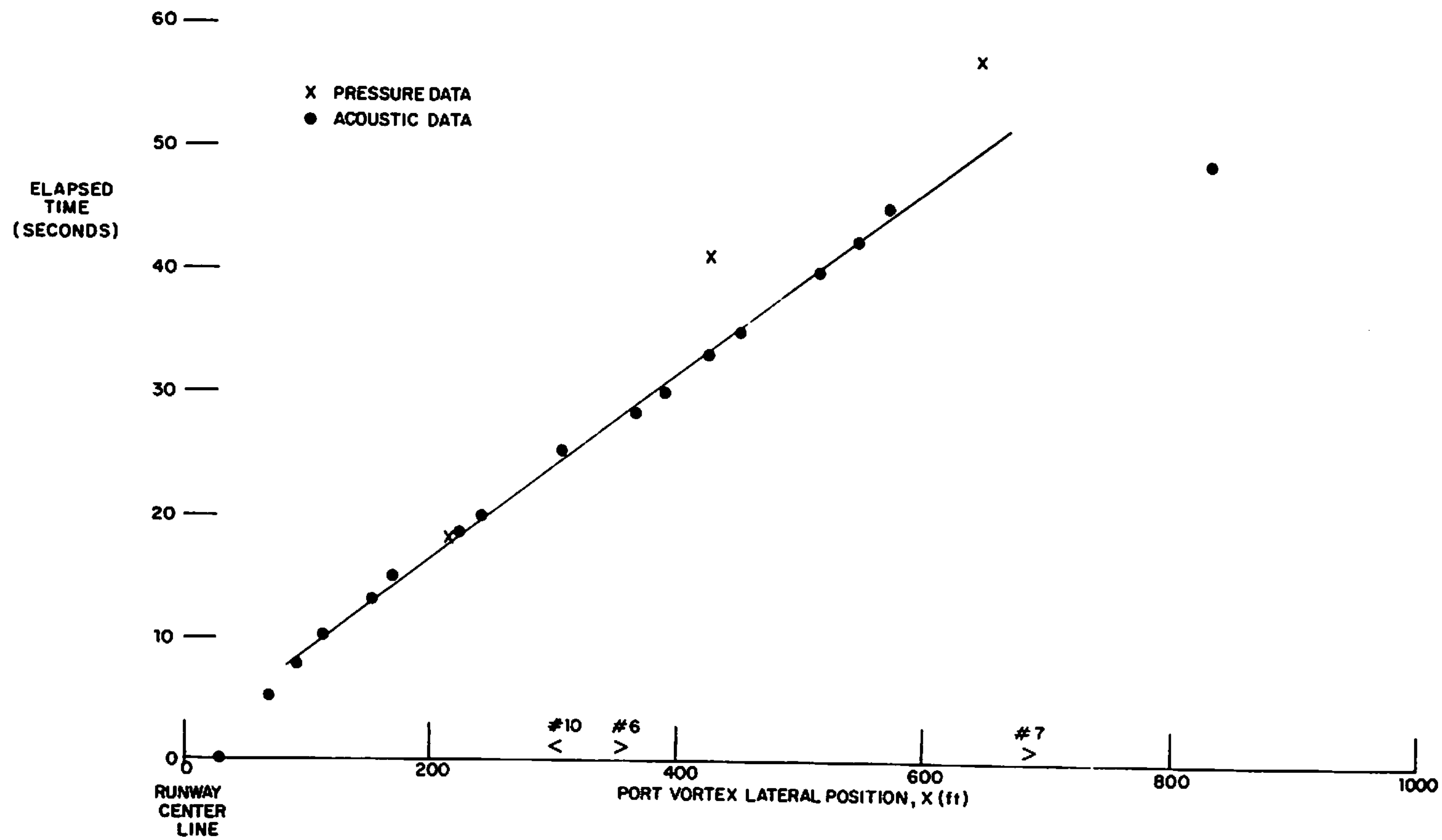

Figure 68. Comparison of port vortex lateral position calculated with the data from acoustic sensors and pressure sensors. Numbers on horizontal scale indicate transceiver positions. Run #47-41 B-727; Kennedy Airport 2/10/72; Middle marker of Runway 31R; Local time: 1035; Configuration: landing

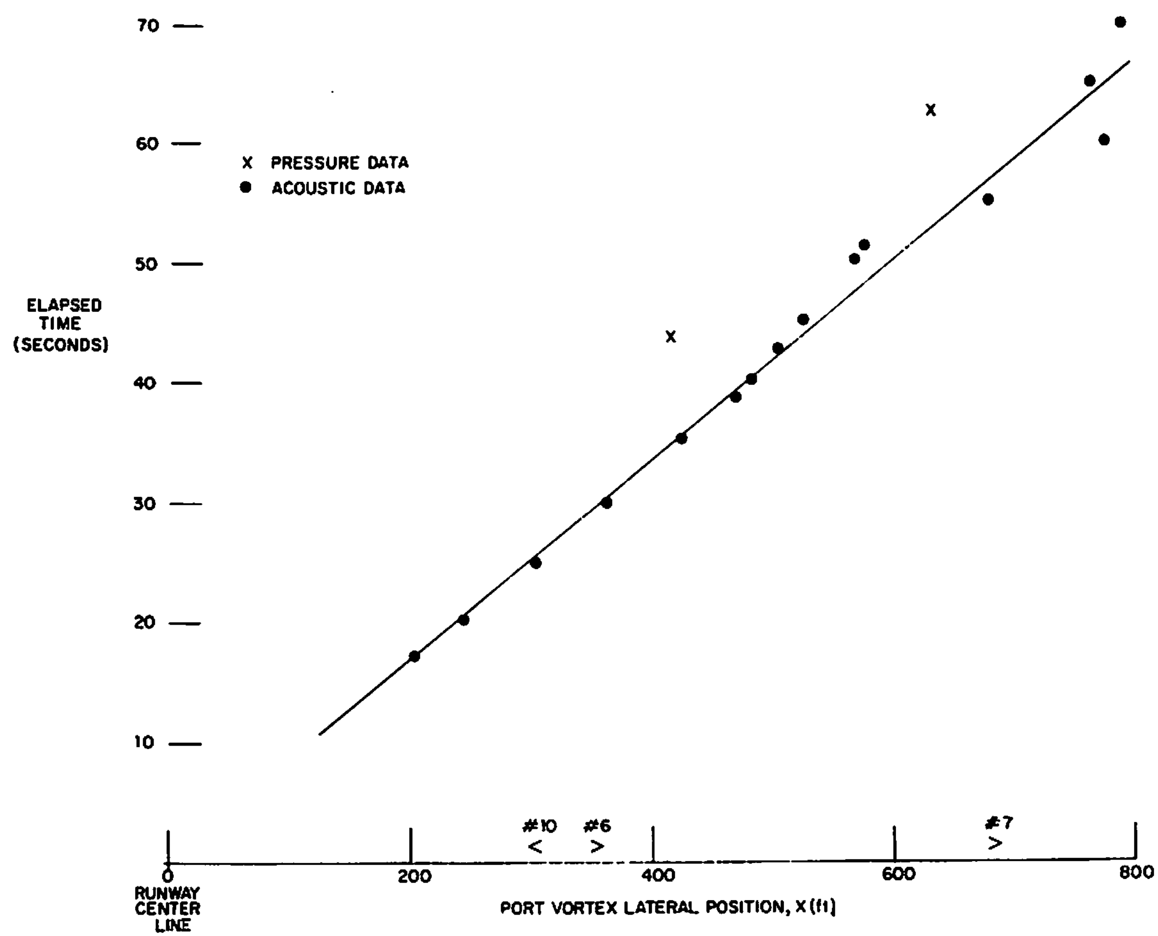

Figure 69. Comparison of port vortex lateral position calculated with the data from acoustic sensors and pressure sensors. Numbers on horizontal scale indicate transceiver locations. Run #47-44 DC-8; Kennedy Airport 2/10/72; Middle marker of Runway 31R; Local time: 1042; Configuration: landing

The transceiver positions for these runs are shown in Figure 70. Enough information was obtained from the time delayed signals using only transceivers #4, 10, 6, 7 and 8 to calculate the vortex track for Figures 64-69. The signals in transceiver #3 were therefore not included in the calculation. The resultant tracks are relatively free of the types of discontinuities which occur in Figures 62-63 for Runs #46-41 and 46-46 where all observed signals were included. The absence of these discontinuities is probably due to the fact that the delayed signals used were relatively free of the systematic errors introduced by the interference of the starboard vortex (See Section 2.3.3).

In Figures 62-69 the discrepancies in vortex location given by the two types of sensors are probably due mostly to errors in the acoustic location x(t). Good pressure data is obtained only for vortices relatively close to the ground, where the largest errors occur in the acoustic system (Appendix B). The maximum disagreement in the lateral positions determined by these two sensors never exceeded one hundred feet. The position of the vortex indicated by the pressure sensors also contains a small error which is entirely a timing error since the positions of the pressure sensors are accurately known. The magnitude of this error depends upon the noise level and upon possible systematic errors in the assumption that the maximum signal occurs when the vortex core is overhead. The timing errors in the pressure data analysis are probably on the order of a few seconds.

The absolute accuracy of the vortex positions measured by these two systems may be determined by comparing them to the positions obtained by photographic tracking with the NAFEC smoke tower. A series of such tests, using pressure sensors, was conducted at NAFEC during the period April 17 - May 5. At the time of this writing this data is being reduced and will be published in a subsequent report. Future tests with the NAFEC smoke tower are being scheduled for the summer and fall of 1972 to calibrate both systems (with priority on the acoustic system) and to resolve some of the systematic problems previously discussed.

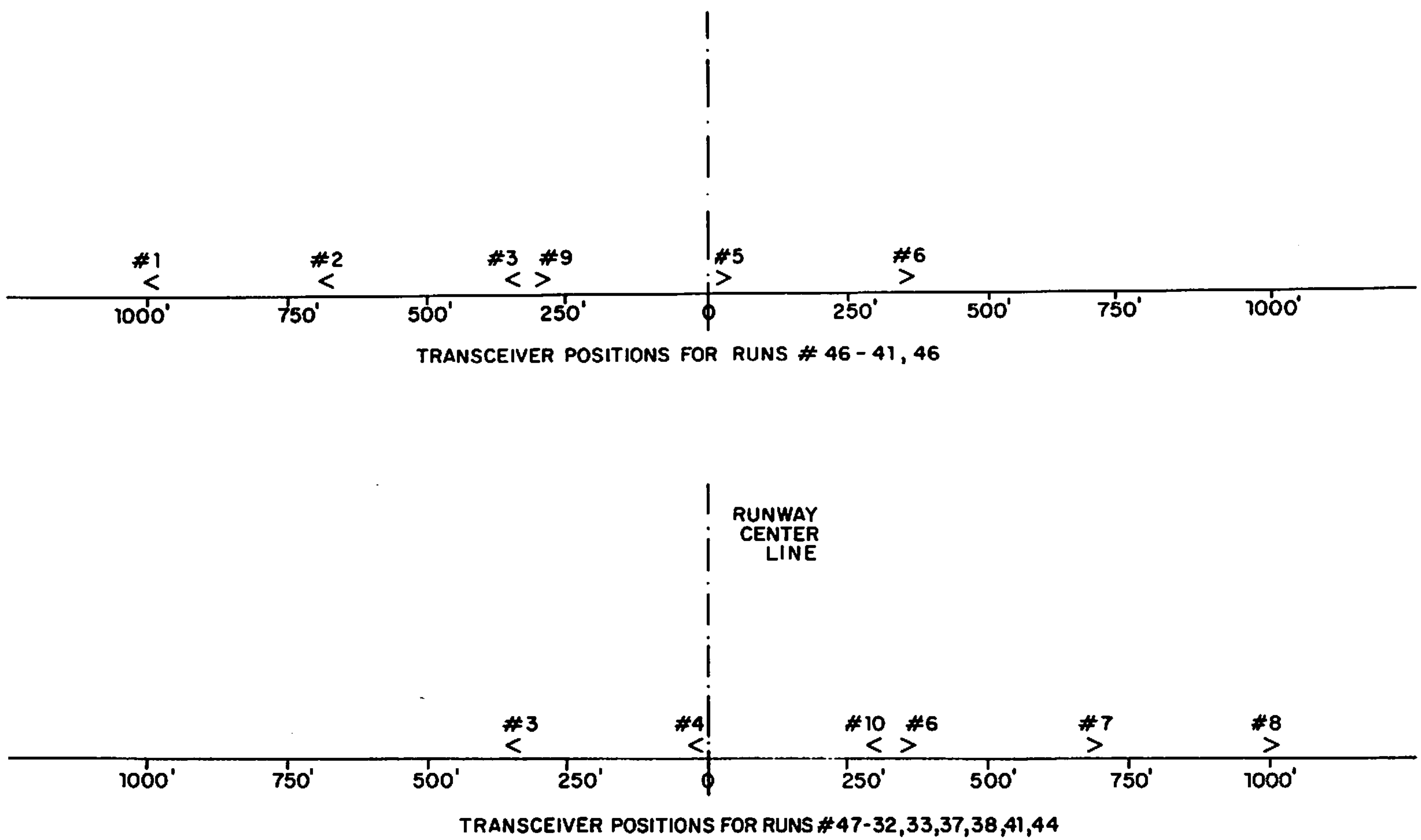

Figure 70. Transceiver Positions

5.0 CONCLUSIONS AND RECOMMENDATIONS

With respect to the acoustic sensor the tests have shown that the best tracking accuracy is achieved with a redundant system. In order for such a system to retain the advantages of simplicity and maintainability in the field, transmission and reception should be accomplished by transceivers. For better S/N these should operate at different frequencies for each of the two functions. As expected, improved ground reference pulses are obtained if the transceivers are elevated above ground level.

Operational problems were encountered by the acoustic sensor due to the interference of one vortex with the signal from the other. This difficulty can probably be overcome by proper data handling procedures. The wind pressure sensors were able to distinguish clearly between the two vortices, (but are not suitable for tracking at altitudes much above 100 feet). Furthermore, wind noise degrades their S/N ratio severely above about 15 knots.

It is recommended that further tests of these sensor systems be oriented toward realtime data processing and the absolute calibration of tracking accuracy. This work should be done at NAFEC where facilities exist for photographically tracking vortices marked with smoke.

APPENDIX A

ACOUSTIC ANTENNA DESIGN

APPENDIX A
ACOUSTIC ANTENNA DESIGN

In this appendix, the properties of various antenna-transducer combinations are compared. It is assumed that the major sources of noise, such as a landing aircraft, are on a line perpendicular to the radar baseline. Table A-1 shows the relative efficiency of the combinations used in various tests. The advantage of a horn-in-dish receiver is large and accounts for the very short streaks of aircraft noise in the Kennedy acoustograms. Table A-2 lists the angular response and other properties of the horns and dishes.

TABLE A-1. SYSTEM EFFICIENCY CALCULATION

Transmitter Efficiency	
Horn	$I = P/\theta_1\theta_2L^2$
Horn in Dish	$I = GP/\theta_1\theta_2L^2$

Receiver Efficiency: Ratio of Front to Side Response	
Omnidirectional Microphone	1
Omnidirectional Microphone in Dish	G
Horn	R
Horn in Dish	GR

Relative Total Efficiency: Product of Transmitter Efficiency and Receiver Efficiencies (assume same θ_1 for all cases)

Configuration	Efficiency	Efficiency at 3KHz
Horn in Dish-Omnidirectional Microphone in Dish (used in previous work)	G^2	500
Horn - Horn (used in Logan Tests)	R/θ_2	40
Horn in Dish - Horn in Dish (used in Kennedy Tests)	RG^2	200,000

Definitions

G = $\theta_3 D/\lambda$ is the gain of the dish (assume $\theta_2=\theta_3$ for a horn in a dish)

θ_1 = Verticle angle of Horn Beam

θ_2 = Horizontal angle of Horn Beam

θ_3 = Angle subtended by a dish at its focal point.

I = Acoustic intensity at reciever

P = Acoustic power transmitted

L = Transmitter - Receiver spacing

TABLE A-2. PROPERTIES OF ANTENNA COMPONENTS

Relative Voltage Response with ID-60TDriver: 3KHz pulse			
Angle	Altec 203B Multicellular horn	University SH Horn	University GH Horn
0°	380 mV	380 mV	250 mV
90°	32	20	7
180°	38	60	20
270°	38	15	7
R	∿100	∿400	∿1200

Horn Physical Characteristics:			
	Altec 203B Multicellular horn	University SH Horn	University GH Horn
Mouth Dimensions	32" (Vertical) X 17"	9" diam.	31" diam.
Nominal Angular Divergence	20° (Vertical) X 40°	100°	65°

Dish Physical Characteristics:

Width (D) = 52"

Height = 36"

Focal Length = 30"

θ_3 = 90°

APPENDIX B

THE INFLUENCE OF TIME DELAY ERRORS ON VORTEX POSITION LOCATION

APPENDIX B
THE INFLUENCE OF TIME DELAY ERRORS ON VORTEX POSITION LOCATION

Errors in the measurement of time delays result in errors in the calculated vortex positions. Expected time delay errors have been empirically determined to be about ±1 millisecond (Figure 10). An example of the resulting position errors for a three transducer system is shown in Figure B-1, where the transducer spacing corresponds to that in Figure 19. Figure B-1 illustrates what happens when one millisecond is subtracted from the time delay observed in receiver 2. The heavy dots represent the correct position calculation and the arrows show the new position when the error is added. Figure B-2 illustrates the effects of adding one millisecond to the time delay observed in receiver 2. The asterick (*) indicates that no real position exists for the incorrect data. Some possible sources of a one msec error are:

1. uncertainty in the position of the ground pulse,
2. one vortex interfering with the path of the signal from the other vortex and/or the ground pulse,
3. wind shear effects,
4. inability to read the data output (Polaroid oscilloscope photographs) to better than one millisecond.

The first three errors are systematic while the last is random.

From a systems point of view it is useful to determine regions where the expected location error is less than a specified amount. The loci of constant position error for a millisecond time delay error are shown in Figure B-3. The loci of constant scattering angle have been superimposed on these curves. The combination of these two types of curves could be used to specify systems parameters. Once a maximum scattering angle and acceptable position uncertainty have been defined, the region that would be adequately monitored lies between the two corresponding curves in Figure B-3. Similar curves could be drawn for any system configuration.

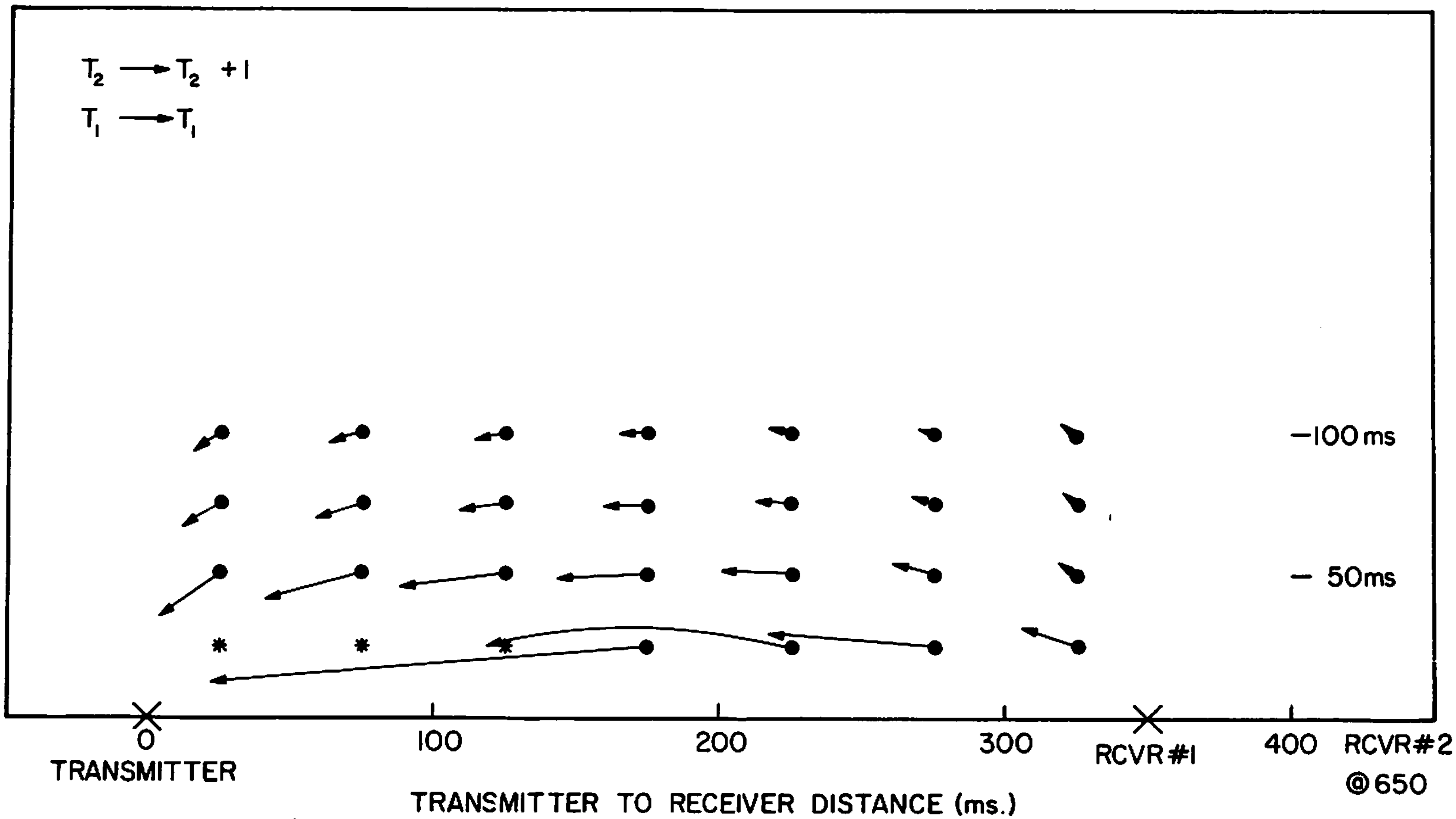

Figure B-1. Displacement of actual position by introducing an error of +1 millisecond in the time delays of receiver #2. Note: all distances have been normalized to c(the speed of sound) = 1.

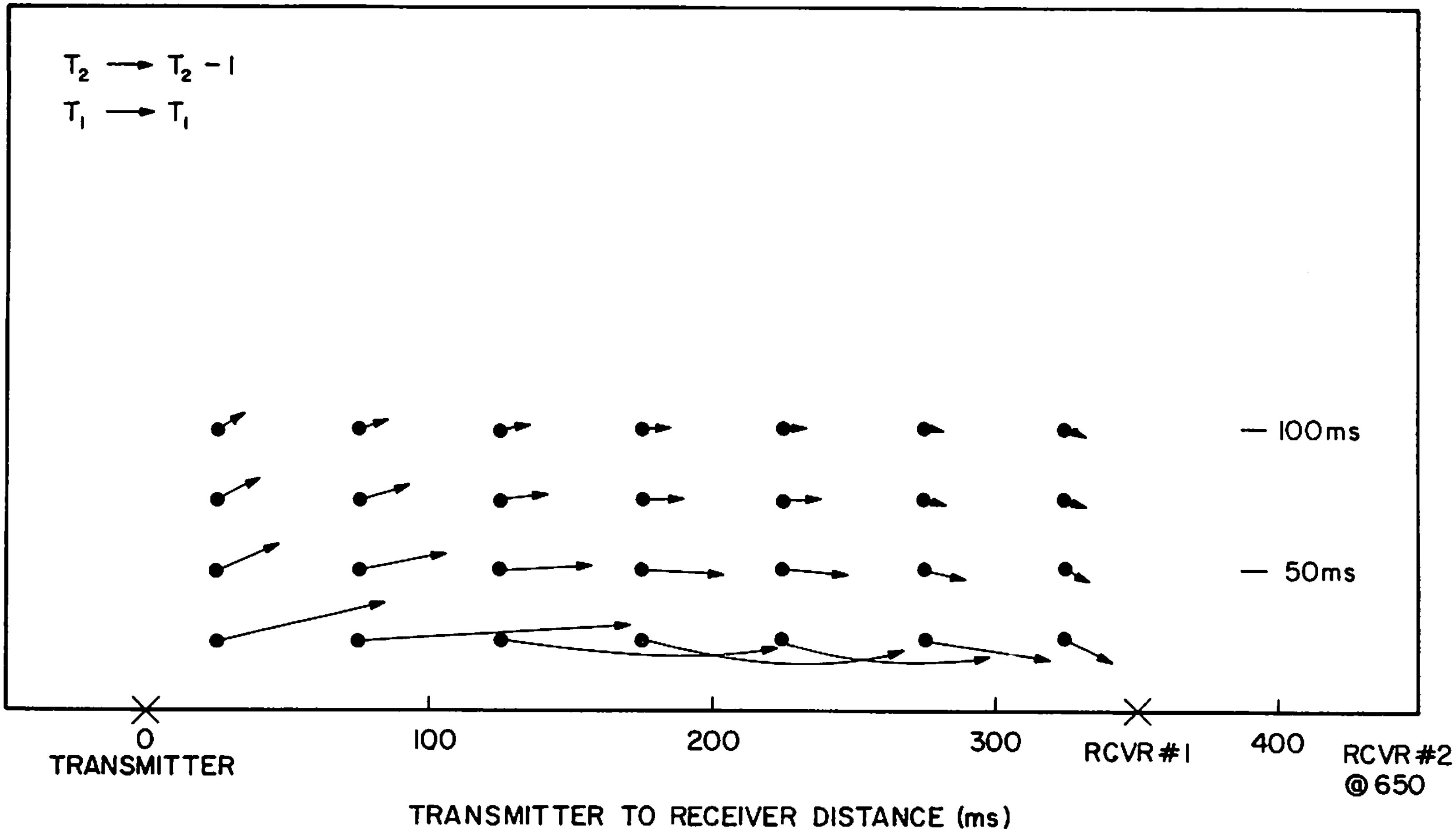

Figure B-2. Displacement of actual position by introducing an error of -1 millisecond in the time delays of receiver #2. Note: all distances have been normalized to c(the speed of sound) = 1.

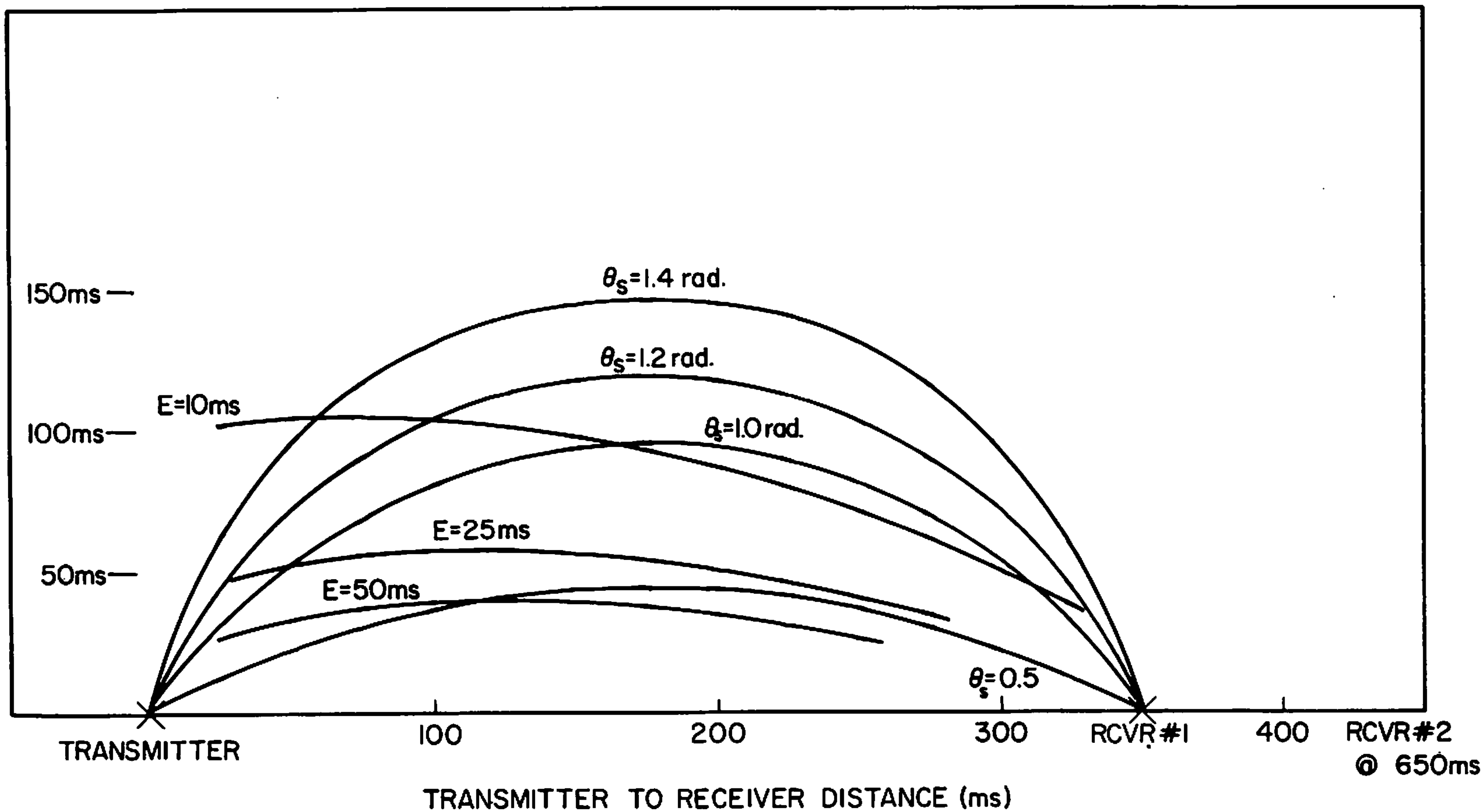

Figure B-3. Loci of constant position shifts and constant scattering angles. Note: all distances have been normalized to c(the speed of sound) = 1.

APPENDIX C

ANALYSIS OF DIRECT ACOUSTIC PULSES

APPENDIX C
ANALYSIS OF DIRECT ACOUSTIC PULSES

This appendix contains the analysis of some direct acoustic pulses obtained under various experimental conditions at Kennedy Airport. Comparisons were made between dishes mounted on ten foot stands (Figure 11) and dishes mounted on the ground. The ten foot stands were designed to increase the magnitude of the up-wind direct signal for large separations between dishes. Signals propagating with the wind used a frequency of 3KHz (Figure C-1) and those against the wind, 2KHz (Figure C-2). The crosswind speed was determined by comparing the pulse transit times in the two directions for pairs of speakers.

The results of the direct pulse analysis are shown in Figures C-1 and C-2. The peak direct signal is plotted as a function of speaker separation and crosswind speed. The reduction in direct signal as a function of distance L is due to three effects:

1. The effect of wavefront expansion (the signal amplitude falls off as L^{-1}).
2. The effect of beam attenuation, which increases at higher turbulence levels.
3. The effect of beam refraction, principally because of wind shear. The beam propagating against the wind is deflected away from the ground and can be lost completely. The beam propagating with the wind is also somewhat attenuated by wind shear.

In Figure C-1 the signal propagating with the wind generally decreases with distance and increasing crosswind. For propagation against the wind in Figure C-2 the attenuation is more dramatic. The actual attenuation is considerably greater than that shown, since the largest signals exceeded the available dynamic range of the tape recorder and were clipped. In the case of a strong crosswind, the signals with one speaker on the ground were smaller as one would expect.

A simple model of wind shear can be used to understand the observed effects of propagation against the wind. Generally, the wind shear $\gamma = dv/dy$ decreases strongly with height. The model therefore assumes (Figure C-3) a uniform wind shear up to height h_o and no wind shear from h_o to the height h of the speaker where the crosswind speed is $v(\gamma = v/h_o)$. One can calculate the limiting separation L_ℓ of two speakers at height h for which the acoustic ray between them just hits the ground. The result is:

$$L = (h+h_o)\ (2c/v)^{1/2}$$

where the ray is assumed to make a small angle with the ground. If one speaker is on the ground, the separation is just half this value. The separations given in Table C-1 for several cross wind values are in rough agreement with observation (Figure C-2).

TABLE C-1. SPEAKER SEPARATION AS A FUNCTION OF CROSSWIND

v	h	h_o	L_ℓ
1.5 ft/sec	10 ft	10 ft	780 ft
5 ft/sec	10 ft	10 ft	420 ft
20 ft/sec	10 ft	10 ft	210 ft

Propagation through the atmosphere not only attenuates the peak signal, but also tends to broaden the pulses and to produce multiple pulses. Figures C-4 - C-6 show some examples of direct pulses obtained with the same speaker pair under different wind conditions. These signals are obtained by filtering the raw acoustic signal, rectifying, and averaging for 15 or 20 seconds at a time when no aircraft or vortices are present.

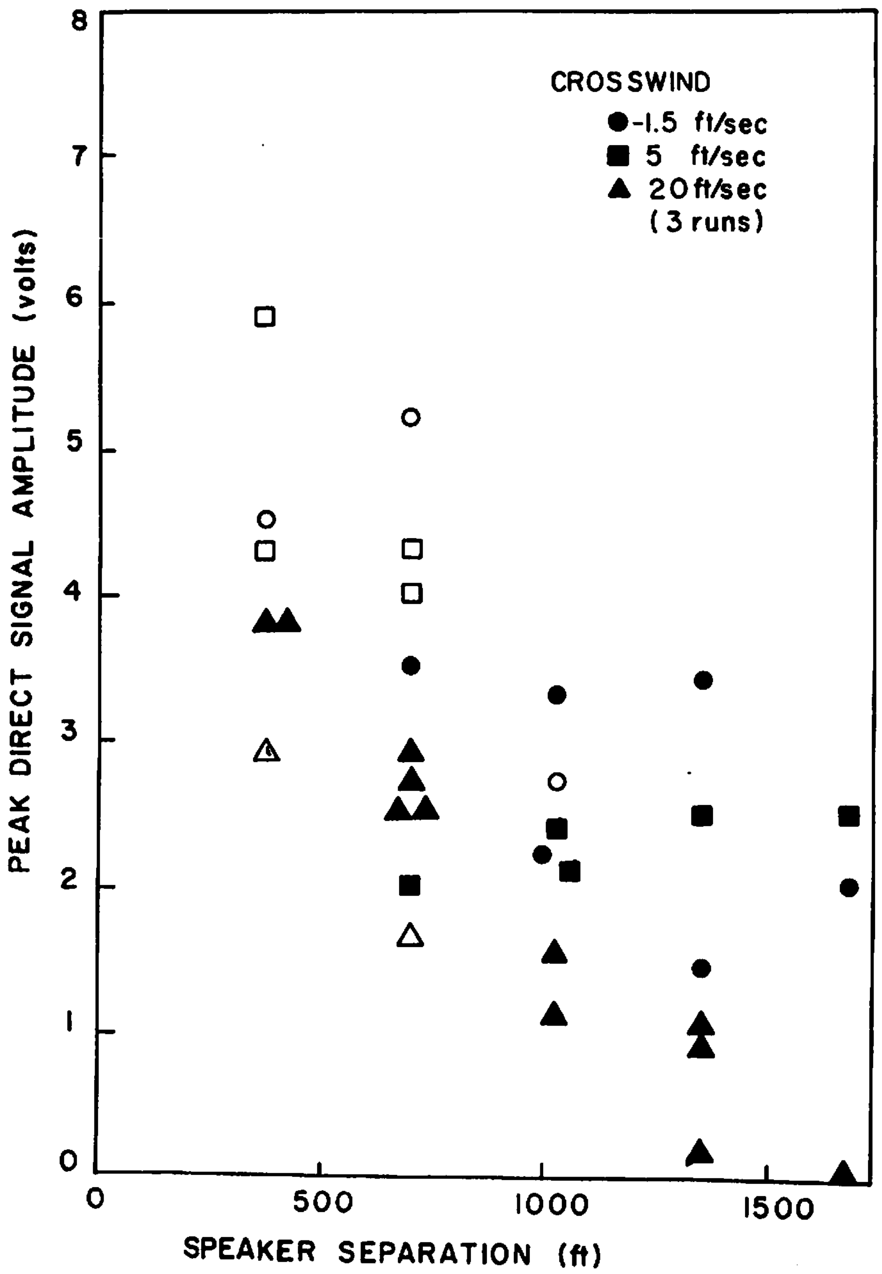

Figure C-1. Peak 3KHz Direct Signal vs Speaker Separation for Three Values of Crosswind. The solid symbols indicate that both speakers were elevated to about 10 Ft. The open symbols indicate that one of the speakers was located at ground level. The wind direction is positive in the direction of 3 KHz propagation.

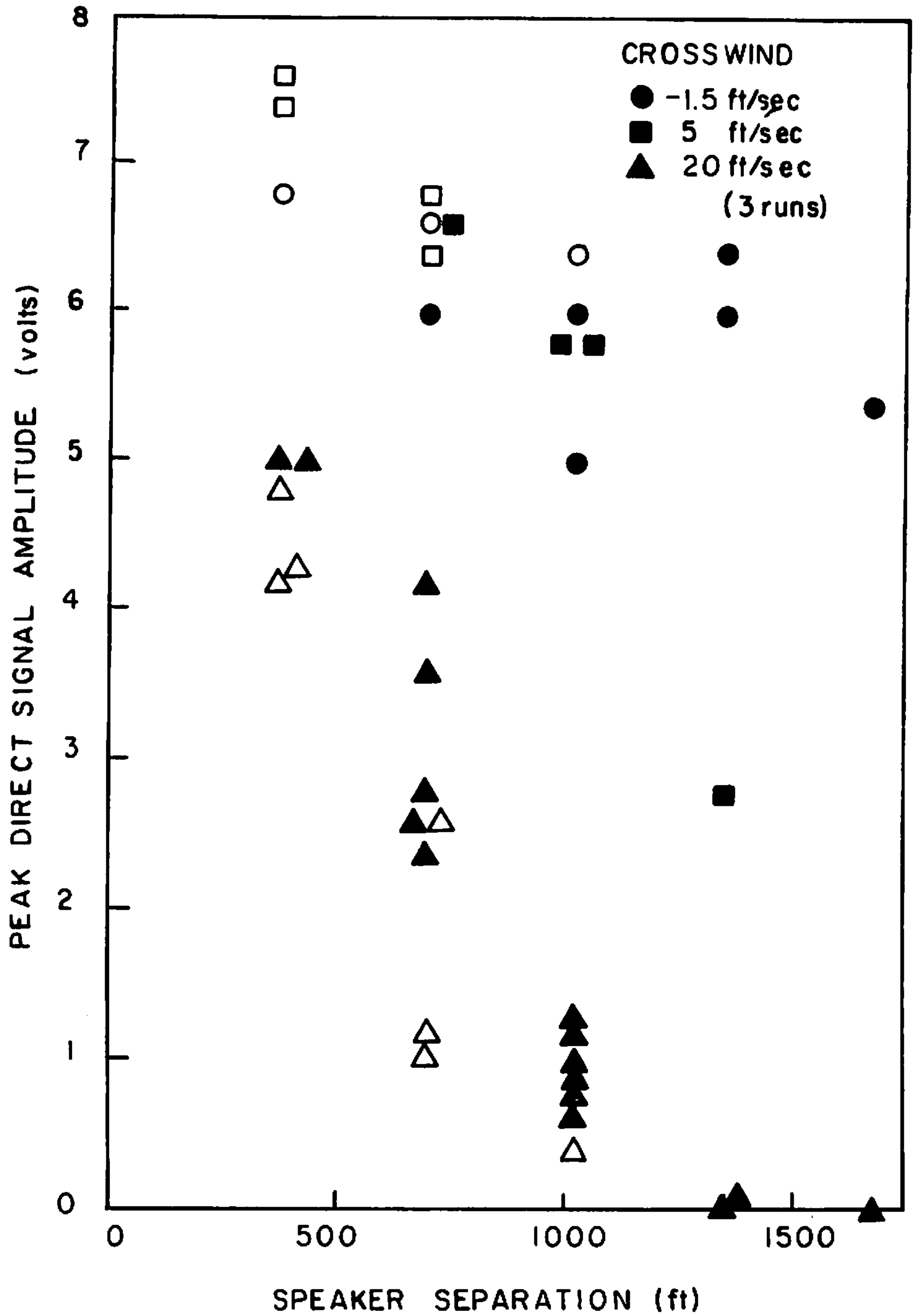

Figure C-2. Peak 2KHz Direct Signal vs Speaker Separation. See comments on Figure C-1.
Note: All signals above 6 volts have been clipped by overdriving the magnetic tape recorder.

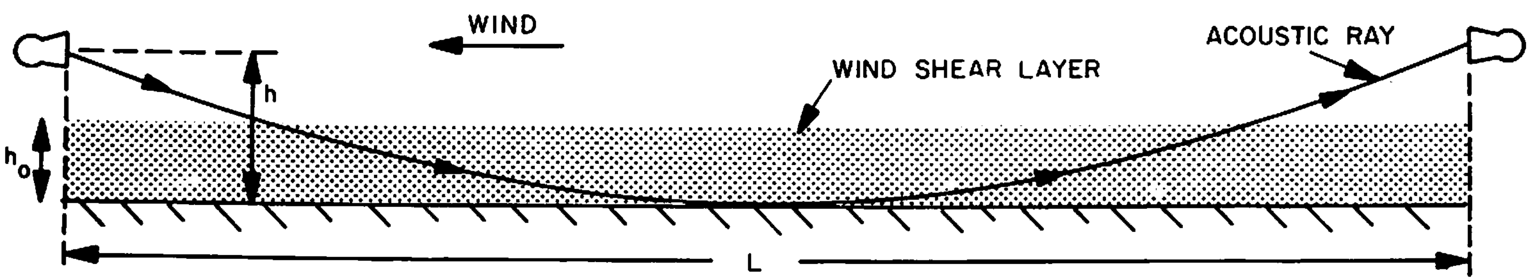

Figure C-3. Acoustic Ray for Propagation Against Wind.

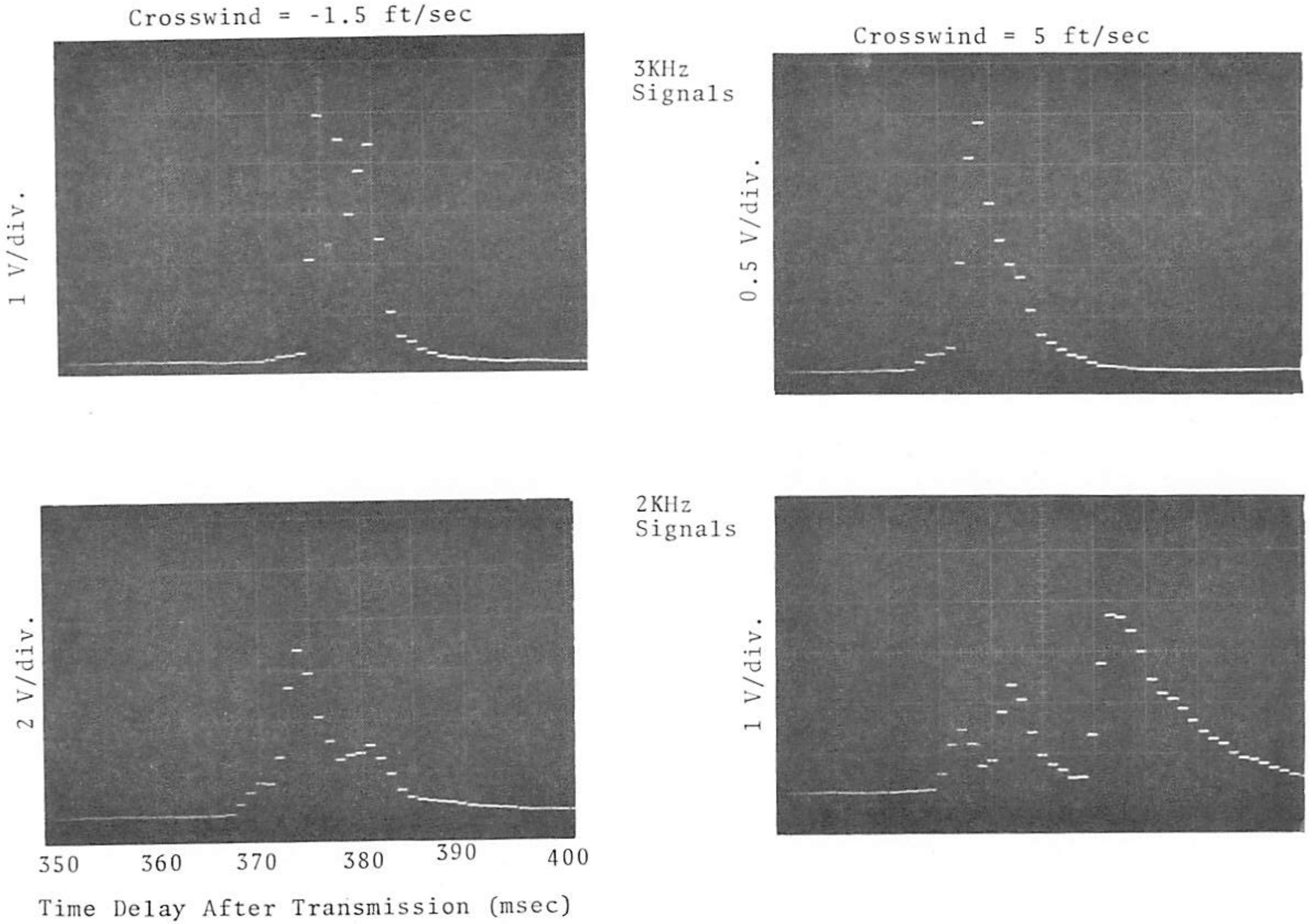

Figure C-4. Direct Signals Between Speaker Locations 3 and 8 (Figure 19) Separation = 1370 Ft.

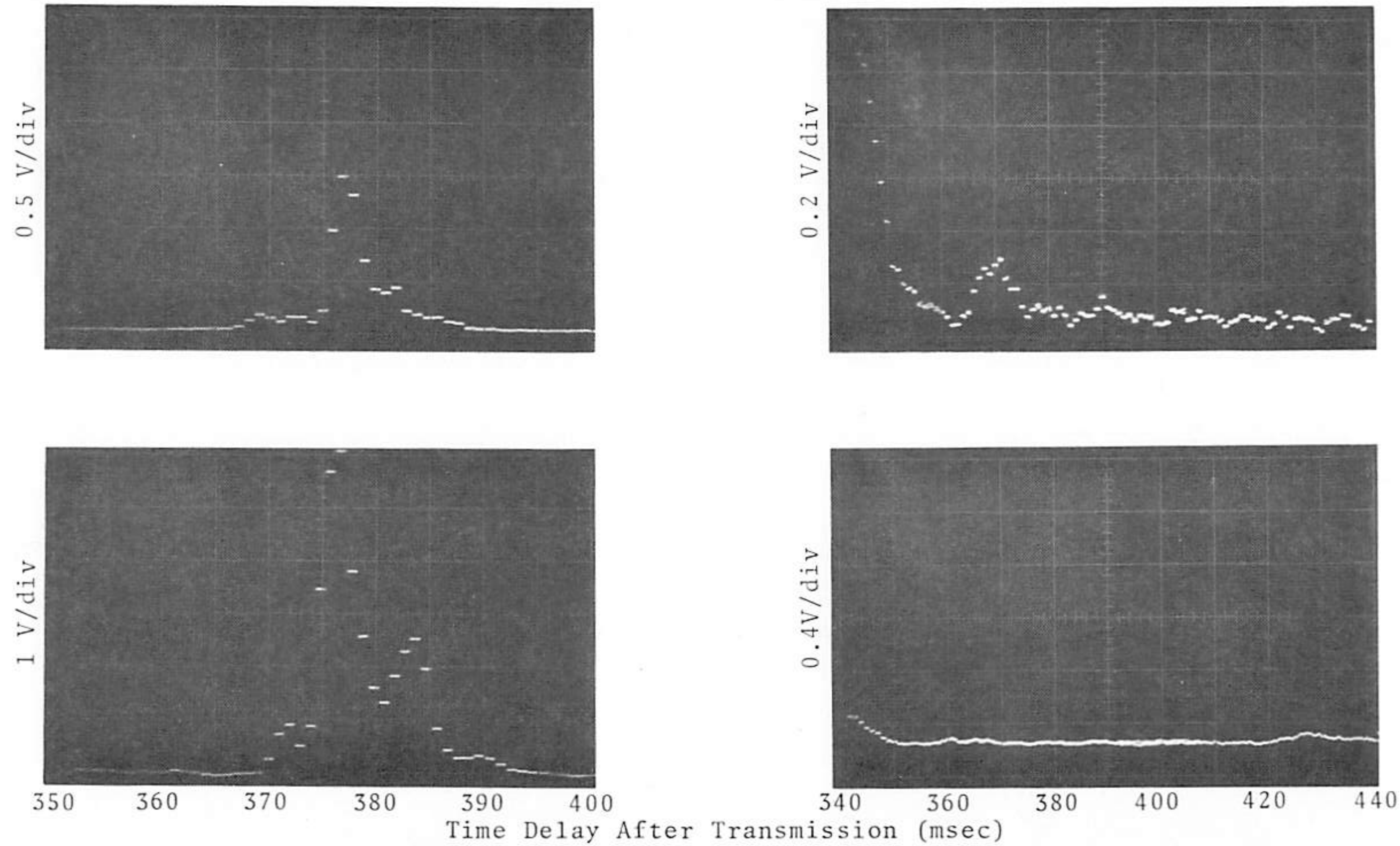

Crosswind = -1.5 ft/sec

Crosswind = 20 ft/sec

Figure C-5. Direct Signals Between Speaker Locations 2 and 7 (Figure 19) Separation = 1370 Ft.

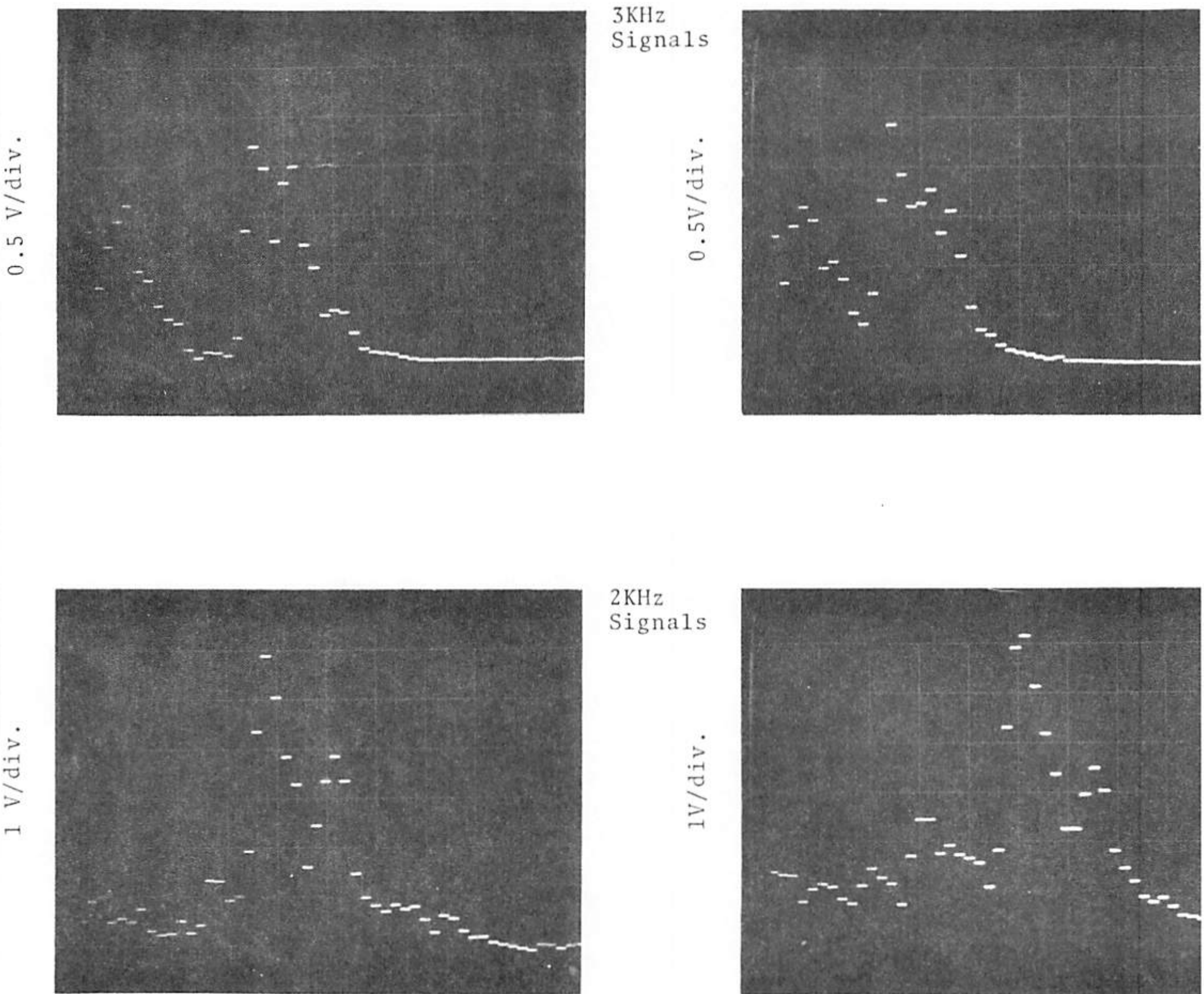

Crosswind = 1.5 ft/sec

Time Delay After Transmission (r

Crosswind = 5 ft/sec

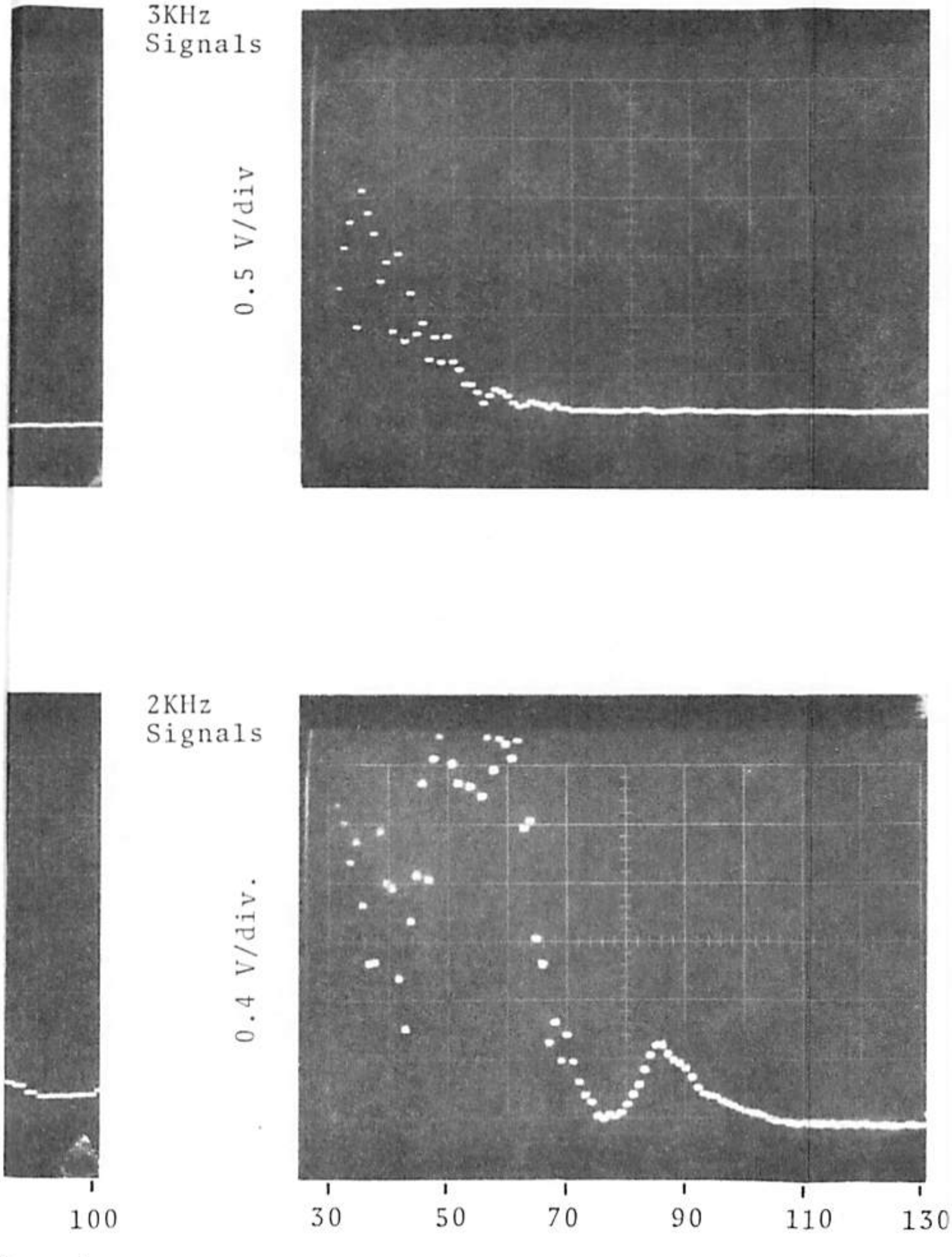

Figure C-6. Direct Signals Between Speaker Locations 3 and 7 (Figu[illegible] 19); Separation = 1040 Ft. Note the disappearance of th[illegible] 3KHz signal into th[illegible] speaker ringing for 20 ft/sec winds.

REFERENCES

1. Burnham, D., Hallock, J., Kodis, R. and Sullivan, T., "Vortex Sensing Tests at NAFEC", Report No. DOT-TSC-FAA-72-2. See also, "Aircraft Wake Vortex Sensing Systems", DOT-TSC-FAA-72-13, which describes earlier work.

2. Simmons, W.R., Wescott, J.W., and Hall, F.F., Jr., "Acoustic Echo Sounding as Related to Air Pollution in Urban Environments", NOAA Technical Report ERL 216-WPL 17, May 1971.

3. Hallock, J.N., "Pressure Measurements of Wake Vortices Near the Ground", J. Aircraft 9, 311 (April 1972).

4. Landau, L.D. and Lifshitz, E.M., Fluid Mechanics (Pergamon Press, London, 1959), p. 19.

5. Burnham, David C., "Effect of Ground Wind Shear on Aircraft Trailing Vortices", AIAA Journal 10, 1114 (August 1972).